Role of Intracellular Oxidant Release in Oxidised Low Density Lipoprotein-Induced U937 Cell Death

A thesis
submitted in partial fulfilment
of the requirements for the Degree of
Master of Science
in Biochemistry

at the
University of Canterbury,
New Zealand

Yan Alpha CHEN

2012

TABLE OF CONTENTS

LIST OF FIGURES v
ABBREVIATIONS vii
ABSTRACT xii
1. INTRODUCTION 1
1.1 Overview 1
1.2 Atherosclerosis 2
1.3 ROS and oxidative stress in atherosclerosis 6
1.4 Oxidative damage 7
1. 4.1 Glutathione (GSH) 8
1. 4.2 Aconitase 9
1.5 Cell death 10
1.6 NADPH oxidase (NOX) 12
1.6.1 NOX structure, location and homology 12
1.6.2 NOX activation 15
1.6.3 NOX and cell death in atherosclerosis 17
1.6.4 NOX inhibitors 18
1.6.4.1 Apocynin 18
1.6.4.2 Diphenyleneiodonium (DPI) 20
1.7 Calcium and atherosclerosis 22
1.8 7,8-Dihydroneopterin (7,8-NP) 24
1.9 Objectives of research 24
2. MATERIALS AND METHODS 26
2.1 Materials 26
2.1.1 Reagents 26
2.1.2 Media 28
2.1.3 Antibodies 28
2.1.4 General solutions, media and buffers 28
2.1.4.1 Phosphate buffered saline (PBS) 28

2.1.4.2 Roswell Park Memorial Institute (RPMI)-1640 Media 28
(with and without phenol red)
2.1.4.3 7,8-Dihydroneopterin (7,8-NP) solution 29
2.1.4.4 Phorbol 12-myristate 13-acetate (PMA) 29
2.2 Methods 29
2.2.1 Cell culture 29
2.2.1.1 Cell culture media 30
2.2.1.2 Preparation of U937 cell line 30
2.2.1.3 Cell experiment procedures 30
2.2.2 Blood collection and plasma preparation for LDL purification 31
2.2.3 LDL preparation 31
2.2.3.1 Extraction of LDL from plasma 31
2.2.3.2 Determination of cholesterol content of LDL 32
2.2.3.3 LDL washing and concentration 32
2.2.4 LDL oxidation 33
2.2.4.1 Dialysis tubing treatment 33
2.2.4.2 Copper oxidation of LDL 33
2.2.5 Cell viability analysis by MTT reduction assay 33
2.2.5.1 MTT assay solutions 33
2.2.5.2 MTT reduction assay 34
2.2.6 Determination of protein concentration 34
2.2.7 Sodium dodecyl sulphate polyacrylamide gel electrophoresis (SDS-PAGE) and Western blot analysis 35
2.2.7.1 Solutions for SDS-PAGE and Western blot analysis 35
2.2.7.2 Cell processing for U937 cells 36
2.2.7.3 SDS-PAGE analysis 36
2.2.7.4 Western blot analysis 36
2.2.7.5 Visualisation 37
2.2.7.6 β-Actin detection 37
2.2.8 Fluorescence microscopy 38
2.2.8.1 Dihydroethidium (DHE) detection for intracellular ROS 39
2.2.8.2 MitoSox Red detection for mitochondrial superoxide 39

2.2.8.3 Fluo-3-acetoxymethyl (AM) ester detection of intracellular calcium 40
2.2.9 DHE and fluo-3AM analysis by flow cytometry 40
2.2.10 Intracellular glutathione (GSH) measurement by high performance liquid chromatography (HPLC) analyses 40
2.2.10.1 Solutions for GSH analysis 41
2.2.10.2 GSH analysis by HPLC 41
2.2.11 Aconitase assay 42
2.2.11.1 Cell extract preparation 42
2.2.11.2 Extraction of cytosol and mitochondrial fractions 43
2.2.11.3 Determination of aconitase activity 43
2.2.12 Succinate dehydrogenase assay 44
2.2.13 Statistical analysis 45

3. RESULTS 46

3.1 Toxicity of oxLDL 46
3.2 Oxidative stress induced by oxLDL 50
3.2.1 The effect of oxLDL on intracellular ROS generation in U937 cells 50
3.2.2 The effect of oxLDL on mitochondrial superoxide generation in U937 cells 55
3.2.3 The effect of oxLDL on intracellular GSH levels in U937 cells 58
3.2.4 The effect of oxLDL on intracellular aconitase activity in U937 cells 59
3.2.5 The effect of oxLDL on intracellular calcium levels in U937 cells 61
3.3 NADPH oxidase (NOX) is the major oxidative stress site 68
3.3.1 The effect of apocynin and DPI on oxLDL-mediated cell death 69
3.3.2 The effect of apocynin and DPI on oxLDL-mediated ROS production 74
3.3.3 The effect of apocynin and DPI on oxLDL-mediated GSH loss 82
3.3.4 The effect of apocynin and DPI on oxLDL-mediated aconitase activity loss 86
3.3.5 The effect of 7,8-NP and apocynin on oxLDL-mediated intracellular calcium influx 93
3.3.6 Mechanism of NOX activation 98
3.4 7,8-NP protection against oxLDL-induced oxidative stress 100

4. DISCUSSION 106

4.1 OxLDL-induced cell death in U937 cells 106

4.2 OxLDL-induced oxidative stress in U937 cells 108

ROS 108

GSH 109

Aconitase 109

4.3 OxLDL-induced calcium influx in U937 cells 110

4.4 NADPH oxidase (NOX) and oxidative stress 116

Mechanism of NOX activation by oxLDL 118

4.5 7,8-NP protection against oxLDL-induced oxidative stress 119

4.5 Summary 121

ACKNOWLEDGEMENTS 123

REFERENCES 124

LIST OF FIGURES

Figure 1.1 Initiating events in the early stage of fatty streak formation 3

Figure 1.2 Development of atherosclerotic lesion 5

Figure 1.3 Schematic representation of NADPH oxidase in a phagocyte (neutrophil or macrophage) 13

Figure 1.4 MPO-mediated dimerization of apocynin 19

Figure 1.5 Proposed mechanism of apocynin inhibition of the cytosolic NOX subunit $p47^{phox}$ 19

Figure 2.1 A representative example of change in the absorbance at 340 nm over 30 minutes in the aconitase assay 44

Figure 3.1 Effect of oxLDL on U937 cell viability loss 47

Figure 3.2 Time course of oxLDL-induced cell viability loss in U937 cells 49

Figure 3.3 Time course study of oxLDL-induced ROS productions in U937 cells . 52

Figure 3.4 Effect of oxLDL on intracellular ROS productions in U937 cells..... 54

Figure 3.5 Effect of oxLDL on mitochondrial superoxide production in U937 cells 57

Figure 3.6 Time course study of oxLDL-induced GSH loss in U937 cells 59

Figure 3.7 Effect of increasing concentrations of oxLDL on aconitase activity..... 60

Figure 3.8 Time course study of oxLDL-induced aconitase activity loss in U937 cells 61

Figure 3.9 Effect of oxLDL on intracellular cytosolic Ca^{2+} levels in U937 cells (by fluorescence microscopy) 64

Figure 3.10 Effect of oxLDL on intracellular cytosolic Ca^{2+} levels in U937 cells (by flow cytometry)..... 66

Figure 3.11 Ca^{2+} ionophore A23187 (Br-A) induced an increase in cytosolic Ca^{2+} in U937 cells 67

Figure 3.12 Effects of increasing concentrations of apocynin or DPI on cell viability in U937 cells 70

Figure 3.13 Effects of apocynin or DPI on oxLDL-mediated cell death in U937 cells 71

Figure 3.14 Effects of 7,8-NP, apocynin and DPI on oxLDL-mediated cell death in U937 cells 73

Figure 3.15 Effect of apocynin on ROS productions in U937 cells 75
Figure 3.16 Effect of DPI on ROS productions in U937 cells 77
Figure 3.17 Effect of apocynin on oxLDL-induced ROS productions in U937 cells 79
Figure 3.18 Effects of DPI on oxLDL-induced ROS productions in U937 cells 82
Figure 3.19 Effects of apocynin or DPI on intracellular GSH level in U937 cells .. 83
Figure 3.20 Effects of apocynin or DPI on oxLDL-induced intracellular GSH loss in U937 cells 85
Figure 3.21 Effects of increasing concentrations of apocynin or DPI on aconitase activity in U937 cells 87
Figure 3.22 Effect of increasing concentrations of DPI on aconitase positive control protein activity 88
Figure 3.23 Effects of 7,8-NP, apocynin and DPI on oxLDL-induced aconitase activity loss in U937 cells 89
Figure 3.24 Effects of 7,8-NP and apocynin on oxLDL-induced aconitase activity loss in cytoplasmic and mitochondrial fractions 92
Figure 3.25 Effects of 7,8-NP and apocynin on oxLDL-induced intracellular Ca^{2+} influx over 6 hours 94
Figure 3.26 Time course study of $p47^{phox}$ activation by oxLDL in U937 cells 97
Figure 3.27 Effects of 7,8-NP and apocynin on $p47^{phox}$ protein expression in U937 cells 99
Figure 3.28 Effect of 7,8-NP on oxLDL-induced ROS productions in U937 cells . 101
Figure 3.29 Effect of 7,8-NP on oxLDL-induced mitochondrial ROS productions in U937 cells 103
Figure 3.30 Effect of 78-NP on intracellular ROS productions in U937 cells 104
Figure 3.31 Effect of 7,8-NP on mitochondrial ROS productions in U937 cells 105
Figure 4.1 Proposed involvement of Ca^{2+} in oxLDL cytotoxicity to U937 cells ... 115

ABBREVIATIONS

7-KC	7-Keto cholesterol
7,8- NP	7,8-Dihydroneopterin
AA	Arachidonic acid
ACN	Acetonitrile
ANOVA	Analysis of variance
Apocynin	4’-hydroxy-3’-methoxyacetophenone
Apo	Apocynin
Apo E	Apolipoprotein E
Apo E-/-	ApoE deficient
ATP	Adenosine triphosphate
BCA	Bicinchoninic acid
BHT	Butylated hydroxytoluene
Br-A	4-Bromo-calcium inophore A23187
BSA	Bovine serum albumin
Ca^{2+}	Calcium ion
$CaCl_2$	Calcium chloride
Cl^-	Chloride ion
CO_2	Carbon dioxide
$CO_3^{\bullet-}$	Carbonate radical
$CuCl_2$	Copper chloride
Cyto b558	Flavocytochrome b558
DCIP	2,6-Dichlorophenolindephenol
DHE	Dihydroethidium
DIC	Differential interference contrast
DMSO	Dimethyl sulphoxide

DNA	Deoxyribonucleic acid
DPI	Diphenyleneiodonium
ECM	Extracellular matrix
ECs	Endothelial cells
EDTA	Ethylenediaminetetraacetic acid
EGTA	Ethylene glycol-bis(2-aminoethylether)-N,N,N’,N’- tetracetic acid
ER	Endoplasmic reticulum
EtOH	Ethanol
FAD	Flavin adenine dinucleotide
FBS	Foetal bovine serum
GAPDH	Glyceraldehydes-3-phosphage dehydrogenase
GCD	Chronic granulomatous disease
GSH	Glutathione
GSSG	Disulfides
GTP	Guanosine triphosphate
H^+	Protons
H_2O_2	Hydrogen peroxide
HCl	Hydrochloric acid
HMDM	Human monocytes-derived macrophage
HOCl	Hypochlorous acid
HPLC	High performance liquid chromatography
IC_{50}	The half maximal inhibitory concentration
IMM	Inner mitochondrial membrane
IMS	Inter-membrane space
INF-γ	Interferon-γ
KOH	Potassium hydroxide

KBr	Potassium bromide
L-	Lipid
$L^{\bullet}$	Lipid radical
LDH	Lactate dehydrogenase
LDL	Low density lipoprotein
LD_{50}	Median lethal dose
LH	Polyunsaturated fatty acyl group
LPL	Lipoprotein lipase
$LOO^{\bullet}$	Lipid peroxyl radical
LOOH	lipid hydroperoxide
MBB	Monobromobimane
MDA	Malondialdehyde
mmLDL	Minimally modified LDL
$MnCl_2$	Manganese chloride
MnSOD	Manganese superoxide dismutase
MOPS	4-Morpholine-propanesulfonic acid
MPO	Mycleoperoxidase
MPT	Mitochondrial permeability transition
MTT	3-[4,5- Dimetylthiazol -2 – yl]-2,5-diphenyl-tetrazolium bromide
$NADP^{+}$	Nicotinamide adenine dinucleotide phosphate
NaCl	Sodium chloride
$NaH_2PO_4 .H_20$	Sodium dihydrogen phosphate monohydrate
NaOH	Sodium hydroxide
NADPH	Reduced nicotinamide adenine dinucleotide phosphate
NF-κB	Nuclear factor kappa B
NO	Nitric acid

$NO_2^{\bullet}$	Nitrogen dioxide
NOS	Nitric oxide synthase
NOX	NADPH oxidase
O_2	Molecular oxygen
$O_2^{\bullet -}$	Superoxide anion
$OH^{\bullet}$	Hydroxyl radical
OMM	Outer mitochondrial membrane
$ONOO^-$	Peroxynitrite
OxLDL	Oxidized LDL
PBS	Phosphate buffered saline
phox	Phagocyte oxidase
PKC	Protein kinase C
PI	Propidium iodide
PLA_2	Phospholipase A2
PMA	Phorbol 12-myristate 13-acetate
PPP	Pentose phosphate pathway
PrOOH	Protein peroxide
PS	Phosphatidylserine
PUFA	Polyunsaturated fatty acid
$R^{\bullet}$	Free radical
$RO^{\bullet}$	Alkoxyl radical
$RO_2^{\bullet}$	Peroxyl radical
ROOH	Protein hydroperoxide
ROS	Reactive oxygen species
Rpm	Revolutions/minute
RPMI-1640	Roswell Park Memorial Institute 1640

RyRs	Ryanodine receptors
SDS	Sodium dodecyl sulphate
SDS-PAGE	Sodium dodecyl sulfate polyacrylamide gel electrophoresis
SEM	Standard error of the mean
SH3	Src homology 3
SMC	Smooth muscle cell
SOD	Superoxide dismutase
SR-A	Scavenger receptor type A
TBARS	Thiobarbituric acid reactive substances
TCA	Trichloroacetic acid
TMRM	Tetramethylrhodamine methyl ester
Tris	Tris (hydroxymethyl) aminomethane
vLDL	Very low density lipoprotein
$^{v}/_{v}$	Volume/volume
$^{w}/_{v}$	weight/volume

ABSTRACT

Atherosclerosis is a complex inflammation condition involving the accumulation of lipid-filled macrophages within the artery wall. Progression of the initial fatty streak to an advanced atherosclerotic plaque is characterized by the development of a necrotic core region containing cholesterol and dead cells. The oxidation of low-density lipoprotein (LDL) to oxidized LDL (oxLDL) and its subsequent uptake by macrophages to form foam cells are the key process in plaque formation. OxLDL is found within atherosclerotic plaque, and it is cytotoxic to a range of cells including macrophages through the generation of reactive oxygen species (ROS) and induction of oxidative stress.

The aim of this study was to examine the cytotoxic effects of oxLDL to U937 human monocyte-like cells. OxLDL caused a rapid concentration-dependent cell viability loss in U937 cells within 6 hours. The progression of oxLDL-induced cell death was found to be strongly correlated with the intracellular ROS production and intracellular glutathione (GSH) loss. OxLDL also caused a rapid loss of intracellular aconitase activity, indicating the impairment of the cellular metabolic function. The cytosolic calcium ion (Ca^{2+}) level was also elevated by oxLDL, which could be from both intra- and extra-cellular sources.

OxLDL also activated plasma membrane superoxide generation complex NADPH oxidase (NOX), and the progression of oxLDL-induced NOX activation was correlated with oxLDL-mediated ROS production, suggesting NOX is the major source of ROS. Further investigations using NOX inhibitors apocynin or diphenyleneiodonium (DPI) found that inhibition of NOX prevented oxLDL-induced cell viability loss, ROS production, GSH loss and aconitase activity decrease. The cytosolic Ca^{2+} elevation caused by oxLDL was also suppressed slightly by inhibiting NOX activity. These results clearly show that NOX is the major site of oxidative stress upon oxLDL activation, contributing to the oxLDL-induced cell death.

This study also examined the protective effect of 7,8-dihydroneopterin (7,8-NP) on oxLDL-induced oxidative stress. 7,8-NP dramatically protected cells from oxLDL-induced cell viability loss, ROS generation and aconitase activity loss. 7,8-NP also inhibited oxLDL-induced cytosolic Ca^{2+} influx particularly after 3 hours. 7,8-NP did not inhibited mitochondrial aconitase activity decrease caused by oxLDL, nor inhibited mitochondrial ROS production. This indicates the protective effect of 7,8-NP against oxLDL damage could primarily in cytoplasm. The failure of 7,8-NP protection from oxLDL activating NOX suggests that the protection of 7,8-NP against oxLDL-induced oxidative stress was not due to the inhibition of NOX activation, but by radical scavenging activity of the NOX products.

1. INTRODUCTION

1.1 Overview

Atherosclerosis is a complex disease characterized by low density lipoprotein (LDL) deposition in the arterial wall. This LDL deposition occurs primarily within macrophages and ultimately begets the formation of well-defined necrotic lesions in the arterial intima. Such lesions then develop and become prone to rupture, and as a consequence, can cause the clinical events such as heart attack and stroke. According to the oxidative modification hypothesis, LDL oxidation is the key event in the early stage of atherosclerosis and oxidized LDL (oxLDL) can be taken up by macrophage cells in an unregulated manner, triggering their transformation into lipid-laden foam cells (Libby *et al.*, 2002).

OxLDL is cytotoxic to a range of cells, and it is responsible for the increased oxidative stress with the overproduction of reactive oxygen species (ROS). ROS can mediate various signalling pathways that underlie vascular inflammation in atherogenesis from the oxidative modification of LDL and initiation of fatty streak development through lesion progression to ultimate plaque rupture (Singh and Jialal, 2006). Therefore, ROS appear to play a causal role in atherosclerosis. Increasing studies support that NADPH oxidase (NOX) is the major source of ROS production and the resultant oxidative stress at the inflammatory sites.

OxLDL-mediated oxidative stress can be reduced by the presence of 7,8-dihydroneopterin (7,8-NP), which is synthesized by macrophages upon interferon-γ (INF-γ) induction during inflammation. 7,8-NP has been found to be an effective antioxidant by scavenging radicals, and thereby protect cells against oxLDL-induced oxidative damage and cell death (Baird, 2003).

This research will investigate the oxLDL-induced oxidative stress by examining the cytotoxic effects of oxLDL in human monocyte-like U937 cells, the contribution of NOX

to the oxLDL-mediated oxidative stress, and examine the protective effect of 7,8-NP against oxLDL-induced oxidative damage.

1.2 Atherosclerosis

Atherosclerosis is a chronic inflammation resulted from the accumulation of lipid-filled macrophages, fibrous protein, lipid deposits and dead cells in the arterial wall (Libby, 2002). This inflammatory process can ultimately lead to the development of complex lesions, or plaques, which protrude into the arterial lumen (Glass and Witztum, 2001). Atherosclerosis and its complications, including cardiovascular disease, heart infarction and stroke are the most common cause of death in Western countries (Murray and Lopez, 1997, Halliwell and Gutteridge, 2007a). Epidemic studies have identified a number of genetic and environmental risk factors associated with atherosclerosis, including age and gender, obesity, smoking, hypertension, diabetes and serum cholesterol levels (Scott, 2004).

Atherosclerosis is also a progressive disease, beginning as fatty streaks within the arterial intima. The lesion formation could be initiated by endothelium dysfunctions particularly at the arterial branch points (Lusis, 2000). In the vicinity of branch points and areas of major curvature, disrupted blood flow is likely to affect endothelial cell (EC) morphology and cause mechanical damage to the endothelium (Jang et al., 1993). The ‘response-to-injury hypothesis’ suggests that the chronic injury to ECs allows the attraction, adherence and transmigration of monocytes through the endothelium (Ross, 1993). LDL enters the arterial intima soon after monocytes recruitment and undergoes modifications, such as oxidation, proteolysis and aggregation, which may be partially caused by exposure to oxidants released by the vascular wall (Lusis, 2000). OxLDL is then taken up by monocytes-differentiated macrophages in an unregulated manner, resulting in the formation of lipid-laden fatty streak, called ‘foam cells’.

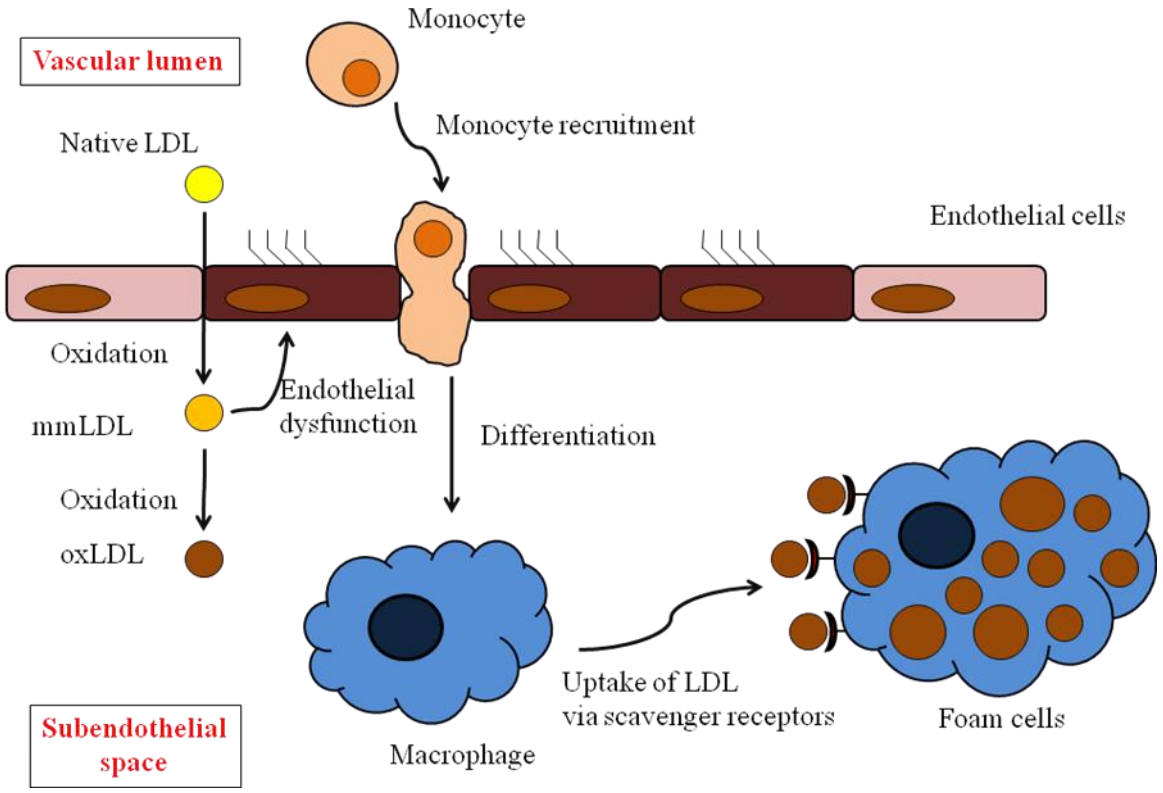

Figure 1.1 Initiating events in the early stage of fatty streak formation
LDL is entrapped in the subendothelial space, where it is oxidatively modified to mmLDL. MmLDL aids the recruitment of circulating monocytes into the intimal space, where monocytes become differentiated into macrophages. In the intima, mmLDL undergoes further oxidation to heavily oxidized LDL (oxLDL). Oxidized modified LDL (both mmLDL and oxLDL) also results in endothelial dysfunction and injury, allowing monocytes to attach to endothelial cells and migrate into the intima through the tight junctions. oxLDL is taken up by macrophages rapidly via scavenger receptors SR-A and CD36 to form lipid-filled foam cells, also called 'fatty streak'. (adapted from Diaz *et al*, 2007).

Controversy surrounds the exact initial events during the early stage of lesion formation. 'Oxidative modification hypothesis', which is the more widely accepted theory, suggests that the LDL may enter first and initially become modified prior to the appearance of monocytes (Figure 1.1) (Rosenfeld, 1996, Napoli et al., 1997). The increased permeability of LDL at the arterial branch points allows the entry and accumulation of LDL in the subendothelial space (Lusis, 2000). Trapped LDL is oxidatively modified to 'minimally oxidized' LDL (mmLDL) by reactive oxygen species (ROS) generated in ECs and smooth muscle cells (SMCs), and several enzymes (Steinberg et al., 1989, Glass and Witztum, 2001). ECs are stimulated by the resulting mmLDL to produce a number of pro-inflammatory molecules, including adhesion molecules, chemotactic proteins and growth

factors, which facilitate the recruitment of circulating monocytes and T cells to the vessel wall as well as the differentiation of monocytes to macrophages. MmLDL can be further oxidized to heavily oxidized LDL, which is no longer recognized by normal LDL receptor. OxLDL and other forms of modified LDL are taken up by macrophages via scavenger receptors, such as scavenger receptor type A (SR-A) and CD36 unregulately and rapidly (Glass and Witztum, 2001, Steinberg et al., 1989). Fast internalization of oxLDL by macrophages leads to the loading of macrophages with cholesterol and cholesteryl esters, resulting in the formation of foam cells which is a hallmark of the early stage atherosclerotic lesion. The cluster of foam cells lead to the development of fatty streak.

Smooth muscle cells (SMCs) are the key participants in the next stage of more complex fibrous plaque formation. In response to cytokines, growth factors and reactive species released from activated macrophages and T cells, SMCs migrate from the medial layer of the artery wall into the intima, where they may take up oxLDL and develop a foam-like appearance (Lusis, 2000, Berliner and Heinecke, 1996). SMCs also synthesis extracellular matrix proteins which are composed of type I collagen, elastin, fibrin, proteoglycans and other forms of collagen (Jang et al., 1993). These extracellular matrix materials lead to the development of the fibrous cap over the plaque (Stary et al., 1995). This fibrous cap covers the lipid core contents that are rich in macrophages, T cells and SMCs, and separates them from the blood in the lumen. SMCs migration, proliferation and extracellular matrix synthesis continuously occur to thicken the fibrous cap and ultimately cause occlusion of the artery lumen (Libby et al., 2002).

Plaque rupture can happen in advanced plaques with large necrotic cores and thin fibrous caps (Lusis, 2000). Cell death of macrophages and SMCs is suggested to disrupt the plaque stability and lead to the development of an acellular necrotic core (Ball et al., 1995). A large number of experimental results suggest that oxLDL is cytotoxic to a range of cells including SMCs, monocytes and macrophages (Harada-Shiba et al., 1998, Baird et al., 2004a, Bjorkerud and Bjorkerud, 1996, Reid et al., 1993), and it is present in the atherosclerotic plaques (Brown and Goldstein, 1984, Ylaherttuala et al., 1989). Therefore, it seems that oxLDL acts as the key driving force of cell death and necrotic core formation. Furthermore, cytokines released by macrophage and T cells amplify a local inflammatory response and induce matrix metalloproteinase to degrade extracellular matrix material,

thereby thinning the fibrous cap and making it more susceptible to rupture (Anderson et al., 2002, Galis et al., 1995). Thus, plaque rupture is often localized to the shoulder regions and fibrous cap of the plaque where apoptotic macrophages and SMCs are abundant (Bjorkerud and Bjorkerud, 1996). Additionally, calcification and neovascularisation can happen to make more complicated and less stable plaques, which are more vulnerable to rapture (Lusis, 2000, Scott, 2004). When plaque ruptures, tissue factors in the necrotic core are exposed to blood, initiating coagulation, the recruitment of platelets and the formation of a thrombus (Figure 1.2) (Glass and Witztum, 2001).

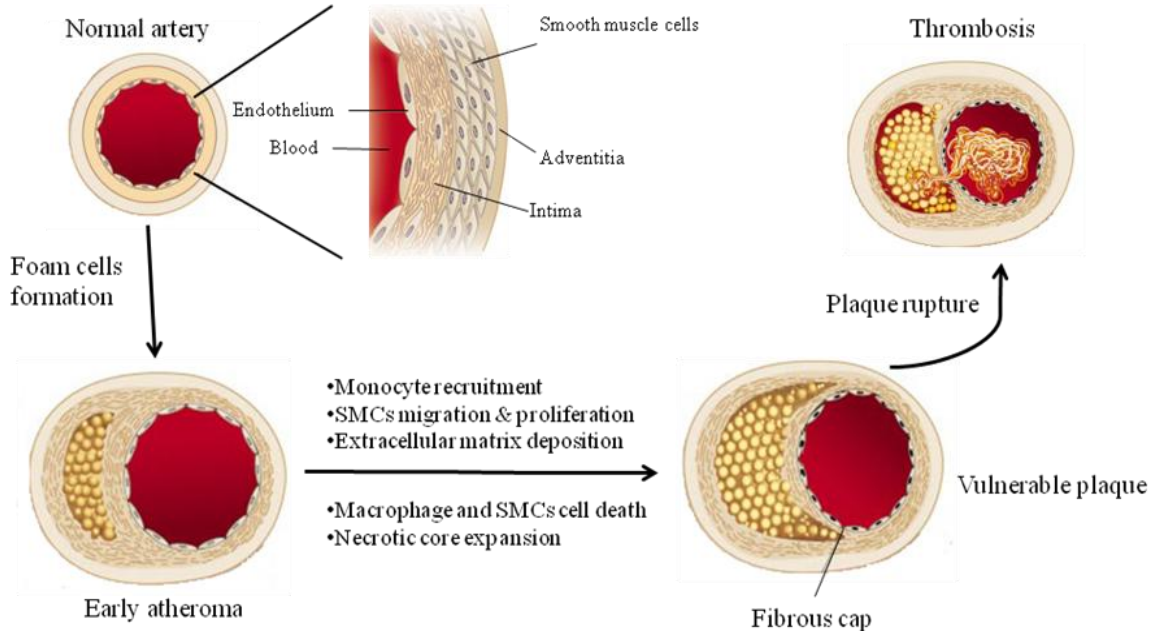

Figure 1.2 Development of atherosclerotic lesion
A normal artery has a typical trilaminar structure. The endothelial cells in contact with the blood in the arterial lumen rest upon a basement membrane. Intima usually contains a smattering of SMCs within the extracellular matrix and elastin. Multiple layers of tightly packed SMCs sit between the outermost layer adventitia and intima, embedded in a matrix rich in elastin and collagen. In the early stages of atherosclerotic lesions, recruitment of monocytes and accumulation of LDL (see Figure 1.1) leads to formation of lipid-laden fatty streaks. The lipid core can grow to more a complex lesion with increased foam cell formation, SMC migration and proliferation, and extracellular matrix degradation. Macrophage and SMCs necrosis contribute to the formation of the necrotic core in the advanced plaque, which eventually constricts the blood flow in the lumen. Plaque containing thin fibrous caps and large lipid pools are susceptible to rupture. Plaque rupture exposes tissue factors in the lipid core to the blood components, resulting in coagulation cascade, platelet adherence, thrombosis and ultimately an acute ischaemic event. (adapted from *Libby, 2002*)

It is widely accepted that LDL oxidation process is a key step in the development of atherosclerosis no matter what the exact initial event is, and oxLDL appears to participate in every stage of lesion formation (Jessup et al., 2004). OxLDL is believed to be

atherogenic and facilitate monocytes adhesion to endothelium and entry into the subendothelial space. OxLDL may cause oxidative stress extracellularly in the plaque by stimulating radical production, leading to endothelial dysfunction and injury. The cytotoxicity of oxLDL also promotes macrophages and SMCs cell death, contributing to necrotic lesion and plaque rupture.

1.3 ROS and oxidative stress in atherosclerosis

ROS appear to play a causative role in the development of atherosclerosis. Collectively ROS are a family of molecules including not only oxygen radicals with unpaired electron(s) such as superoxide ($O_2^{\bullet -}$), peroxyl ($LOO^{\bullet}$) and hydroxyl radical ($OH^{\bullet}$), but also some non-radical derivatives such as hydrogen peroxide (H_2O_2), hypochlorous acid (HOCl) and peroxynitrite ($ONOO^-$) (Stadtman and Berlett, 1998). When the generation of ROS is overwhelming and outstripping endogenous antioxidant defense system, oxidative stress is generated. An increasing body of evidence suggest that oxidative stress contributes to atherosclerosis by inducing endothelial dysfunction, mediating redox signaling that can alter protein and enzyme activities, and causing oxidative damage to cellular lipids, proteins and DNA (Gackowski et al., 2001, Han et al., 1998, Haramaki and Packer, 1994, Ito et al., 1996, Kagan et al., 2002). The importance of oxidative stress in atherosclerosis is further supported by the observed impairment of vascular function and enhanced atherogenesis in animal models that have deficiencies in antioxidant enzymes (Madamanchi et al., 2005).

ROS can contribute to atherosclerosis lesion formation in many ways, starting from the initiation of fatty streak development though lesion progression to the ultimate plaque rupture. ROS can participate in the oxidative modifications of lipid and protein (apolipoprotein B-100) components of LDL, hence transforming LDL to a high uptake form that can be internalized by macrophages and leading to foam cell formation (Cathcart et al., 1989). ROS, in particular H_2O_2, can act as intracellular messengers in pro-inflammatory signaling, leading to activation of the redox sensitive transcription factor nuclear factor kappa B (NF-κB) and expression of adhesion molecules and chemokines in the vascular endothelium, all of which have long been implicated in atherosclerosis (Halliwell and Gutteridge, 1999, Stocker and Keaney, 2004). Superoxide radical can rapidly decrease endothelial nitric oxide (NO) bioavailability. NO is an important

endogenous vasodilator, thereby reducing NO bioavailability resulting in endothelial dysfunction via impairing endothelium-dependent vasorelaxation (Cai and Harrison, 2000). Loss of NO can also lead to vascular SMCs proliferation and migration, as well as promoting leukocyte and platelet adhesion (Nushjira, 2009). Moreover, ROS can trigger cell death, contributing to the necrotic core formation. The presence of oxidation products of lipids and proteins in atherosclerotic plaques further support the roles of ROS play in the lesion development (Stocker and Keaney, 2004, Leeuwenburgh et al., 1997).

There are several potential sources of deleterious ROS in most cells, including mitochondria, xanthine oxidase, NADPH oxidase (NOX) and uncoupled NO synthase (Nushjira, 2009). Among these, NOX is believed to be the predominant $O_2^{\bullet-}$-generating enzyme, and it is especially important for redox signaling (Dworakowski et al., 2006).

1.4 Oxidant damage

Growing evidence have suggested a causal role of oxidative stress in the development of atherosclerosis. It appears that oxLDL can induce oxidative stress by down-regulating antioxidant enzymes and increasing ROS production, causing oxidative damage to cellular components. Cellular proteins seems to be the primary target of free radicals since they make up the majority of the cells' components. The oxidative damage on proteins can inactivate key metabolic enzymes, disrupt ligand bindings, and cause loss of plasma membrane ion channel functions, which in turn leads to metabolic function failure and resultant cell death. Previous studies have shown an activity loss of glyceraldehydes-3-phosphage dehydrogenase (GAPDH) caused by ROS (Morgan et al., 2002a, Morgan et al., 2002b, Souza and Radi, 1998). GAPDH is an essential enzyme in glycolysis whose function is critical to metabolism. GAPDH inactivation can result in an reduction in the efficiency of the tricarboxylic acid (TCA) cycle and decreased ATP production, leading to metabolism dysfunction and cell death (Sukhanov et al., 2006). The oxidative damage to GAPDH can be prevented by the presence of glutathione (GSH) (Arosio et al., 1997). Therefore, GSH has been studied as an antioxidant. Intracellular GSH content has been found to decrease rapidly upon exposure to oxLDL in U937 cells and macrophages (Baird et al., 2004b, Gieseg et al., 2009b). Another important enzyme in TCA cycle is aconitase,

which is also known to be easily inactivated by oxidants (Bulteau et al., 2003). The following section will describe GSH and aconitase in detail.

1.4.1 GSH

GSH is a key component of intracellular antioxidant defence system and exists primarily in the thiol-reduced form (Meister, 1988). GSH synthesis occurs in the cytoplasm from its precursor amino acids (glutamate, cysteine and glycine) via a series of reactions catalyzed by ATP-dependent γ-glutamylcysteine synthetase and GSH synthetase (Forman et al., 2009). GSH is delivered to intracellular compartments including mitochondria, endoplasmic reticulum (ER), nucleus and the extracellular space after synthesis to act as an antioxidant.

GSH plays a crucial role in a multitude of cellular processes such as cell differentiation, proliferation and apoptosis. The disturbances in GSH homeostasis are implicated in the progression of many human diseases including atherosclerosis (Ballatori et al., 2009). The primary function of GSH lies in reducing oxidative stress and maintaining the thiol-redox status of the cell (Forman et al., 2009). GSH loss appears to be a potential indicator of oxidative stress within cells. GSH can scavenge ROS by rapidly reacting with a wide range of oxidants including $OH^{\bullet}$, HOCl, ONOO-, $RO^{\bullet}$, $RO_2^{\bullet}$, $CO_3^{\bullet}$-, and $O_2^{\bullet}$-, resulting in the generation of glutathione disulfides (GSSG) (Halliwell and Gutteridge, 2007). GSH can be regenerated from GSSG at the expense of NADPH by the enzyme GSH reductase, implying that cells can withstand a certain level of oxidative stress. Depletion of intracellular GSH through complete oxidation of GSH or inhibition of GSH regeneration through oxidative damage to metabolic enzymes can result in further oxidative damage to cellular contents and ultimate cell death (Kappler et al., 2007). This study showed that protein peroxide (PrOOH) formation and cell death in THP-1 cells treated with peroxyl radicals occurred only after loss of GSH. Previous studies from this laboratory have also shown one of the earliest cellular events in U937 cells and humane monocytes-derived macrophages (HMDMs) with the treatment of oxLDL or HOCl is the rapid decrease in intracellular GSH content, followed by cell death (Yang, 2009, Baird et al., 2004b, Rutherford, 2010). Protection of GSH store with the macrophage generated antioxidant

7,8-dihydroneoptein seems to prevent cellular death in U937 cells to peroxyl radicals or oxLDL (Baird et al., 2005b, Duggan et al., 2002).

1.4.2 Aconitase

Aconitase is an iron-sulfur enzyme containing a [4Fe-4S] cluster that catalyses the stereo-specific isomerisation of citrate to isocitrate in the TCA cycle (Beinert et al., 1996). Aconitase exists in both cytosol and mitochondria. The cytosolic aconitase is a bi-functional protein, not only converting citrate to isocitrate, also binding to RNA as a transcription regulatory factor (Beinert and Kennedy, 1993). The distribution ratio between mitochondrial and cytosolic aconitase varies with animal species or cell types (Konstantinova and Russanov, 1996).

Aconitase has been shown to be very prone to oxidative damage, since the [4Fe-4S]cluster is highly sensitive to oxidation especially by $O_2^{\bullet}$- radicals (Yan et al., 1997, Gardner and Fridovich, 1992). $O_2^{\bullet}$- can readily inactivate aconitase by distracting a labile iron from the [4Fe-4S] cluster, giving an inactive [3Fe-4S]cluster (Gardner et al., 1995). This aconitase inactivation can be prevented by mitochondrial manganese superoxide dismutase (MnSOD) (Gardner et al., 1995). Several studies have shown that aconitase is the only target undergoing a significant oxidative modification during aging or hyperoxia treatment (Gardner et al., 1994, Morton et al., 1998, Yan et al., 1997, Yarian and Sohal, 2005). Decreased aconitase activity plays a causal role in the subsequent cell death by initiating the cascade with the potential to cause a dramatic increase in the cellular burden to oxidative damage. Oxidative inactivation of aconitase can contribute to a decline in the overall efficiency of mitochondrial bio-energetics by blocking electron flow to oxygen, which results in an accumulation of reduced metabolites, such as NADH, leading to ‘reductive stress’ (Yan et al., 1997). The increased reductive stress causes an increased production of ROS through autoxidation of the reduced metabolites, thus further increasing oxidative damages to macromolecules. The free iron released from the [4Fe-4S] cluster upon oxidants’ attack could also contributes to further ROS production via Fenton reaction (Yarian and Sohal, 2005). The oxidative inactivation of aconitase causes increased ROS production, resulting in further oxidative damage to cellular contents, and also renders the

energy deficiency or ATP deficiency contributing to the subsequent metabolic function failure. Both events will eventually lead to cell death.

1.5 Cell death

Cell death is the key event in the progression of atherosclerosis. OxLDL is cytotoxic to a variety of cell types including macrophages, monocytes, ECs and SMCs, causing both necrotic or apoptotic cell death (Gieseg et al., 2009a, Baird et al., 2005a). How exactly oxLDL causes cell death *in vitro* is unclear. It has been previously suggested that the oxysterols, in particular, 7-ketocholesterol (7-KC), is the main cytotoxic agent within oxLDL, contributing to cell death (Colles et al., 2001, Monier et al., 2003). Yet the recent study from this laboratory has clearly shown that 7-KC is not the cytotoxic component of oxLDL (Rutherford, 2010). It is more likely the elevated oxidative stress induced by oxLDL is responsible for the cell death. There are two common cell death mechanism: necrosis and apoptosis.

Necrosis is characterized by swelling and rupture of internal organelles, loss of ion homeostasis, which prevents further ATP production, followed by plasma membrane lysis and release of denatured proteins, DNA fragments, lysosomal contents and other cell debris into the extracellular space (Lelli et al., 1998). Inflammation is another hallmark of necrosis, where cells of the immune system ingest the necrotic cells to clear away debris and limit the infection. The activities and secretions of immune cells, however, can also damage normal tissues in the vicinity because of the environmental pH's changes (Duke et al., 1996). Calcium-dependent activation of calpain or cathepins can cause severe damage to cytoskeletal proteins, resulting in the irreversible membrane blebbing and eventually necrosis (Weber et al., 2005, Yang et al., 2012).

In contrast, apoptosis, is an active and highly regulated process resulting in the controlled shut down of cells without rupture of organelle membranes. The cell can break into small membrane-surrounded fragments, called apoptotic bodies (Haunstetter and Izumo, 1998). The feature of apoptosis include morphological changes, such as chromatin condensation

and margination, DNA fragmentation and apoptotic body formation (Yuan et al., 2000). The apoptotic bodies can be cleared by phagocytosis without triggering an inflammatory response. Typical biochemical changes comprise cytochrome c release from mitochondria, activation of cysteine-dependent caspase, and the redistribution of phosphatidylserine (PS) to the outer surface of plasma membrane which enables the recognition of apoptotic bodies by phagocytes (Tabas, 2005). If the apoptotic bodies are not phagocytosed, the secondary necrosis can occur, in which the membrane of apoptotic bodies lyse and the contents of bodies are released (Skepper et al., 1999, Tabas, 2005).

Apoptosis can occur in caspase-dependent or –independent pathways. Early studies usually considered the presence of caspase activation as the definitive evidence of apoptosis, since their cleavage of structural and regulatory proteins are responsible for the irreversible dismantling of cells. Caspase activation has been found along with the apoptotic cell death in oxLDL-treated THP-1 cells and HOCl-oxidized LDL-treated U937 cells (Vicca et al., 2000, Vicca et al., 2003). However, later investigations revealed that cells can undergo apoptosis in the absence of caspase inactivation. Studies of the cytotoxicity of oxLDL in THP-1 and U937 cells showed that PS exposure occurred in both cell types, but caspase activation was only detected in THP-1 cells. Absence of caspase activation was observed in U937 cells, associated with an intense ROS production and a dramatic decrease in intracellular thiols upon treatment with oxLDL (Baird et al., 2004b). The oxidation of free thiols within the active site of various caspase renders them inactive (Hampton et al., 2002), generating a caspase-independent apoptotic cell death. The difference in response between U937 and THP-1 cells to oxLDL may be related to varying mechanism of uptake of oxLDL (Baird et al., 2004b). It has been previously found that U937 cells express 4-fold higher levels of CD36 scavenger receptor than doTHP-1 cells (Nguyen-Khoa et al., 1999), which may result in an initial burst of oxLDL uptake and more intensive oxidative stress in U937 cells. It is suspected that the exact pathway of apoptosis initiated by oxLDL may vary in the atherosclerotic lesion depending on the cell type and the local environment (Baird et al., 2004b).

1.6 NADPH oxidase (NOX)

The NADPH oxidase complex (NOX) is a plasma membrane associated enzyme complex found in a variety of cells, including neutrophils and endothelial cells (Nushjira, 2009, Griendling et al., 2000). The significance of NOX was originally addressed as a key enzymatic system in host defence against microbial pathogen. Deficiency in phagocyte NOX impairs superoxide generation, resulting in chronic granulomatous disease (GCD) which is characterized by recurrent bacterial and fungal infections (Kirk et al., 2000, Babior, 1999). NOX is the predominate enzyme complex generating $O_2^{\bullet}$- via the one-electron reduction of molecular oxygen, using NADPH as the electron donor:

$$2\ O_2 + NADPH \longrightarrow 2\ O_2^{\bullet}- + NADP^+ + H^+$$

1.6.1 NOX structure, location and homology

Despite of the existence in various cell types, it appears that the structure of NOX is somehow different between phagocytic and non-phagocytic cells (Griendling et al., 2000). In the past 40 years, majority of the efforts have been focused on exploring NOX in phagocytes such as neutrophils due to their significant role in innate immune systems, and therefore the best-characterized NOX is that found in phagocytes (**Figure 1.5**) (Nushjira, 2009).

Phagocytic NOX system comprises two membrane-bound components, a large subunit gp91^{phox} (phox for *ph*agocyte *ox*idase) and a small subunit p22^{phox}, and several cytoplasmic subunits. Gp91^{phox} and p22^{phox} occur as a heterodimeric flavocytochrome b 558 (cyto b558), existing in a dormant state in the absence of the other cytosolic components. The gp91^{phox}, also known as NOX2, contains two heme groups and binds the redox cofactor flavin adenine dinucleotide (FAD), serving as the catalytic core of the enzyme (Rotrosen et al., 1992, Sumimoto et al., 1996). The p22^{phox} protein has a src homology 3 (SH3)-binding domain, which serves as the site of linkage with the cytosolic components (Parkos et al., 1988). Besides, there are three multi-domain cytosolic subunits p47^{phox}, p67^{phox} and p40^{phox}, all of which contain one or two SH3 domains. SH3 domain specifically binds to proline-

rich peptides, and it is the key driving force for the protein-protein interactions in NOX activation process (Koch et al., 1991, Rodaway et al., 1990, Leto et al., 1994, De Mendez et al., 1996). Compared to the catalytic role of membrane-associated cyto b558 in NOX activity, these cytoplasmic subunits appear to be the major regulatory factors during NOX activation by tightly controlling protein-protein interactions occurred among multiple domains. NOX also contains a small G protein Rac in the cytoplasm, serving as a regulatory protein by switching between GDP-bound (inactive) and GTP-linked (active) forms (Nushjira, 2009, Kirk et al., 2000, Babior, 1999). To date various studies have provided the evidence for the presence of $p22^{phox}$, $p47^{phox}$, $p67^{phox}$ and Rac in non-phagocytes, including endothelial cells, VSMC and fibroblasts (Griendling et al., 2000).

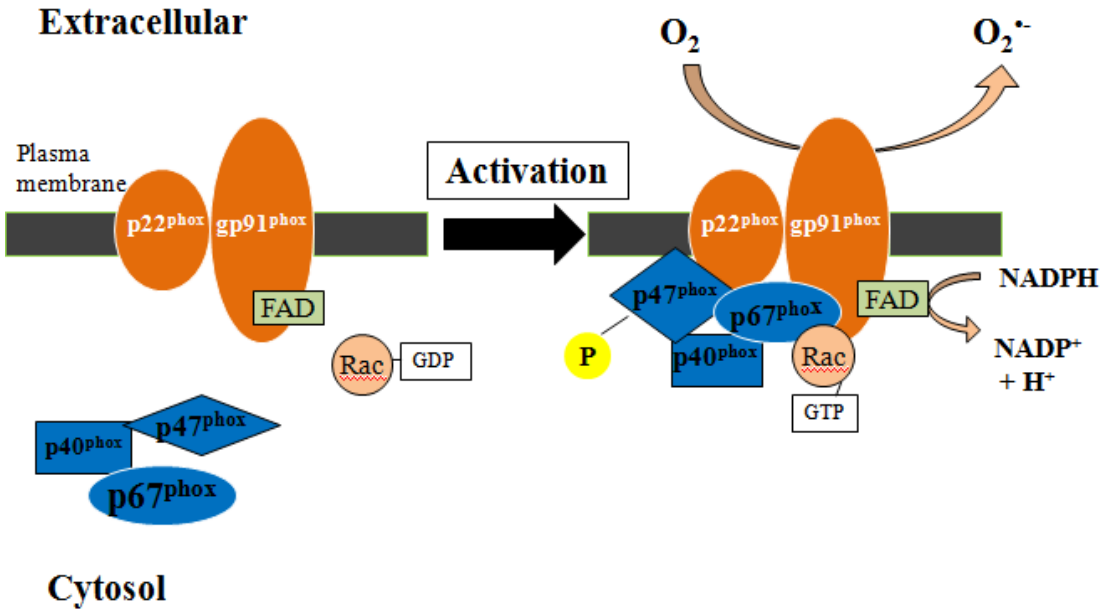

Figure1.3 Schematic representation of NADPH oxidase assembly in a phagocyte (neutrophil or macrophage).

In the resting cells, three NOX components-$p40^{phox}$, $p47^{phox}$ and $p67^{phox}$-exist in the cytosol, whereas the other two components-$p22^{phox}$ and $gp91^{phox}$-are located in the plasma membrane. The small G protein, Rac, stays in the inactive form with the association of GDP. Upon activation, there is an exchange of GDP with GTP on Rac, leading to its activation. Extensive phosphorylation of the cytosolic $p47^{phox}$ subunit leads to the conformational changes allowing the interaction with $p22^{phox}$. The movement of $p47^{phox}$ brings with it the other cytosolic subunits, $p67^{phox}$ and $p40^{phox}$, resulting in the migration of the three cytosolic subunits to the plasma membrane, where they assemble with the $p22^{phox}$ and $gp91^{phox}$ to form the active enzyme. The fully assembled NOX transport electrons from cytoplasmic NADPH to oxygen to generate superoxide.

Membrane-associated and cytosolic subunits are distributed distinctly between subcellular compartments ensuring that NOX is inactive in resting cells. Yet in response to stimulation, the cytosolic components migrate almost instantly to the inner surface of the plasma membrane where they assemble with the cyto b558 to form the active enzyme. This process is tightly regulated by protein-protein interaction and by phosphorylation. The detailed mechanism of this activation process will be discussed further in detail later.

NOX was originally found to be associated with the plasma membrane in neutrophils (Wientjes et al., 1997), but later studies indicated that NOX also locates in the membrane of some phagocytic granules, such as phagosome (Kobayashi et al., 1998). Kobayashi *et al.* used cytochemical staining to show that superoxide production in activated neutrophils initially took place in small alkaline phosphatase-containing cytoplasmic vesicles. These vesicles fused together to form larger vesicles which then merged with the plasma membrane. These results strongly imply that membrane-associated NOX components are located exclusively in intracellular organelles (Kobayashi et al., 1998).

To date a family of NOX homologues has been discovered. These homologues are designated as NOX 1, NOX 2, NOX 3, NOX 4, NOX 5, DUOX 1 and DUOX 2. NOX 1 is primarily expressed in many epithelial cells of the digestive tract (Szanto et al., 2005). NOX 2 generally represents pg91^{phox} in phagocytic NOX, though it is also widely expressed in endothelial cells, cardiomyocytes and fibroblasts in addition to its classical expression in neutrophils (Cassatella et al., 1985, Meier et al., 1993, Bayraktutan et al., 1998, Jones et al., 1996, Jones, 1994, Bayraktutan et al., 2000). NOX 3 is found in the foetal tissues and adult inner ear, and it is required for otoconia formation (Paffenholz et al., 2004). NOX 4, formerly known as Renox, was firstly found in kidney but is indeed widely expressed in many tissues including placenta, endothelial cells, vascular smooth muscular cells, cardiomyocytes, fibroblasts, ovary, testis and skeletal muscle (Geiszt et al., 2000). NOX 1-4 share up to 60% homology and are characterized by their calcium-independency (Brandes and Kreuzer, 2005). In contrast, the activity of NOX 5 is mostly expressed in spermatozoa and lymphocytes and increased by calcium (Banfi et al., 2001). DUOX 1 and DUOX 2 are very similar to NOX 5, but they carry an additional peroxidase domain,

exhibiting high expression in the thyroid gland and the intestine (Geiszt et al., 2003, Denke et al., 2002).

1.6.2 NOX activation

In resting cells, $p47^{phox}$, $p67^{phox}$ and $p40^{phox}$ form a ternary complex in the cytoplasm, whereas Rac is found to associate with Rho-GDP dissociation inhibitor. In response to various stimuli, NOX is activated by assembling three cytosolic factors, $p47^{phox}$, $p67^{phox}$, $p40^{phox}$ and Rac, into a functional complex with the membrane components cyto b558 (Rotrosen et al., 1992, Leto et al., 1994).

$P47^{phox}$ is the key organizer of the NOX active enzyme, and it is responsible for transporting the cytosolic complex to the membrane. Over a dozen sites on $p47^{phox}$ have been shown to undergo phosphorylation when cells are activated (Huang and Kleinberg, 1999). Cell activation by a variety of stimuli drives the protein kinase C (PKC)-mediated phosphorylations of $p47^{phox}$ on several serine residues located in the polybasic region of the C-terminus and causes a conformational change in $p47^{phox}$, leading to the immediate and irreversible interaction with $p22^{phox}$ subunit on the membrane through an SH3 domain (Huang and Kleinberg, 1999). This event triggers further phosphorylations of $p47^{phox}$ and increasingly tight association of $p47^{phox}$ with cyto b558 on the membrane (Rotrosen and Leto, 1990).

The $p67^{phox}$ subunit also undergoes phosphorylation on residue Thr^{233} upon stimulation, although to a lesser degree than $p47^{phox}$, allowing its binding to $p47^{phox}$ and $p40^{phox}$ through direct protein-protein interactions (Finan et al., 1994, Leto et al., 1994). This process leads to the migration of the assembled cytosolic components to the plasma membrane, where they form a functional complex with cyto b558, followed by the electron transfer from NADPH to FAD and then donated to the heme of cyto b558 and finally to oxygen, whose reduction leads to the formation of superoxide (Nisimoto et al., 1999). The assembly of the three cytosolic factors with cyto b558 leads to a conformational change in cyto b558,

which may enhance NADPH binding and/or facilitate electron transfer between NADPH and FAD and/or from FAD to heme (Cross and Curnutte, 1995).

The NOX activation also requires the translocation of Rac, which occurs simultaneously, but dissociably, from the translocation of the $p47^{phox}$/$p67^{phox}$ complex (Sumimoto et al., 1994). Being a G protein, Rac switches between GDP-bound (inactive) and GTP-linked (active) forms. The replacement of GDP with GTP upon NOX activation re-orients key residues in Rac protein. The third phosphate of GTP attracts Tyr^{32} on a peripheral loop, twisting the adjacent residues into position. This moves the adjacent Glu^{31} and Ile^{3} so that they may associate with neighbouring proteins. Asp^{38} appears to move away (Abo et al., 1991, Abo et al., 1994). The association of Rac-GTP with $p67^{phox}$ at the membrane aids the electron flow from NADPH to FAD and then to oxygen to produce superoxide (Rinckel, 1999). Protons dissociated from NADPH are moved through the membrane via protein channels and are available to interact with superoxide to produce H_2O_2.

The assembly and activation of NOX appears to be regulated by cytosolic Ca^{2+}. When cells are activated by a variety of stimulus, cytosolic Ca^{2+} level is elevated due to the extracellular Ca^{2+} influx and the release of intracellular Ca^{2+}, causing Ca^{2+}-dependent activation of PKC (Cathcart, 2004). PKCδ activation triggers the $p47^{phox}$ phosphorylation, and PKCα activation is responsible for the subsequent activation of phospholipases A_2 (PLA_2). PLA_2 can cleave membrane phospholipids, causing disruption of membrane organization and facilitating Ca^{2+} influx and Ca^{2+} release from internal stores (Nicotera and Orrenius, 1998). Activation of PLA_2 also results in the release of arachidonic acid (AA) and related polyunsaturated fatty acids (PUFA), which can be further oxidized by lipoxygenases or cyclooxygenases with concomitant generation of ROS. AA production promotes the translocation of $p47^{phox}$ and $p67^{phox}$ to the plasma membrane (Cathcart, 2004).

1.6.3 NOX and cell death in atherosclerosis

NOX, as the main ROS producer within the macrophage cells, is a double edge sword whose physiopathological role may be greatly different, depending on the extent and duration of its activation. In the past ten years, the importance of NOX in inflammatory diseases such as atherosclerosis has been increasingly described (Singh and Jialal, 2006, Nushjira, 2009, Harrison et al., 2003, Aviram and Rosenblat, 2003). In hypercholesterolemic rabbits prone to atherosclerosis, increased NOX-mediated superoxide production by angiotensin II was associated with endothelia dysfunction (Warnholtz et al., 1999). NOX has also been assessed for its contribution to the development of atherosclerosis with apolipoprotein E (apoE)-deficient (apoE-/-) mice (Barry-Lane et al., 2001, Kirk et al., 2000, Hsich et al., 2000). ApoE -/- mice develop marked hyperlipidemia and progressive atherosclerotic lesions, so they have been used extensively as an accepted model of atherosclerosis (Palinski et al., 1994). In these studies, apoE -/- mice with gene knockouts of either of two central components of NOX ($gp91^{phox}$ or $p47^{phox}$) had less lesion area than apoE -/- mice, suggesting NOX is involved in the formation of the atherosclerotic plaque.

A variety of *in vitro* studies further emphasize the importance of NOX in atherosclerosis. NOX and superoxide production is increased in vascular cells by a variety of agonists relevant to the atherosclerosis, including angiotensin II (Qin et al., 2006), thrombin (Patterson et al., 1999), platelet-derived growth factor (Movitz et al., 1997), and tumor necrosis factor (Li et al., 2002). Atherosclerotic levels of LDL stimulate NOX-generated superoxide, which in turn contributes to LDL oxidation. OxLDL may act as an especially potent stimulus for NOX activation, both in the vasculature and in macrophages, thereby accentuating the progression of atherosclerosis (Nushjira, 2009). The excessive production of NOX-derived ROS, in addition to serve as intracellular signaling molecules, contributes to the pathogenesis of atherosclerosis in numerous ways as outlined above (see **section 1.3**). An excessive level of ROS in SMCs caused the loss of GAPDH, leading to necrosis as the cells are unable to generate sufficient ATP (Morgan et al., 2002b). This can be prevented by NOX inhibitors (Sukhanov et al., 2006). Anti-CD36 antibodies also blocked ROS production and GAPDH loss, suggesting activation of NOX could be triggered by oxLDL

binding to CD36 (Nguyen-Khoa et al., 1999). As mentioned earlier, uptake of oxLDL by CD36 triggers ROS production in a number of cell types, especially U937 cells which have a high expression level of CD36 (Nguyen-Khoa et al., 1999, Baird et al., 2004b). These observations imply that in cells which express high levels of CD36 and NOX, such as U937 cells, the resulting ROS production overtakes the caspase-dependent cell death. The excessive ROS production derived from NOX can oxidize cysteine protease, which prevent caspase activation, meaning cells will slide into necrosis and cell lysis instead of a controlled apoptosis.

1.6.4 NOX inhibitors

At present , no specific NOX inhibitors exist (Bedard and Krause, 2007). In sharp contrast with this statement, a large number of studies aim at investigating the role of NOX in a great deal of physiopathological process are based on the use of NOX inhibitors, mainly apocynin and diphenyleneiodonium (DPI).

1.6.4.1 Apocynin

Apocynin, is the name given to the aromatic ketone 4-hydroxy-3-methoxyacetophenone, which is also known as acetovanillone. It is an ortho-methoxy-substituted catechol, naturally occurring in roots of the medicinal herb *Picrorhiza kurroa* which grows in the Himalayan mountains (Aldieri et al., 2008). Apocynin has been used as an efficient NOX inhibitor in many *in vitro* and *in vivo* experimental models to study the involvement of NOX in any physiopathological events. Human cellular studies using neutrophils revealed that apocynin has a half maximal inhibitory concentration (IC_{50}) of 10 μM when cells are stimulated with PMA (Simons et al., 1990). Holland *et al.* reported incubation of stimulated endothelia cells with apocynin showed NOX inhibition, resulting in a significant impaired ROS production (Holland et al., 1998). Treatment of isolated rat arteries with apocynin decreased NOX-derived superoxide production and increased NO bioavailability (Hamilton et al., 2002). In addition, in human arteries and veins, NOX-mediated superoxide production was also inhibited by apocynin and endothelium-dependent vasodilation was improved (Hamilton et al., 2002). Apocynin was also shown to

be effective at suppressing atherogenesis i*n vivo* in spite of highly elevated serum LDL levels using a rabbit model (Holland, 1999). The mechanism of apocynin inhibition is not totally known, but it appears to involve the impairment of the intracellular translocation to the membrane of two cytosolic components of NOX, $p47^{phox}$ and $p67^{phox}$ (Stolk et al., 1994). In human monocytes, the treatment of apocynin decreased the expression of $p47^{phox}$ (Barbieri et al., 2004), and a similar effect was observed on $p67^{phox}$ expression in THP-1 cells (Juliet et al., 2003). Studies on the effect of phagocyte NOX suggested that apocynin must be metabolized by H_2O_2 and myeloperoxidase (MPO) to form an apocynin radical which reacts with the essential thiol groups in the NOX subunits, preventing the oxidase complex from assembling and activating (t Hart and Simons, 1992, Stolk et al., 1994). Alternatively, it has been proposed that MPO catalyses the oxidation of apocynin and convert it to a symmetrical dimer, as shown in **Figure 1.4**. Further oxidation and hydroxylation of apocynin dimer can form a trimer (Ximenes et al., 2007). It has been proposed that apocynin radical and/or its dimer radical may inhibit the activation of the cytosolic $p47^{phox}$ by reacting with the essential thiol groups of $p47^{phox}$ (**Figure 1.5**) (Ximenes et al., 2007).

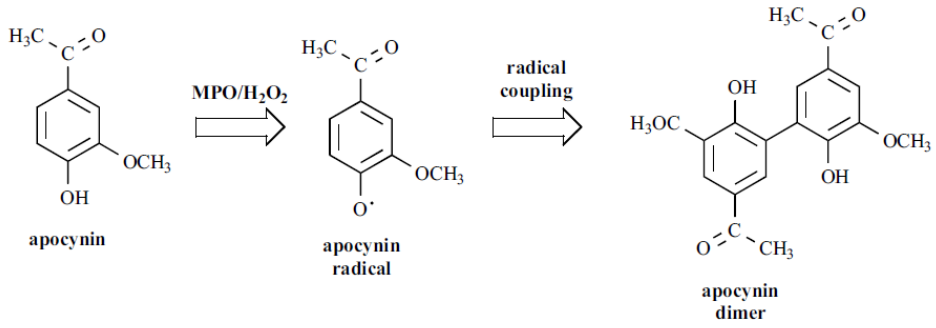

Figure 1.4 MPO-mediated dimerization of apocynin (modified from *Ximenes et a.l, 2007*)

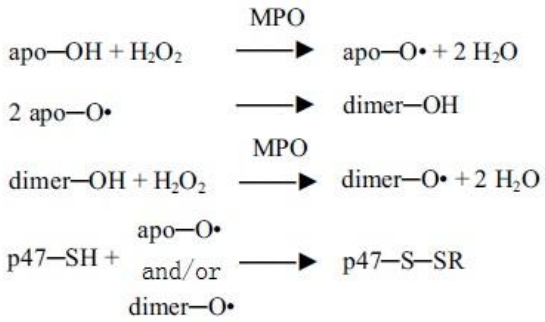

Figure 1.5 Proposed mechanism of apocynin inhibition of the cytosolic NOX subunit $p47^{phox}$. R could be another protein thiol or GSH (modified from *Ximenes et a.l, 2007*).

There are, however, potential drawbacks to the use of apocynin. A serious potential problem comes from studies showing that apocynin may actually increase oxidative stress in different cell types, and it could be pro-oxidant due to the formation of MPO-mediated apocynin radicals. Vejrazka *et al.* showed that apocynin stimulated ROS production in rat vascular fibroblasts and inhibited respiratory burst in rat monocytes stimulated with zymosan. They supposed that apocynin could act as an inhibitor of phagocyte NOX and a stimulator of ROS production in non-phagocyte cells (Vejrazka et al., 2005). Furthermore, in N11 glial cells, apocynin was reported to evoke an increase of H_2O_2 production and a decrease of the GSH/GSSG ration, accompanied by augmented efflux of GSH (Riganti et al., 2008, Riganti et al., 2006). Apocynin induced the activation of both pentose phosphate pathway (PPP) and TCA cylce, which was subsequent to the oxidative stress, and this can be prevented when cells were incubated with GSH together with apocynin (Riganti et al., 2008). Previous study also found that GSH level was decreased in response to apocynin treatment in alveolar epithelial cells (Riganti et al., 2006). Castor *et al.* suggested that the pro-oxidant activity of apocynin radical takes the responsibility for the GSH oxidation (Castor et al., 2010). Therefore, it is suggested that apocynin per se can induce an oxidative stress and exert a cytotoxic effect in some cell types. It is conceivable that when NOX is maximally activated, the inhibition of respiratory burst is the prevailing effect of the apocynin, as a wide body of literature has already shown, but in the absence of a stimulation of NOX, the pro-oxidant effect of apocynin itself could predominate.

1.6.4.2 Diphenyleneiodonium (DPI)

Diphenyleneiodonium (DPI) is known as an uncompetitive inhibitor of flavoproteins. It was originally identified as a hypoglycaemic agent blocking gluconeogenesis and respiration in rat liver (Holland et al., 1973). Later research found that DPI inhibits NOX activity. DPI is thought to attenuate NOX activity by withdrawing an electron from the complex to form a covalent adduct with FAD, inhibiting NOX superoxide production (O'Donnell et al., 1993). DPI shows the inhibitory effect on NOX activity in cell free assays of human neutrophils as well as in whole cells (O'Donnell et al., 1993, Cross and Jones, 1986). As suggested by the mechanism of action, DPI is a nonspecific inhibitor of many different electron transporters. A large amount of research has reported that DPI

inhibits many other flavoproteins, including xanthine oxidase, (Doussiere and Vignais, 1992), nitric oxide synthase (NOS) (Stuehr et al., 1991), xanthine oxidase, mitochondrial complex I (Li and Trush, 1998), and cytochrome p450 reductase (Prabhakar, 2000). They suggest that the electron transport through the flavin moieties of these enzymes causes reduction of DPI to its radical form, followed by irreversible phenylation of either the flavin or the adjacent amino acids and haem groups (Aldieri et al., 2008). Due to the lack of specificity, DPI can cause deleterious effects on cell functions. For example, inhibition of NOS by DPI can suppress NO production, which is critical for vasodilation, and therefore contributes to hypertension (Wang et al., 1993).

DPI may elicit oxidative stress and increase ROS generation in some conditions dependent on either the DPI concentration and incubation time or on the cell type investigated. For instance, in human promyelocytic leukemia HL-60 cells and isolated rat heart submitochondrial particles, DPI (100 μM, 10-60 min) induced increased ROS production and subsequent apoptosis (Li et al., 2003). In rat pulmonary artery endothelial cells, DPI promoted increased expression of stress protein haem oxygenase-1, which is a frequent event in cells under oxidative stress (Ryter et al., 2002). A 24-hour incubation with 10 μM DPI caused increased ROS generation in human retinal pigment epithelial cells (Park et al., 2007). Riganti *et al.* also observed that DPI (1-100 μM) inhibited the PPP in N11 glial cells after a 3-hour incubation by directly inhibiting the activity of the regulatory enzyme glucose-6-phosphate dehydrogenase (G6PD) (Riganti et al., 2004). The same study also showed that DPI caused a concentration-dependent increase in ROS production and lipid peroxidation, an increased leakage of lactate dehydrogenase (LDH) in the extracellular medium, a decrease of the GSH/GSSG ration and an increased efflux of GSH out of the cells (Riganti et al., 2004). These effects were prevented with the addition of GSH. It suggests that the oxidative damage caused by DPI was subsequent to the G6PD and PPP inhibition. Furthermore, the NAD-dependent enzymes, such as LDH and GAPDH, were also found to be inhibited by DPI, and the subsequent blockade of glycolysis could partly explain the inhibition of glucose flux through the TCA cycle. These data together suggest that DPI can exert oxidative stress and lead to cell metabolic dysfunction. Similar to apocynin, it is very likely that when NOX is not maximally activated, the prevailing effect of DPI is to stimulate, rather than to inhibit, ROS production (Aldieri et al., 2008).

1.7 Calcium and atherosclerosis

Free calcium ions (Ca^{2+}) are key signaling molecules. Resting cells tightly regulate free Ca^{2+} in the range of 100 to 200 nM in both the cytosol and the mitochondria, whereas the extracellular free Ca^{2+} concentration is approximately 2 mM (Yang et al., 2012). This concentration gradient is maintained by a number of Ca^{2+} transport systems on the plasma membrane and intracellular Ca^{2+} 'pool' membranes. Typically, plasma membrane contain three systems: a specific ATPase which is a ATP-dependent Ca^{2+} pump responsible for the extrusion of Ca^{2+} out of cells, voltage-gated L- or T-type Ca^{2+} channels, and a Na^{+}/Ca^{2+} exchanger which can release Ca^{2+} out of cells against its concentration gradient with the entry of Na^{+}. Mitochondria contain an electrophoretic uniporter that is used exclusively for the uptake of Ca^{2+} from cytosol, as well as a Na^{+}/Ca^{2+} exchanger used for the release of Ca^{2+} from the mitochondrial matrix to the cytosol. ER also contains a specific ATPase for the uptake of Ca^{2+} from cytosol into ER, and ryanodine receptors (RyRs) responsible for the Ca^{2+} release out of ER (Carafoli, 1987).

Several lines of studies have indicated the importance of Ca^{2+} signaling in the development of atherosclerosis (Berthier et al., 2004, Meilhac et al., 1999, Plank et al., 2007, Wang et al., 2000, Wang et al., 2001). OxLDL-induced rise in cytosolic Ca^{2+} appears to be a common event or trigger for both necrosis and apoptosis in a range of cells (Berthier et al., 2004, Deng et al., 2009, Deniaud et al., 2008, Porn-Ares et al., 1998). Studies have illustrated that a rapid redistribution of Ca^{2+} throughout cells occurs upon oxLDL treatment in U937-derived macrophages-like cells, resulting in the transient elevations of the cytosolic Ca^{2+} due to both the extracellular Ca^{2+} influx through the plasma membrane voltage-gated L- or T-type Ca^{2+} channels and the Ca^{2+} depletion from intracellular ER store through RyRs in the ER membrane (Deng et al., 2009, Deng et al., 2005). Whether this occurs in actual macrophages or U937 monocytes is not known.

An abnormal increase in cytosolic Ca^{2+} can trigger a number of cellular events. An elevation in cytosolic Ca^{2+} can promote NOX activation by activating PKC and PLA_2, which triggers the phosphorylation of NOX subunit $p47^{phox}$ (Cathcart, 2004). The excessive cytosolic Ca^{2+} can also be taken up by mitochondria to trigger mitochondrial ROS production and the mitochondrial permeability transition (MPT) pore opening, which then leads to either apoptotic or necrotic cell death (Madamanchi and Runge, 2007, Whiteman et al., 2004, Deng et al., 2009). Stimulation of the TCA cycle and oxidative phosphorylation by Ca^{2+} would enhance ROS output by accelerating the mitochondrial metabolism and O_2 consumptions, leading to more superoxide radical leakage from the mitochondrial respiratory chain (Nicotera and Orrenius, 1998). The mitochondrial ROS production can serve as the oxidizing agent for MPT pore activation via the oxidation of essential thiol groups in membrane proteins (Inoue et al., 2008, Kowaltowski et al., 1997). It is the MPT pore opening that triggers the mitochondrial membrane potential loss and the subsequent rupture of the outer mitochondrial membrane and mitochondrial dysfunction (Yang et al., 2012, Deng et al., 2009). Apoptotic factors can be released from mitochondria via the opened MPT pore, such as cytochrome c, leading to caspase-3 activation and subsequent apoptotic cell death (Nicotera and Orrenius, 1998).

Furthermore, cytosolic Ca^{2+} increase can activate Ca^{2+}-dependent calpain, a class of non-lysosomal cysteine proteases (Dong et al., 2009, Miyoshi et al., 1996). Activated calpain can cleave a few cytoskeletal proteins, including spectrin (an actin-binding protein controlling the polymerization and reorganization of actin), talin (cytoskeletal protein connecting actin filaments with the plasma membrane) and α-actin, resulting in the elimination of the plasma membrane anchorage to the cytoskeleton and contributing to the plasma membrane blebbing (Miyoshi et al., 1996, Weber et al., 2005). When blebbing proceeds to such an extent that bleb rupture occurs without immediate resealing, the cells loses its ion gradient and is effectively dead. The cellular contents are released into the surrounding area, causing necrotic cell death. Calpain activation also mediates lysosomal destabilization with the subsequent release of cathepsins, a protease responsible for degradation of cellular components, resulting in the caspase-independent apoptosis (Yang et al., 2012, Vindis et al., 2005).

1.8 7,8-Dihydroneopterin

Activated T cells release IFN-γ which stimulates the synthesis and secretion of 7,8-dihydroneopterin (7,8-NP) by macrophages. 7,8-NP has been found in the atherosclerotic lesion, and it may function within inflammatory sites to protect macrophages from the oxidants present (Gieseg et al., 2009b). *In vitro* studies have shown that 7,8-NP is a potent antioxidant that can prevent oxidative damage to cells, cellular membranes, cellular proteins and protein thiols (Gieseg *et al.*, 2000, Gieseg *et al.*, 2001, Duggan *et al.*, 2002). The protective effects of 7,8-NP appears to be attributed to its radical scavenging capability. 7,8-NP can scavenge free radicals such as $OH^{\cdot}$ (Heales et al., 1988), $O_2^{\cdot-}$, H_2O_2 (Shen, 1994), peroxyl radicals (Oettl et al., 2004), lipid peroxyl radicals (Gieseg et al., 1993) and HOCl (Yang, 2009). 7,8-NP can also prevent copper-, peroxyl radical- and cell-mediated LDL oxidation by scavenging the lipid-derived radicals which promote the protein peroxidation (Gieseg *et al.*, 2003, Gieseg *et al.*, 1995). In addition, 7,8-NP has been shown to prevent oxLDL-induced intracellular GSH loss in U937 cells by scavenging oxLDL-mediated ROS, which in turn maintained the intracellular redox environment and hence prevented cell death (Baird, 2003). Apart from scavenging radicals, 7,8-NP can also protect HMDMs from oxLDL-mediated cell death via down-regulation of scavenger receptor CD36, thereby decreasing CD36-mediated uptake of oxLDL (Gieseg et al., 2010a).

1.9 Objectives of research

OxLDL accumulates in the atherosclerotic lesions, driving macrophage cell death and formation of advanced plaque with necrotic regions. Numerous studies have shown oxLDL induces increased oxidative stress in macrophages and monocytes, resulting in the rapid loss of intracellular GSH and cell death. To confirm this finding, the following research will investigate the oxLDL-induced oxidative stress in human monocyte-like U937 cells by examining the effects of oxLDL on cell viability, ROS production, intracellular GSH content, aconitase activity, and cytosolic Ca^{2+} level.

The source of oxidative stress and how oxLDL triggers oxidant production remains unclear. Since NOX is the predominant protein complex producing superoxide, it is appears that

NOX is the major source of oxidative stress in the atherosclerotic lesion. In the study it is hypothesized that NOX can be activated by oxLDL, and the NOX-derived ROS production triggers the intracellular GSH depletion, inducing oxidative stress. The resulting oxidative stress may inactivate aconitase, leading to the metabolism failure and eventually cell death. NOX activation may also promote the cytosolic Ca^{2+} increase, which in turn cause mitochondrial uncoupling and subsequent mitochondrial ROS production, resulting in the mitochondrial aconitase inactivation. Cytosolic Ca^{2+} may also participate in the NOX activation. To validate this hypothesis, NOX inhibitors apocynin and DPI will be used to study the effect of NOX on oxLDL-induced oxidative stress

.

Another aim of this project is to examine the antioxidative effect of 7,8-NP on oxLDL-induced oxidative stress in U937 cells and whether 7,8-NP protects cells from oxLDL damage via interaction with NOX.

2. MATERIALS AND METHODS

2.1 Materials

2.1.1 Reagents

All reagents used in this research were of analytical grade or better. Water was de-ionized and ultrafiltered using a NANOpure ultrapure water system from Barnstead/ Thermolyne(IA/USA). Unless otherwise stated, all solutions were prepared in this nanopure water.

β-mercaptoethanol	Sigma Chemical Co., Missouri, USA
2,6-dichlorophenolindephenol (DCIP)	Sigma Chemical Co., Missouri, USA
2-Thiobarituric acid (TBA)	Sigma-Aldrich Chemical Co., Steinheim, Germany
3-[4,5-Dimethylthiazol-2-yl]-2,5-diphenyl-tetrazolium bromide (MTT)	Sigma Chemical Co., Missouri, USA
4-bromo-calcium ionophore A23187 (Br-A)	Sigma Chemical Co., Missouri, USA
4-Morpholine-propanesulfonic acid (MOPS)	Sigma Chemical Co., Missouri, USA
7,8-Dihydroneopterin (7,8-NP)	Schirck Laboratories, Switzerland
Acetic acid (glacial)	Merck Ltd, Poole, England
Acetonitrile (ACN)	J.T.Baker (USA)
Acetone	Merck Ltd, Poole, England
Aconitase positive control	Sapphire Bioscience, Australia
Anchor non fat milk powder	Fonterra Brand New Zealand, Ltd, NZ
4'-hydroxy-3-methoxyacetophenone (apocynin)	Sigma Chemical Co., Missouri, USA
Argon gas	BOC Gases, Auckland, New Zealand
Barium (±) – fluorocitrate	Sigma Chemical Co., Missouri, USA
Bicinchoninic acid (BCA) protein determination kit	Pierce, Illinois, USA
Bovine serum albumin (BSA)	Gibco Invitrogen Corporation, Auckland, New Zealand
Bromophenol blue	Sigma Chemical Co., Missouri, USA
Butylated hydroxytoluene (BHT)	Sigma Chemical Co., Missouri, USA
Chelex 100 resin	Bio-Rad Laboratories, California, USA
Cholesterol reagent	Roche Diagnostics, USA
Copper chloride ($CuCl_2$)	Sigma Chemical Co., Missouri, USA
Coumassie blue	Bio-Rad Laboratories, California, USA
Cysteine	Sigma Chemical Co., Missouri, USA

Dihydroethidium (DHE)	Invitrogen,, Oregon, USA
Dimethyl sulphoxide (DMSO)	BDH Laboratory Supplies Ltd., Poole, England
Diphenyleneiodonium (DPI)	Sigma Chemical Co., Missouri, USA
Dipotassium phosphate (K_2HPO_4)	Scharlau Chemie, Italy
Ethanol	Merck, Darmstadt, Germany
Ethylenediaminetetraacetic acid (EDTA)	Sigma Chemical Co., Missouri, USA
Ferrous ammonium sulphate	Sigma Chemical Co., Missouri, USA
Glutathione (reduced form)	Sigma Chemical Co., Missouri, USA
Glycerol	Sigma Chemical Co., Missouri, USA
Glycine	Bio-Rad Laboratories, California, USA
Hydrochloric acid, fuming 37 % (HCl)	Merck, Darmstadt, Germany
Isopropanol	Mallinckrodt Chemicals, New Jersey, USA
Magnesium chloride ($MgCl_2$)	BDH Laboratory Supplies Ltd., Poole, England
Methanol	Merck, Darmstadt, Germany
MitoSox red	Invitrogen,, Oregon, USA
Molecular Weight Marker	Fermentas International Inc, Ontario, Canada
Monobromobimane (MBB)	Fluka Analytical, Switzerland
Nicotinamide adenine dinucleotide phosphate ($NADP^+$)	Sigma Chemical Co., Missouri, USA
Nitrogen gas	BOC Gases, Auckland, New Zealand
NuPAGE 4-12% Bis-Tris Gel, 1.0 mm x 10 well	Invitrogen, California, USA
Phorbol 12-myristate 13-acetate (PMA)	Sigma Chemical Co., Missouri, USA
Ponceau S	Sigma Chemical Co., Missouri, USA
Porcine heart isocitrate dehydrogenase (ICD)	Sigma Chemical Co., Missouri, USA
Potassium bromide (KBr)	Merck, Darmstadt, Germany
Potassium chloride (KCl)	Merck Darmstadt, Germany
Potassium dihydrogen phosphate (KH_2PO_4)	Scharlau Chemie, Italy
Potassium hydroxide (KOH)	Merck, Darmstadt, Germany
Sodium acetate ($C_2H_3NaO_2$)	Merck, Darmstadt, Germany
Sodium azide (NaN_3)	BDH Laboratory Supplies Ltd., Poole, England
Sodium chloride (NaCl)	Merck, Darmstadt, Germany
Sodium citrate	BDH Laboratory Supplies Ltd., Poole, England
Sodium dihydrogen orthophosphate monohydrate ($NaH_2PO_4.H_20$)	Scharlau Chemie, Italy
Sodium dodecyl sulphate (SDS)	Sigma Chemical Co., Missouri, USA
Sodium hydrogen carbonate ($NaHCO_3$)	Merck, Darmstadt, Germany
Sodium hydroxide (NaOH)	Scharlau Chemie, Italy
Succinate acid	Sigma Chemical Co., Missouri, USA
Supersignal West Dura chemiluminescence	Pierce Biotechnology Inc., Illinois, USA

Thimerosal	Sigma Chemical Co., Missouri, USA
Trichloroacetic acid (TCA)	Sigma Chemical Co., Missouri, USA
Tris (hydroxymethyl) aminomethane (Tris)	Roche Diagnostics GmbH, Mannheim, Germany
Trypan blue solution (0.4%)	Sigma Chemical Co., Missouri, USA
Tween-20	Sigma Chemical Co., Missouri, USA

2.1.2 Media

Foetal bovine serum (FBS)	Invitrogen, California, USA
Penicillin/Streptomycin (10000 units/ml penicillin G and 10000 μg/ml streptomycin)	Gibco Invitrogen, Auckland, New Zealand
Roswell Park Memorial Institute (RPMI) -1640 media, with phenol red	Sigma-Aldrich Chemical Co., Missouri, USA
Roswell Park Memorial Institute (RPMI) -1640 media, without phenol red	Sigma-Aldrich Chemical Co., Missouri, USA

2.1.3 Antibodies

Mouse monoclonal against β-Actin	Sigma-Aldrich Chemical Co., USA
Mouse monoclonal IgG_1 p47-phox	Santa Cruz Biotechnology Inc., USA
Goat Anti-mouse IgG HRP-conjugated	Santa Cruz Biotechnology Inc., USA

2.1.4 General solutions, media and buffers

2.1.4.1 Phosphate buffered saline (PBS)

Phosphate buffered saline (PBS), containing 150 mM sodium chloride (NaCl) and 10 mM sodium dihydrogen orthophosphate (NaH_2PO_4) (pH 7.4), was treated with 1g of washed chelex-100 resin for at least two hours to remove any transition metals before vacuum filtered through a 0.45 μm Phenex filter membrane (Phenomenex). If required for cell culture, the PBS solution was sterilized by autoclaving (15 minutes, 121 ℃ and 15 psi) and stored at 4 ℃. PBS was warmed in the water bath to 37 ℃ prior to use with cells.

2.1.4.2 Roswell Park Memorial Institute (RPMI)-1640 media (with or without phenol red)

Media was prepared as per manufacturer's instructions. Powdered RPMI (with or without phenol red) was dissolved in nanopure water, followed by addition of sodium bicarbonate and pH adjustment to 7.4 with 1 M sodium hydroxide (NaOH). The media was filter-

sterilised using a peristaltic pump (CP-600, Life Technologies) and a 0.20 µm Sartolab®-P20 filter (Sartorius AG, Goettingen, Germany) into sterile bottles. Media was stored at 4 ℃ and warmed to 37 ℃ in the water-bath before use.

2.1.4.3 7,8-Dihydroneopterin (7,8-NP) solution

A 2 mM stock of 7,8-dihydroneopterin (7,8-NP) (MW= 255.2 g/mol) was prepared fresh, immediately before each experiment. 7,8-NP was dissolved in degassed ice cold RPMI-1640 medium during a 5-10 minute sonication. 7,8-NP solution was subsequently filter-sterilised using a 0.22 µm MS® PES syringe filter (Membrane Solutions, USA) and diluted to working concentrations in warm RPMI-1640 media.

2.1.4.4 Phorbol 12-myristate 13-acetate (PMA)

A stock solution of phorbol 12-myristate 13-acetate (PMA) was made by dissolving PMA in DMSO to give a final concentration of 0.1 mg/ml, which was stored at -20 ℃, and diluted to 100 ng/ml in RPMI 1640 without phenol red before addition to the cells.

2.2 Methods

2.2.1 Cell culture

All cell experiments were carried out under aseptic conditions in a class II biological safety cabinet (Clyde-Apex BH 200). Sterile plastic wares were supplied by Falcon, Terumo, Unomedical and Greiner Bio-one. Media and solutions were sterilized either by autoclaving or by filtration through a sterile 0.22 µm membrane filter. All equipment and tissue culture items were sprayed thoroughly with 70% ($^{v}/_{v}$) ethanol before being transferred to the class II biological safety cabinet.

Cells were maintained in an incubator at 37 ℃ in a humidified atmosphere containing 5% CO_2 (Sanyo CO_2 Incubator). Viable cells were counted using a haemocytometer and a light microscope after staining with trypan blue at a ratio of 1:1.

2.2.1.1 Cell culture media

RPMI-1640 medium (with phenol red) supplemented with 100 units/ml penicillin G and 100 µg/ml streptomycin was combined with foetal bovine serum (FBS) to a final concentration of 5% ($^{v}/_{v}$) for normal cell maintenance.

2.2.1.2 Preparation of U937 cell line

The U937 cell line was originally developed from the pleural fluid of a 37-year old man with generalised histiocytic lymphoma (Sundstrom and Nilsson, 1976). Due to the easy maintenance and many macrophage-like characteristics, U937 cells are widely used as an *in vitro* model for biomedical research. Our U937 cells were a gift from the Haematology Research Laboratory at the Christchurch School of Medicine, University of Otago. A 1 ml vial containing 20 x 10^6 cells/ml was removed from liquid nitrogen storage and defrosted in the 37 ℃ water-bath until almost completely thawed. The concentrated cell suspension was poured into 30 ml of RPMI-1640 medium in a 50 ml centrifuge tube and centrifuged at 500 g for 5 minutes to separate the DMSO freezing medium and cells. The resulting cell pellet was re-suspended in 10 ml of RPMI-1640 medium in a 25 cm^2 tissue culture flask. Cell density was maintained at 0.3-1.5 x 10^6 cells/ml by passaging in Cellstar® 75 cm^2 tissue culture flasks (Greiner Bio-one) every 2-3 days.

2.2.1.3 Cell experiment procedures

Cell experiments were generally performed using Cellstar® 6 or 12-well suspension culture plates (Greiner Bio-one) which were coated with 8 µl of 5% bovine serum albumin (BSA) per well, to prevent cells adhering to the plastic in the absence of FBS. Five percent BSA solution was made up in RPMI-1640 (without phenol red) immediately prior to each experiment. Viable cells were counted using a haemocytometer and a light microscope after staining with trypan blue at a ratio of 1:1. The required quantity of cells for the experiment was pelleted by centrifugation at 500 g for 5 minutes at room temperature and re-suspended in RPMI-1640 (with or without phenol red) at 37 ℃, to a concentration of 1 x 10^6 cells/ml. The cell suspension was then aliquoted into wells containing RPMI-1640 (with or without phenol red) and any reagents specific to the experiment, to give a final concentration of 5 x 10^5 cells/ml.

2.2.2 Blood collection and plasma preparation for LDL purification

Written consent was first obtained from all healthy blood donors who were required to fast overnight (ethics approval from Upper South A Ethics Committee, CTY/01/04/036). Blood was collected from donors by venipuncture using a 21G x $^{3}/_{4}$ inch or 19 G needle attached to a 30 ml syringe (Terumo, USA). The blood was then collected directly into 50 ml centrifuge tubes (Greiner Bio-one) containing 0.5 ml of 100 mg/ml EDTA (pH 7.4), to give a final concentration of 0.1% EDTA.

Whole blood was centrifuged at 4,100 g for 20 minutes at 4 ℃ with the brake off to separate red blood cells and plasma. The resulting top yellow plasma was subsequently transferred to SS34 rotor centrifuge tubes and centrifuged at 11,000 g for 30 minutes at 4 ℃, with slow acceleration/deceleration, to remove remaining cellular debris in the plasma. Plasma from all donors was then pooled together into a single measuring cylinder, to minimize inter-individual variation. Plasma was stored at -80 ℃ in 32 ml aliquots for up to 6 months until required.

2.2.3 LDL preparation

2.2.3.1 Extraction of LDL from plasma

This method of LDL isolation was performed utilizing a Beckman Near Vertical Rotor which employs the method of Chung *et al.* (1980) with modifications described by Gieseg and Esterbauer (1994), which was directly adapted from Dr. Wendy Jessup (Heart Research Institute Ltd, Sydney) for LDL preparation in a vertical rotor. The method involves setting up a one step gradient that, during ultracentrifugation, redistributes to form a gradient that separates the lipoproteins.

A 32 ml tube of frozen human plasma was defrosted under cold running water and centrifuged at 4,700 rpm for 10 minutes at 4 ℃ to pellet precipitated fibrinogen. The supernatant was decanted into a beaker and placed immediately on ice. The plasma density was adjusted to 1.24 g/ml by gradually adding 11.4g of solid potassium bromide (KBr). The solution was gently stirred to prevent the formation of foam, which is the sign of LDL denaturation. Plasma was maintained on ice and under argon gas until ultracentrifugation.

Eight milliliters of 1 mg/ml EDTA (pH 7.4) was added to each of 8 OptiSeal™ polyallomer centrifuge tubes (Beckman Coulter, USA) before under-layering with 4 ml of KBr-plasma, using a long luer-fitting needle attached to a 5 ml syringe. Ultracentrifuge tubes were transferred to the NVTi-65 rotor and centrifuged at 60,000 rpm for 2 hours at 10 ℃ using slow acceleration/deceleration. Following centrifugation, a yellow/orange colored band of LDL in the density range of 1.019 – 1.063 g/ml was collected using a 90^{o} needle attached to a 20 ml syringe. Freshly prepared LDL can be stored at 4 ℃ under argon gas until use.

2.2.3.2 Determination of cholesterol content of LDL

LDL concentration was determined as a function of cholesterol level using a cholesterol kit supplied by Roche Diagnostic. Ten microliters of LDL was incubated with 1 ml of cholesterol reagent at room temperature for 10 minutes. The absorbance was read at 500 nm against a blank containing only cholesterol reagent.

LDL concentration was then calculated from the absorbance, based on the estimate of cholesterol accounting for 31.69% of the entire LDL particle, by weight, and LDL having a molecular weight of 2.5 kDa (Gieseg and Esterbauer, 1994).

Calculation: absorbance x 14.9 = [cholesterol] (mM)
[cholesterol] (M) x 386.64 g/mol = [cholesterol] (g/l)
[cholesterol] (g/l) x 100/31.69 = [LDL] (g/1 or mg/ml)

2.2.3.3 LDL washing and concentration

The LDL was adjusted to a final concentration of 10 mg/ml (total mass) before any subsequent manipulations or use in experiments. LDL was concentrated using Amicon® Ultra-15 filter tubes (Millipore, USA). LDL was transferred to two filter tubes. Each was made up to 15 ml with chelex-treated PBS and centrifuged at 3,000 g for 30 minutes at 10 ℃. This step was then repeated twice. The duration of the third centrifugation was adjusted according to the desired final volume/concentration of LDL, as determined by cholesterol assay (see **section 2.2.3.2**). If no further manipulations were to be made to the LDL, it was filter-sterilised using a 0.22 μm syringe filter and stored at 4 ℃ in the dark, under argon gas.

2.2.4 LDL oxidation

2.2.4.1 Dialysis tubing treatment

The dry dialysis tubes (Medicell International, UK) with 14.4 mm flat width and molecular weight cut off, 14,000 Daltons, were cut in to approximately 25 cm length, and then boiled on a heating block in a glass beaker containing solution of 5% $^{w}/_{v}$ sodium hydrogen carbonate ($NaHCO_3$) and 1mM EDTA for 20 minutes. Following washing with distilled water, the tubes were boiled again in a glass beaker containing distilled water. After 20 minutes of boiling, the tubes were washed thoroughly with distilled water and stored in 50% ethanol at 4 ℃.

2.2.4.2 Copper oxidation of LDL

LDL at 10 mg/ml (total mass) was transferred to a piece of dialysis tubing secured at one end with a double knot and a weighted closure at the other. Fifty millimolar copper chloride ($CuCl_2$) solution was combined with the LDL inside the dialysis tubing to give a final concentration of 0.5 mM $CuCl_2$. The LDL-containing dialysis tubing was placed in a large bottle containing 1 L PBS/50 mg LDL, plus $CuCl_2$ at a final concentration of 0.5 mM $CuCl_2$. LDL was dialyzed against 0.5 mM $CuCl_2$ in PBS overnight at 37 ℃ in a heated shaker. Complete oxidation of LDL occurred when the LDL colour turned colourless.

The dialysis tubing containing oxLDL was then transferred to a fresh bottle containing 1L of PBS and stirred with 1 g of washed chelex-100 at 4 ℃ for two hours in order to remove the excessive copper ion. This was repeated twice, with the final incubation taking place overnight. OxLDL was filter-sterilized using a 0.22 μm syringe filter and stored at 4 ℃.

2.2.5 Cell viability analysis by MTT reduction assay

2.2.5.1 MTT assay solutions

Five mg/ml of 3-[4,5-Dimethylthiazol-2-yl]-2,5-diphenyl-tetrazolium bromide (MTT) was prepared in RPMI 1640 without phenol red. This solution was filter-sterilized using a 0.22 μm MS® PES syringe and stored at -20 ℃ in dark until use.

A 0.01M HCl solution was made up from 11.44 M HCl and nanopure water. Sodium dodecyl sulphate (SDS) powder was added to this solution and stirred slowly to give a final concentration of 10% ($^{w}/_{v}$) SDS.

2.2.5.2 MTT reduction assay

The MTT reduction assay is a widely used method for measuring cell viability. This laboratory has previously shown that results produced by this method agree well with results obtained by the trypan blue exclusion assay (Baird, 2003). The yellow tetrazolium MTT compound is reduced by metabolically active cells, via the action of NADPH dehydrogenase enzymes, to give an insoluble purple formazan product. This purple product can be solubilised and quantified spectrophotometrically so that the colour intensity provides an indication of both the concentration of cells and their metabolic activity (Mosmann, 1983).

Following experimental treatment, U937 cells from each well were washed with warm PBS and then incubated with 1 ml of RPMI-1640 medium (without phenol red) containing 0.5 mg/ml MTT for 2 hours. The purple formazan product was then dissolved by the addition of 1 ml of 10% ($^{w}/_{v}$) SDS in 0.01 M HCl to each well with thorough mixing. Absorbance was read at 570 nm, against a blank that contained all reagents but was without cells.

2.2.6 Determination of protein concentration

Protein concentration was determined using the bicinchoninic acid (BCA) protein determination kit from Pierce (Global Scientific, USA). The working reagent was freshly prepared by mixing Reagent A (sodium carbonate, sodium bicarbonate, BCA and sodium tartrate in 0.1 M sodium hydroxide) and Reagent B (4% $CuSO_4.5H_2O$) at a 50:1 ratio.

Fifty microliters of sample were mixed with 1ml of working reagent and incubated at 60 ℃ for 30 minutes with gentle shaking in a heated shaking block. The reaction was subsequently stopped by placing samples on ice before reading the absorbance at 562 nm against a water blank. Protein concentration was determined from a standard curve prepared by the incubation of known concentrations of BSA (0-250 μg/ml) in 1 ml of working reagent.

2.2.7 Sodium dodecyl sulfate polyacrylamide gel electrophoresis (SDS-PAGE) and Western blot analysis

2.2.7.1 Solutions for SDS-PAGE and Western blot analysis

Cracker buffer was prepared by dissolving SDS (MW = 288.38 g/mol), glycerol (MW = 92.10 g/mol), bromophenol blue (MW = 670.02 g/mol) in 0.5 M Tris-HCl in nanopure water (pH 6.8) and making up to a final volume of 50 ml. Prior to use, 1 ml of the above solution was mixed with 20 µl of β-mercaptoethanol and 2 ul of 100 mg/ml EDTA. The final cracker buffer hence consisted of 0.125 M Tris-HCl (pH 6.8), 1% ($^{w}/_{v}$) SDS, 20% ($^{w}/_{v}$) glycerol, 0.1% ($^{w}/_{v}$) bromophenol blue, 2% ($^{v}/_{v}$) β-mercaptoethanol, and 0.5 mM EDTA.

Lysis buffer consisted of 40 mM of HEPES (MW = 238.31 g/mol), 50 mM of NaCl (MW = 58.44 g/mol), 1 mM EDTA (MW = 372.24 g/mol), and 1 mM EGTA (MW = 380.4 g/mol) in nanopure water, with pH adjusted to 7.4 using 10 M NaOH and stored at 4 ℃. Prior to use, Complete, Mini protease inhibitor stock (7×) was added to lysis buffer. The 7× stock protease inhibitor solution was prepared as per manufacturer's instructions. One Complete, Mini protease inhibitor cocktail tablet (Roche, Germany) was dissolved in 1.5 ml of nanopure water to give a 7× stock solution. The completed lysis buffer was stored on ice until use.

MOPS (4-morpholine-propanesulfonic acid) buffer consisted of 50 mM MOPS, 50 mM Tris base, 0.1% ($^{w}/_{v}$) SDS, and 1 mM EDTA in nanopure water, with the pH adjusted to 7.7 by adding concentrated HCl.

Transfer buffer for Western blot analysis consisted of 25 mM Tris, 192 mM glycine (MW = 75.07 g/mol), and 20% ($^{v}/_{v}$) methanol in nanopure water, which was stored at 4 ℃ until use. Ponceau S stain consisted of 0.01% ($_{w}/_{v}$) Ponceau S and 5% ($_{v}/_{v}$) acetic acid.

The TBS washing solution consisted of 40 mM Tris-HCl (pH 7.5), 150 mM NaCl, 0.05% ($^{w}/_{v}$) Tween-20, and 0.01% ($^{w}/_{v}$) thimerosal (contains Hg) in nanopure water. The 5% ($^{w}/_{v}$) blocking solution (TBSM) was prepared by dissolving 10 g of Anchor non-fat milk powder in 200 ml of TBS and was stored at 4 ℃. 2% TBSM, were made up by diluting the 5% TBSM with TBS.

2.2.7.2 Cell processing for U937 cells

After treatment, cell samples were collected and washed twice with cold PBS by spinning at 500 g for 5 minutes at room temperature. One hundred and fifty µL of ice cold complete lysis buffer was used to lyse U937 cell pellet. The cell lysate was then transferred into a 1.7 ml eppendorf tube and incubated on ice to properly lyse the cells. After 30 minutes, the cell lysate was vortexed briefly and 5 µl was taken for protein assay (see **section 2.2.6**), while the rest was stored at -80 ℃ until use.

After protein analysis, the volume of cell lysate containing 75 µg of protein was transferred to a new 1.7ml eppendorf tube. Ice cold acetone was then added to precipitate the proteins (the ratio of cell lysate to acetone was 1:10). After incubation on ice for 5 minutes, the sample was centrifuged at 20,800 g for 5 minutes at 4 ℃. The resulting protein pellet was dissolved in "cracker" buffer for SDS-PAGE analysis (see **section 2.2.7.3**).

2.2.7.3 SDS-PAGE analysis

Cracker buffer (30 µl) was used to dissolve the acetone-precipitated protein pellet described above to give a final protein concentration of 2.5 µg/µl. The sample was then heated in a heating block at 95 ℃ for 3 minutes and centrifuged for 5 minutes at 20,800 g at room temperature to remove any cell debris.

A gradient polyacrylamide gel, 4-12% (Bis-Tris Gel, Invitrogen, Carslband, CA, USA), was placed in the XCell SureLock™ Mini-Cell system (Invitrogen, US) and the MOPS running buffer added to the buffer reservoir. Five microliters of Fermentas pre-stained molecular weight marker mix (Fermentas International Inc, Canada) and 20 µL of samples (containing 50 µg proteins) were loaded into the wells of the gel, before electrophoresis at 200 V for approximately 1 hour until the loading buffer dye reached the bottom of the gel.

2.2.7.4 Western blot analysis

After SDS-PAGE, the separated proteins on the SDS-PAGE gel were electrophoretically transferred onto a nitrocellulose membrane with 0.45 µm pore size (Invitrogen, USA) using a Hoefer™ TE22 tank transfer unit (USA) filled with cold transfer buffer, with voltage set at 70 V using the PowerPac 300 power supply (BioRad). After approximately 15 hours, the nitrocellulose membrane was stained with Ponceau S stain for 1 minute to

ensure that the transfer was successful.

The following membrane washing and incubation were performed on a rocking platform mixer (Ratex Instruments, Australia). After briefly rinsing with water, the membrane was blocked using 5% TBSM for 2 hours, followed by three consecutive 5-minute washes in TBS. The membrane was then probed with the primary mouse monoclonal IgG_1 antibodies against $p47^{phox}$ (Santa Cruz Biotechnology Inc, USA) in 1:250 dilution using 2% TBSM. After 1.5 hours, the membrane was washed 5 times in TBS 5 minutes each, followed by 1 hour incubation in the secondary antibody goat anti-mouse IgG-HRP (Santa Cruz Biotechnology Inc, USA) diluted to 1:750 with 2% TBSM. The membrane was then washed as above, followed by brief washing in nanopure water twice to remove any residual TBS. TBS contains Tween-20, which inhibits the peroxidase from reacting with the chemiluminescence substrates, and hence interferes with visualisation (see **section 2.2.7.5**). The membrane was then left in nanopure water and taken for visualization immediately.

2.2.7.5 Visualisation

Detection of the secondary HRP-coupled antibody was conducted using "Supersignal West Dura chemiluminescence" substrates (Pierce, USA), which consist of the luminol solution and the peroxide solution. These two solutions were mixed at 1:1 ratio to give the working solution immediately before use. When applied to the membrane, the luminol in the working solution reacts with the horseradish peroxidase (HRP) on the secondary antibody on the membrane and hydrogen peroxide in the working solution to generate 3-aminophthalate plus the emission of light at 425 nm.

The working solution (0.5 ml) was evenly applied to the membrane and the image was recorded for 10 minutes on a Syngene Chemigenius-2 bioimaging system using Genesnap software (Global, NZ). The membrane was then stored in TBS at 4 ℃ for β-actin detection (see **section 2.2.7.6**).

2.2.7.6 β-actin detection

The membrane (see **section 2.2.7.5**) was re-probed for β-actin as an internal control to confirm equal loading of proteins. The membrane was incubated for 1.5 hours with the

primary mouse monoclonal antibodies against β-actin (Sigma-Aldrich Chemical Co., USA) diluted to 1:10000 in 1% TBSM. The procedures and visualisation were the same as those mentioned in **sections 2.2.7.4** and **2.2.7.5.** The two exception were that the secondary antibody goat anti-mouse IgG-HRP (Santa Cruz Biotechnology Inc, USA) was diluted to 1:1000 in 2 % TBSM, and the exposure time for visualisation was 2 minutes.

2.2.8 Fluorescence microscopy

Intracellular ROS production, mitochondrial superoxide production and cytosolic calcium ion (Ca^{2+}) level were monitored by probing the cells with particular fluorescent dyes followed by examination using fluorescence microscopy.

U937 cells at 0.5 $x10^6$ cells/ml were incubated with fluorescence dyes either before or after oxLDL treatment depending on the type of fluorescence dye used, but always at 37 ℃ in the dark. The cells were then washed twice with warm PBS, and the cell pellets were re-suspended in 20 μL PBS before placing on to a microscope slide (25.4×76.2 mm, 1mm-1.2mm thick, Sail brand).

The cells were viewed using a Zeiss AxioImager.M1 epifluorescent microscope (Carl Zeiss (NZ) Ltd, Auckland, New Zealand), equipped with a Differential Interference Contrast (DIC) condenser and fitted with an HBO 100 W mercury vapour lamp. Cells were viewed using 40 × Plan-NEOFLUAR objectives. Different fluorescent filters were used depending on the fluorescent dyes employed. The images were captured using a Zeiss AxioCam HRc CCD camera with AxioVision Rel. 4.5 software (1300 × 1030 pixel resolution) and processed with Adobe Photoshop 8.0. To ensure accuracy within experimental treatments and to avoid fluorescent dye quenching, the time for sample irradiation and image capture was kept constant. The resulting fluorescence intensities for the detection of superoxide productions were converted to numerical values using the online software Image J. The fluorescence intensities of 500 cells per treatment were converted and averaged using Microsoft Excel software.

2.2.8.1 Dihydroethidium (DHE) detection for intracellular ROS

Dihydroethidium (DHE) has been widely used for detecting intracellular superoxide anions. This cell permeable dye reacts with superoxide resulting in the formation of a two-electron oxidised product, ethidium (E^+), which binds to DNA and leads to enhancement of red fluorescence (λex/λem = 510/605 nm) (Budd *et al.*, 1997; Zhao *et al.*, 2003). DHE (MW = 315.4 g/mol) stock was prepared in DMSO and stored at -20 ℃.

After treatments and PBS washing, U937 cells were incubated with 150 µl of 10 µM DHE in sterile PBS for 20 minutes at 37 ℃ in the dark. Cells were subsequently washed twice with warm PBS to wash off excess DHE. Cell pellets were re-suspended in 20 µl of PBS, and then transferred to microscope slide, with the coverslip placed on a glass slide. The fluorescent filter used for DHE was Zeiss filter set 00 (excitation: band path 530-585; beam-splitter: FT600; emission: LP615).

2.2.8.2 MitoSox Red detection for mitochondrial superoxide

Mitosox Red is a novel fluorogenic dye for highly selective detection of mitochondrial superoxide of live cells. The probing principle of this cell permeable dye is very similar to that of DHE, but it is more selectively targeted to the mitochondria. Once in the mitochondria, MitoSox Red is readily oxidized by superoxide but not other ROS and exhibits red fluorescence (λex/λem = 510/580 nm) (S.Janes et al., 2004). The oxidation product becomes highly fluorescent upon binding to nucleic acid. Five millimolar MitoSox Red (MW = 759 g/mol) reagent stock solution is prepared by dissolving one vial (50µg) of MitoSox Red in 13µl DMSO only before use.

After treatments and PBS washing, U937 cells were incubated with 1ml of 5 µM MitoSox Red in sterile PBS for 10 minutes at 37 ℃ in the dark. Cells were then washed twice with warm PBS to wash off excess MitoSox Red. Cell pellets were re-suspended in 20 µl of PBS, and then transferred to microscope slide, with the coverslip placed on a glass slide. The fluorescent filter used for DHE was Zeiss filter set 00 (excitation: band path 530-585; beam-splitter: FT600; emission: LP615).

2.2.8.3 Fluo-3-acetoxymethyl (AM) ester detection of intracellular calcium

Fluo-3-acetoxymethyl (AM) ester is used to detect cytosolic free calcium and it is cell permeable due to its AM ester structure. After entering the cells, it is cleaved by intracellular esterases to form Fluo-3 and AM. Upon excitation by blue light (λex 488 nm), Fluo-3 emits a green fluorescence (λem 530 nm) when bound to free calcium ions in the cytosol (Minta *et al.*, 1989; Kao *et al*., 1989). Fifty-hundred micro molar of fluo-3AM ester (MW = 1129.9 g/mol) stock was prepared in DMSO and stored at -20 ℃.

U937 cells were pre-incubated with 200 µl of 10 µM fluo-3AM in non phenol red RPMI-1640 medium for 40 minutes, followed by PBS washing and experimental treatments. The fluorescence filter used for fluo-3 was the Zeiss filter 38HE (FITC).

2.2.9 DHE and fluo-3AM analysis by flow cytometry

Flow cytometry is a powerful technique that simultaneously measures and analyzes multiple characteristics of single cells, such as cell size, granularity and relative fluorescence intensity, as they flow in a fluid stream through a beam of light. It gives high-throughput (for a large number of cells) automated quantification of fluorescence instead of producing fluorescent images.

Cells were probed with DHE or fluo-3AM for intracellular superoxide or calcium detection as above (see **section 2.2.8.1** and **2.2.8.3**). Cell samples were then re-suspended in 500 µl of PBS in eppendorf tubes, and analyzed using the Accuri$^{@}$ C6 flow cytometer (BD Biosciences, USA). DHE-probed and fluo-3AM-probed cells were detected using the 585/40 band-pass (BP) filter in FL-2 and 530/30 BP filter in FL-1, respectively. Approximately 10,000 cells were analyzed for each sample. All data were collected and analyzed using the cFlow Plus software.

2.2.10 Intracellular glutathione (GSH) measurement by high performance liquid chromatography (HPLC) analyses

HPLC, a system for the separation, identification and quantification of compounds, was used for a number of analyses. The HPLC system used (Shimadzu Corporation, Japan) comprised a controller (LC-20AD), a fluorescence detector (RF-10AXL), a UV-Vis

detector (SPD-M20A), an auto sampler (SIL-20AC HT), a column oven (CTO-20A), inline vacuum degasser (DGU-20A_5) and a communication bus module (CBM-20A).

Before use in the HPLC system, all mobile phases were degassed by sonication (Alphatech Systems Ltd & Co., Auckland) for 5 minutes. Chromatogram results consisting of peak areas were quantified using Shimadzu LCSolution software package (version 1.22 SP1, 2002-2006). Analytes in samples were standardised against the correlating pure standards of known concentrations for their quantification.

2.2.10.1 Solutions for GSH analysis

A 40 mM stock of monobromobimane (MBB) was prepared by dissolving MBB (MW = 271.1 g/mol) in acetonitrile (ACN), which was stored at 4 ℃ in the dark for up to 2 weeks.

A 10 mM reduced GSH stock was freshly made prior to experiment by dissolving GSH (MW = 307.3 g/mol) in cold PBS. This stock solution was diluted to 5 and 10 µM with PBS immediately prior to HPLC analysis for use as standards.

Mobile phase A consisted of 0.25% acetic acid and mobile phase B was 100% ACN.

2.2.10.2 GSH analysis by HPLC

Monobromobimane (MBB) is a cell-permeable fluorescent dye that binds thiol group, and therefore it is used for the detection of intracellular GSH. MBB alkylates thiol groups to form a GSH-MBB adduct that is then detected by the fluorescence detector after protein precipitation (Cotgreave and Moldeus, 1986). All procedures involving MBB were performed under minimum exposure of light as MBB is light sensitive.

After treatment and two PBS washes, cell pellets were re-suspended in 400 µl of warm PBS, 9 µl of 0.1 M NaOH (to increase pH to 8) and 10 µl of 40 mM MBB, in this order. Following a 20-minute incubation in dark at room temperature, 20 µl of 100% ($^{w}/_{v}$) trichloroacetic acid (TCA) was added to lyse the cells. After thorough mixing, the cell lysate was centrifuged at 11,000 rpm for 5 minutes at 4 ℃ to pellet cellular proteins. Eighty microlitres of the resulting supernatant was transferred to an autosampling vial insert and

10 µl was injected onto the Phenosphere reverse phase C-18, 150 x 4.6 mm, 5 µm column (Phenomenex, Auckland, NZ) which was heated to 35 ℃.

GSH-MBB adducts were detected by the fluorescence detector with excitation and emission wavelengths set at 394 nm and 480 nm respectively. Mobile phases A and B were pumped through the column at a flow rate of 1.5 ml/minute with the following gradient program. GSH concentrations in all samples were quantified by comparing with the peak areas of 5 µM and 10 µM GSH standards.

Time (minutes)	Mobile Phase A	Mobile Phase B
0	90 %	10 %
10	90 %	10 %
11	0 %	100 %
15	0 %	100 %
16	95 %	5 %
20	95 %	5 %

2.2.11 Aconitase assay

Aconitase is an iron-sulfur protein containing a $[Fe4\text{-}S4]^{2+}$ cluster that catalyzes the stereo-specific isomerization of citrate to isocitrate via cis-aconitate in the tricarboxylic acid cycle, a non-redox-active process. Iso-citrate is then catalyzed by iso-citrate dehydrogenase to form α-ketoglutarate in the presence of $NAD^+/NADP^+$ (Beinert et al., 1996). There are two kinds of aconitase in cells, mitochondrial aconitase and cytosolic aconitase. They are related, but distinctly different enzymes and are coded for on different chromosomes. Loss of aconitase activity in cells treated with pro-oxidants has been interpreted as a measure of oxidative damage (Yarian et al., 2005).

2.2.11.1 Cell extract preparation

U937 cells were washed in warm PBS twice after treatment by centrifugation at 500 g for 5 minutes, and the cell pellets were disrupted in 1ml of ice cold lysis buffer (50 mM Tris.HCl (pH 7.4), 0.6 mM $MnCl_2$ and 20 µM flurocitrate) by applying sonication with a microtip sonic oscillartor (Fisher Scientific) in 1-s pulses for 1 minute. Cell lysate was then

centrifuged at 14,000g for 5 minutes at 4 °C, and the supernatant was transferred to the eppendorf tubes and promptly assayed for combined intracellular (cytoplasmic and mitochondrial) aconitase activity.

2.2.11.2 Extraction of cytosol and mitochondrial fraction

After treatment, washed cell pellets were re-suspended in 1 ml of ice cold lysis buffer and kept on ice for 30 minutes. Cell lysate was then passed through a 23 G needle for 20 times to break open and homogenise the cells further. The cell homogenate was centrifuged at 230,000 g for 30 min at 4°C. The pellet was used as a mitochondrial fraction, and the supernatant was the cytosolic fraction. The mitochondrial fraction was resolved in 1 ml of the lysis buffer and sonicated using the microtip of a sonic oscillartor in 1-s pulses for 1 minute to lyse the mitochondrial membrane. Both cytosolic and mitochondrial fractions were kept on ice until use.

2.2.11.3 Determination of aconitase activity

The aconitase activity is measured based on measurement of the concomitant formation of NADPH from $NADP^+$, and the formation of NADPH is monitored by the increase in absorbance at 340 nm. Under appropriate conditions, the rate of NADPH production is proportional to aconitase activity.

After protein concentration analysis (see **section 2.2.6**), 200 µl of cellular supernatants or fractions were added to 800 µl of reaction mixture containing 20 mM Tris.HCl, 12 mM $MnCl_2$, 20 mM sodium citrate, 1 mM $NADP^+$ and 2 units of isocitrate dehydrogenase. The change of absorbance at 340nm was recorded at 30°C for 30 minutes. One milliunit of aconitase activity was defined as enzymatic activity required to catalyze formation of 1nmol of isocitrate per minute with an extinction coefficient of 0.0062 (Powell and Jackson, 2003). A positive aconitase standard at 2units/ml was diluted in 800 µl of reaction buffer and assayed simultaneously after reactivation in 1 ml of activation buffer containing 50 mM Tris.HCl, 0.5 mM ferrous ammonium sulfate and 5 mM cysteine on ice for 1 hour.

In this assay, an initial lag phase (approximately 5 minutes) in NADPH formation was seen (**Figure 2.1**), which was previously suggested as a reflection of the delayed accumulation of *cis*-aconitate due to the reaction equilibrium (Gardner et al., 1994). Therefore, linear

rates during the latter half of the 30-min assay were used for the determinations of aconitase activity.

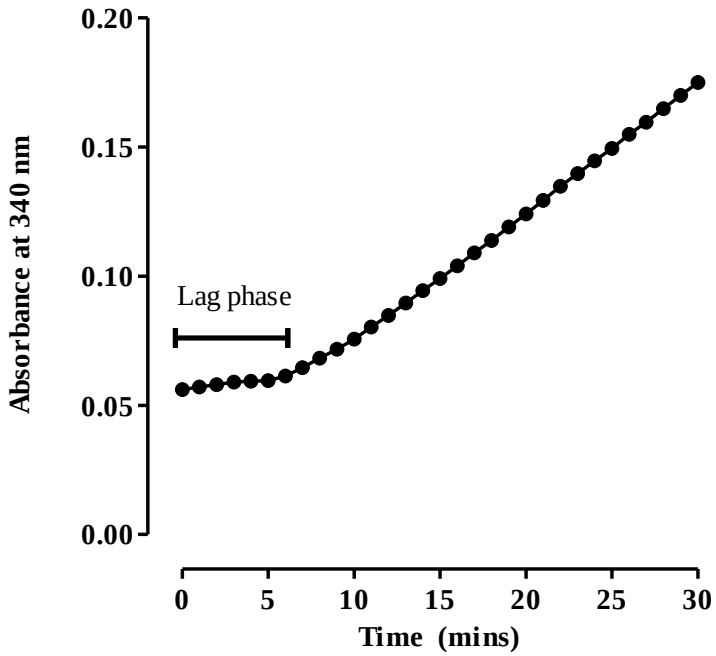

Figure 2.1 A representative example of change in the absorbance at 340 nm over 30 minutes in the aconitase assay

2.2.12 Succinate dehydrogenase assay

Succinate dehydrogenase (SDH) is one of the best studied enzyme in the Kreb cycle which catalyzes the oxidation of succinate to fumarate by transferring two electrons from succinate to flavin adenine dinucleotide (FAD), forming $FADH_2$. SDH is an unique protein among the Kreb cycle enzyme in the mitochondria as it is tightly bound to the inner mitochondrial membrane. Thus, it is recognized as a specific maker for the existence of mitochondria. The *in vitro* analysis of SDH activity is carried out by introducing an artificial electron acceptor, 2,6-dichlorophenolindophenol (DCIP), the reduction of which can be monitored spectrophotometricallly. When the normal path of electrons through the mitochondrial electron transport chain is blocked by sodium azide (NaN_3), the electron from $FADH_2$ can picked up by DCIP, which is a blue dye in oxidized form, forming the colourless reduced DCIP. The colour change can be monitored by the change of the

absorbance at 600nm. Therefore, the SDH activity is assayed by following the reduction of DCIP (Powell and Jackson, 2003).

One hundred microliters of mitochondrial or cytoplasmatic fraction was diluted in 600 µl of assay buffer (6 mM KH_2PO_4, 14 mM K_2HPO_4, 10 mM KCl and 5 mM $MgCl_2$), which was then added to 1.0-ml cuvette tube containing 100 µl of 40 mM NaN_3, 100 µl of 5 mM DCIP and 100 µl of 50 mM succinate. The reaction mixture was incubated for 1 minute at 30°C, and then the decrease in absorbance at 600 nm was measured for 30 minutes at 30°C for the determination of SDH activity, which was calculated based on the molar extinction coefficient (ε=21,000). The amount of SDH in the subcellular fraction is an indicator of how successful mitochondria is isolated from cytosol during the organelle separation process.

2.2.13 Statistical analysis

Data were graphed and analysed statistically using GraphPad Prism version 5.0 for Windows (GraphPad Software, San Diego, California, USA). Significance was confirmed via a one-way analysis of variance (ANOVA) followed by Tukey's multiple comparison test. Where data were expressed as a percentage of control, significance was done on the raw data. Significant levels are indicated in the following manner: (*) $p \leq 0.05$, (**)$p \leq 0.01$ and (***)$p \leq 0.001$.

Most results shown in this thesis are taken from one experiment which is representative of three separate experiments. The mean and standard error of the mean (SEM) shown within each experiment were calculated from triplicate samples in every case. Some results, such as western blots, are the combined result of several separate experiments, with the mean and SEM shown and calculated from those experiments. This will be stated in the legend.

3. RESULTS

3.1 Toxicity of oxLDL

This research began with an investigation of oxLDL toxicity in U937 cells, to confirm the previous findings regarding the effect of oxLDL on U937 cell viability.

The toxicity of oxLDL to U937 cells was examined by exposing cells to increasing concentrations of oxLDL for 24 hours, and cell viability was subsequently measured using the MTT reduction assay (**Figure 3.1A**). A concentration-dependent decrease in the cell viability with increasing amount of oxLDL was found. Final oxLDL concentrations of 0.1, 0.2 and 0.5 mg/ml reduced the cell viability by approximately 8, 18, 90 % of the control, respectively. With the treatment of 1.0 and 1.5 mg/ml oxLDL, less than 10 % of cells were still viable.

Changes in U937 cells morphology after oxLDL treatment were also examined under the light microscope (**Figure 3.1B**). The control cells treated with 0 mg/ml oxLDL showed classic round-shaped U937 cell morphology. U937 cells treated with 0.1 and 0.2 mg/ml oxLDL showed a swelled appearance, and some cell debris were present. Cells treated with 0.5 mg/ml oxLDL had more distorted cell membranes and much more cell debris. OxLDL at 1.0 and 1.5 mg/ml caused significant cell damage with disruption of cell membranes and loss of cellular contents.

Figure 3.1 A)

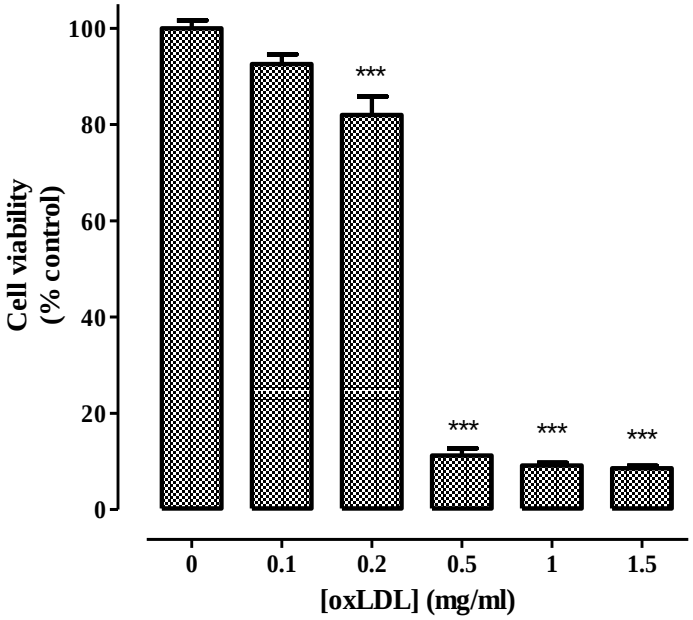

Figure 3.1 B)

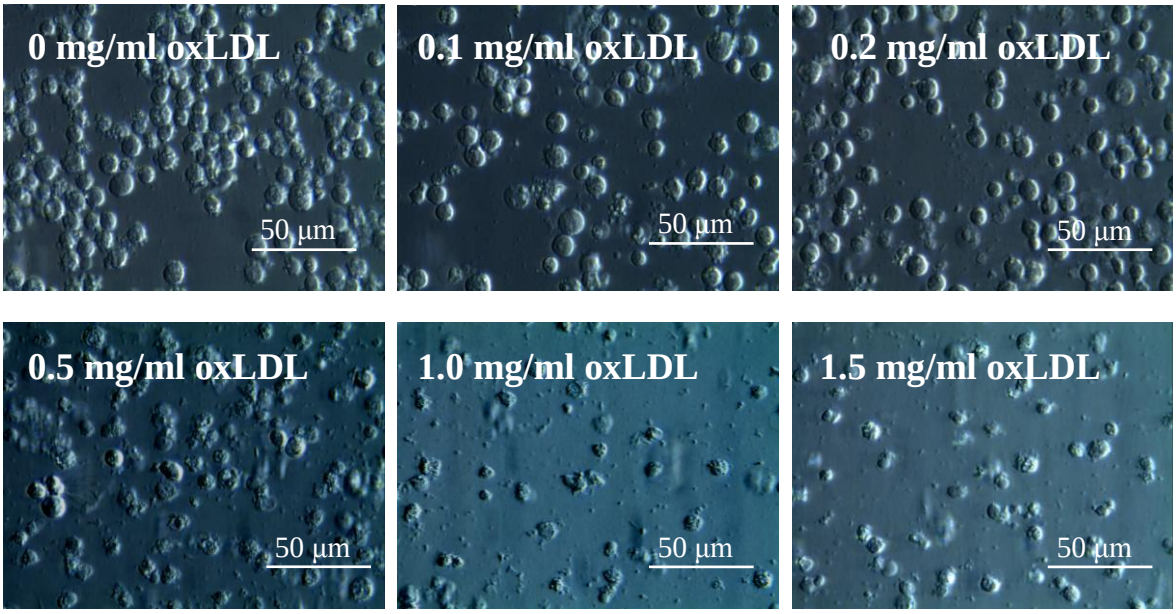

Figure 3.1 Effect of oxLDL on U937 cell viability loss.
U937 cells (0.5×10^6 cells/ml) were treated with the increasing concentrations of oxLDL, followed by incubation at 37 ^{o}C in non-phenol red RPMI-1640 for 24 hours. A) Cell viability was measured using the MTT reduction assay at various oxLDL concentrations. Data are expressed as a percentage of the respective control (0 mg/ml oxLDL added), and the actual absorbance reading for this 100 % control value is 0.625 at 570 nm. Significance is indicated from this control. Results are displayed as mean ± SEM of triplicates from a single experiment, representative of three separate experiments. B) Cells treated with various concentrations of oxLDL were viewed *in situ* in tissue culture wells through an inverted microscope (400x magnification) after 24 hours. Images were taken using a Leica C-Mount camera and processed using Leica Application Suite software.

It is noteworthy that the toxicity of oxLDL to U937 cells appeared variable between different batches prepared, with the median lethal dose (LD_{50}) between 0.2 and 0.5 mg/ml oxLDL, which agrees with the previous findings; although the exact reason is still unknown (Gieseg et al., 2009a). Consequently, the toxicity of each batch of oxLDL was tested to determine LD_{50} prior to be used, and the LD_{50} oxLDL concentration was used in the subsequent experiments..

A time course study was also performed to examine the progression of oxLDL-mediated cell death in U937 cells by incubating cells with 0.25 mg/ml oxLDL for 12 hours. Cell samples were collected at each time point, and the cell viability was determined by the MTT reduction assay (**Figure 3.2A**). The cell viability dropped significantly by 25% following a 3 hour incubation with oxLDL compared to the 0 hour control, and it continued to decrease by 40% after 6 hours. Cell viability decreased by 75% after 9 hours and continued to decline until only 20% of cells remained viable at 12 hours. **Figures 3.2B** illustrates the morphological changes in U937 cells observed under an inverted microscope during their incubation with oxLDL. After 3 and 6 hours incubation with oxLDL, the cells had a swelled appearance with distorted cell membranes and bleb formation. A large number of cells were found to undergo serious cell damage, also cell membrane disruption and loss of cellular contents were observed after 9 hours of incubation. After 12 hours the majority of cells appeared lysed and much cellular debris was detected. These morphological changes caused by oxLDL appeared to follow the characteristics of necrotic cell death.

Figure 3.2 A)

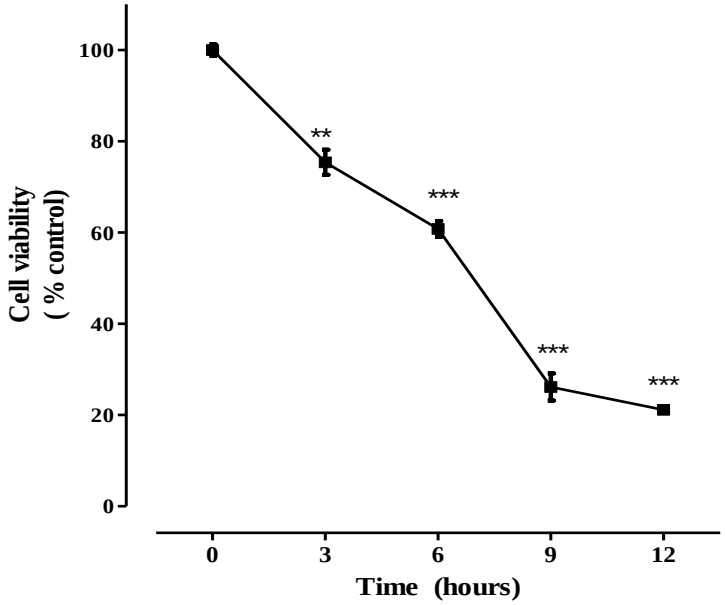

Figure 3.2 B)

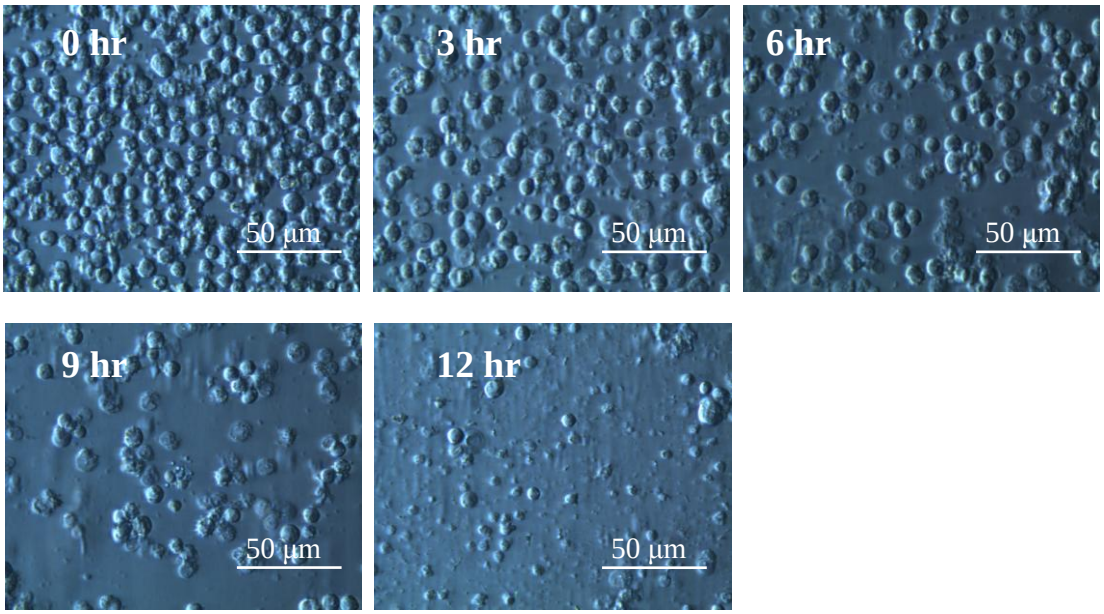

Figure 3.2 Time course study of oxLDL-induced cell viability loss in U937 cells.
U937 cells (0.5×10^6 cells/ml) were incubated at 37°C in non-phenol red RPMI-1640 with 0.25 mg/ml of oxLDL. A) At various times, cell samples were removed and cell viability was measured using the MTT reduction assay. Data are expressed as a percentage of the respective control at 0 hour, and the actual absorbance reading for this 100% control value is 0.661 at 570nm. Significance is indicated from the 0 hour data. Results shown are mean ± SEM of triplicates from a single experiment, representative of three separate experiments. B) Cells were viewed *in situ* in tissue culture wells through an inverted microscope (400x magnification) after 0, 3, 6, 9 and 12 hours. Images were taken using a Leica C-Mount camera and processed using Leica Application Suite software.

3.2 Oxidative stress induced by oxLDL

An increasing body of evidence has addressed the involvement of oxidative stress in the development of atherosclerosis via over-production of reactive oxygen species (ROS) or failure of antioxidant defence system (Stocker and Keaney, 2004, Harrison et al., 2003). Previous findings showed that oxLDL triggered an increased oxidative stress in HMDM, resulting in the excessive production of intracellular superoxide, the rapid loss of cellular glutathione (GSH), and eventual loss of cell viability (Gieseg et al., 2010b). In this section, the oxLDL-induced oxidative stress in U937 cells was investigated by studying the effect of oxLDL on intracellular superoxide and mitochondrial superoxide production using the fluorescent probes dihydroethidium (DHE) and MitoSox Red, respectively. Additionally, the cellular GSH levels, intracellular aconitase activity and free calcium (Ca^{2+}) concentration were also studied to define oxLDL-induced oxidative stress.

3.2.1 The effect of oxLDL on intracellular ROS generation in U937 cells

In order to study whether oxLDL induces superoxide production in U937 cells and how fast this occurs, a time course study was initially conducted by treating cells with 0.5 mg/ml oxLDL, followed by probing with DHE at various times (see **section 2.2.8.1**) and examination of the fluorescence intensity. The oxLDL-treated cells displayed a time-dependent increase in the DHE fluorescence during the first 3 hours incubation, followed by a sharp reduced fluorescence at 6 hours (**Figure 3.3A**). The quantification of fluorescence intensities converted from the fluorescent images (**Figure 3.3B**) showed that the fluorescence intensity increased markedly by 55 % following a 1 hour incubation with oxLDL, and a maximum was reached after 3 hours with a 94 % rise. The DHE fluorescence intensity then dropped dramatically to the control level after 6 hours, and continued to decline to 80 % of the control at 8 hours. This decrease may be due to the fact that many cells started to lyse after 3 hours and the oxidants leaked out of the cells, so that the fluorescence signal could not be detected any more. It is also possible that the ROS-generating enzyme, such as NADPH oxidase (NOX), reached the maximum activity at 3 hours. These results demonstrate that ROS generation induced by oxLDL in U937 cells was an early event occurring, as fast as 1 hour post-treatment and reaching the maximum after 3 hours.

To further confirm that it was oxLDL that induced intracellular superoxide production, U937 cells were also treated with increasing concentrations of oxLDL for 3 hours, followed by the DHE staining. The intracellular fluorescence intensity was significantly elevated with the addition of oxLDL compared to the control (**Figure 3.4A**). The fluorescence intensity was elevated by 80 % with the treatment of 0.15 mg/ml oxLDL compared to the control, and then gradually increased by 100 % when the oxLDL concentration raised to 1 mg/ml (**Figure 3.4B**). These results clearly show that oxLDL provoked the intracellular ROS production, in turn resulting in the increased oxidative stress.

Figure 3.3 A)

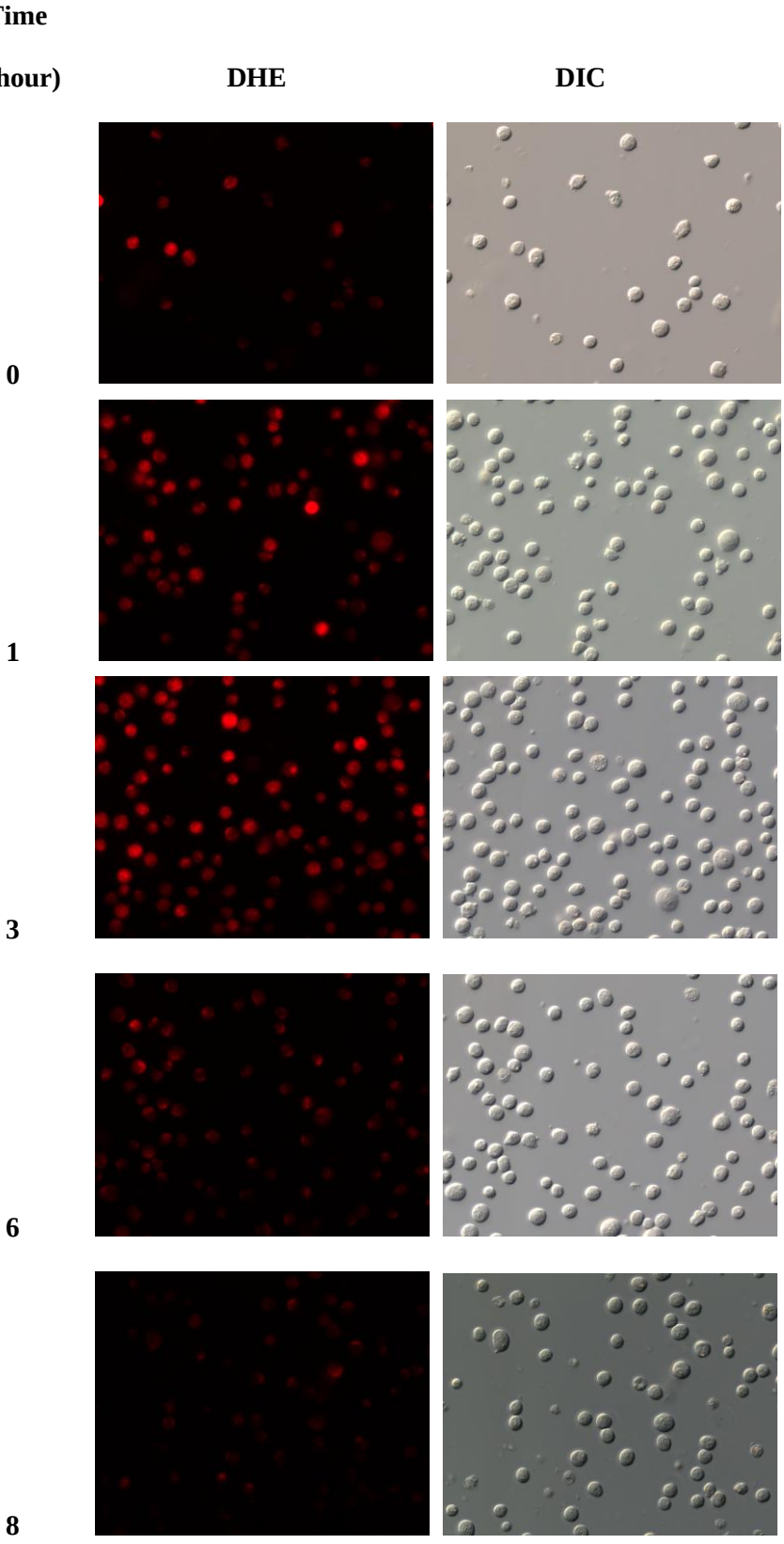

Figure 3.3 B)

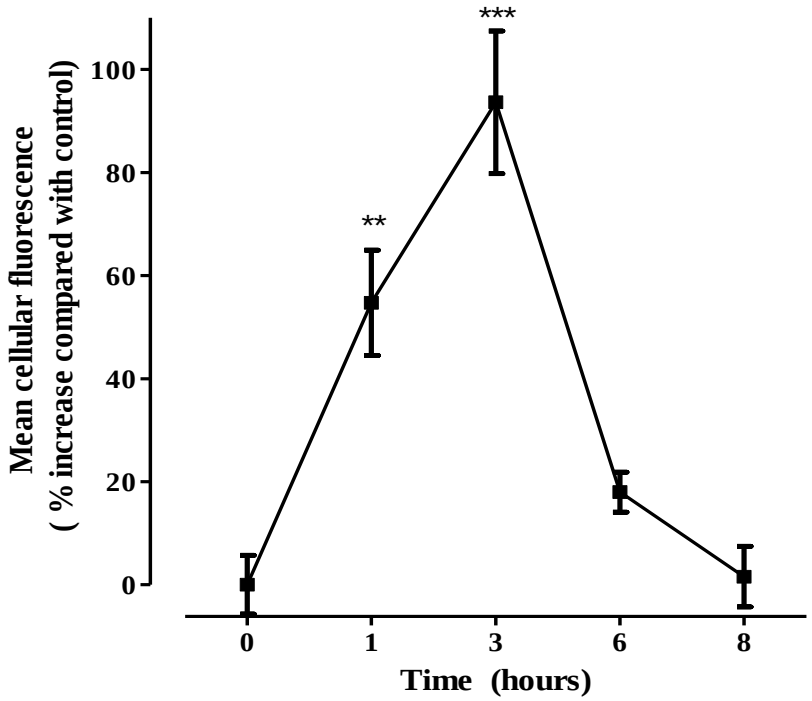

Figure 3.3 Time course study of oxLDL-induced ROS productions in U937 cells.

U937 cells (0.5×10^6 cells/ml) were incubated in RPMI-1640 containing 0.5 mg/ml oxLDL at 37 ^oC. At various times, washed cells were collected and stained with 10 μM DHE for 20 minutes in dark for the fluorescence probing of intracellular superoxide. A) The cells were then viewed under a fluorescence microscope (λex/λem of 500-530 nm/590-620 nm). DIC photos for each of the respective fluorescence photos are shown. B) Cellular fluorescence intensities are converted to numerical values using Image J software, and results are presented as a percentage of control (0 hr data). Significance is detected from this control value. 500 cells in each treatment were collected for quantification, and results shown are mean fluorescence ± SEM of triplicate experiments.

Figure 3.4 A)

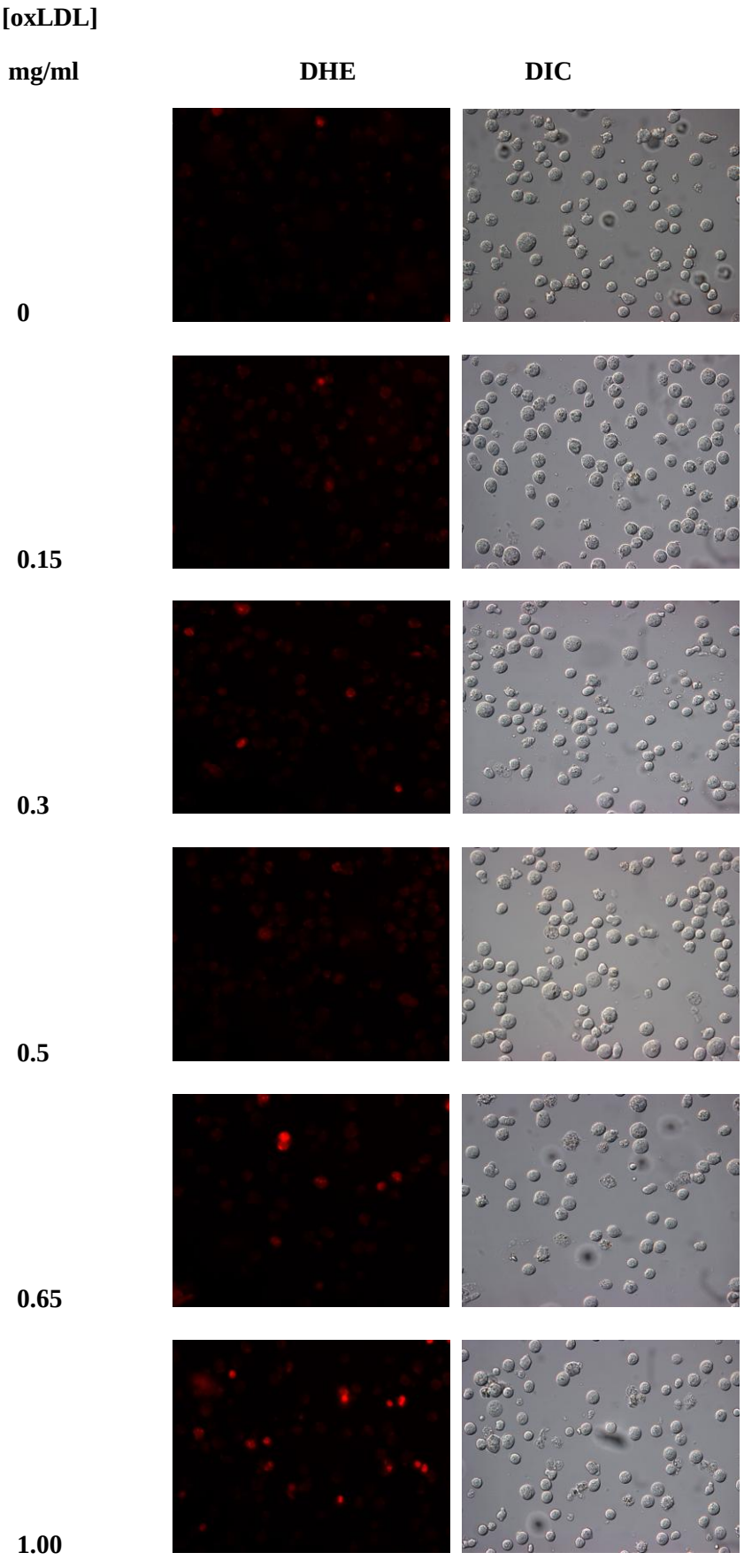

Figure 3.4 B)

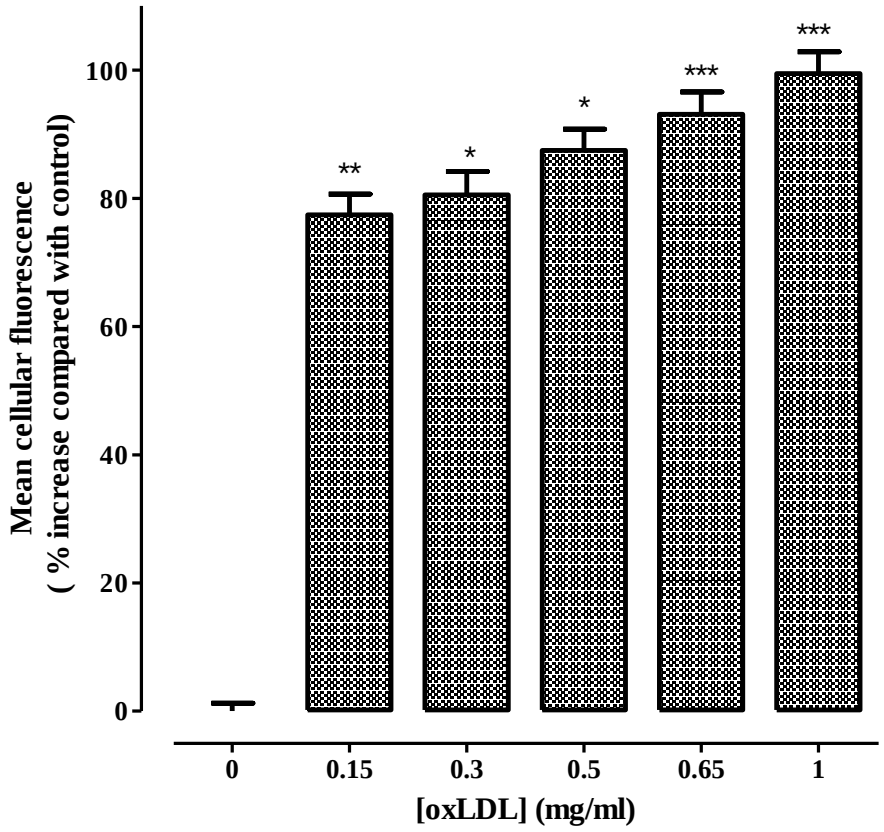

Figure 3.4 Effect of oxLDL on intracellular ROS production in U937 cells.

U937 cells (0.5×10^6 cells/ml) were incubated in RPMI-1640 containing the increasing concentrations of oxLDL for 3 hours at 37 ^{o}C. A control with 0 mg/ml oxLDL added was also included. At the end of treatment, washed cells were stained with 10 μM DHE for 20 minutes in dark for the fluorescence probing of intracellular superoxide. A) The cells were then viewed under a fluorescence microscope (λex/λem of 500-530 nm/590-620 nm). DIC photos for each of the respective fluorescence photos are shown. B) Cellular fluorescence intensities are converted to numerical values using Image J software, and results are presented as a percentage of the control value (0 mg/ml oxLDL added). Significance is indicated from this control. 500 cells in each treatment were collected for quantification, and results shown are mean fluorescence ± SEM of triplicate experiments.

3.2.2 The effect of oxLDL on mitochondrial superoxide generation in U937 cells

It is known that mitochondria is a potential source of superoxide production, and the organelle undergoes oxidative damage upon exposure to oxLDL (Zmijewski et al., 2005). Therefore, the effect of oxLDL on mitochondrial superoxide production in U937 cells was studied by treating cells with increasing concentration of oxLDL for 3 hours, followed by

staining with MitoSox Red which is specifically targeted to mitochondrial superoxide (see **section 2.2.8.2**).

The fluorescence images (**Figure 3.5A**) and the numerical values converted from those images (**Figure 3.5B**) illustrate a concentration-dependent increase in the MitoSox Red fluorescence. Cells exposed to 0.15 mg/ml oxLDL did not show significant fluorescence change compared to the non-treated control cells. OxLDL at the concentration of 0.3 and 0.5 mg/ml caused an increase in the fluorescence intensities by 20 % and 30 %, respectively. Cells treated with 0.65 and 1 mg/ml oxLDL showed a dramatic rise in the fluorescence intensities by 55 % and 90 % compared to the control, respectively, suggesting that oxLDL induced mitochondrial superoxide production as early as 3 hours incubation. Also noteworthy is that this experiment was performed concurrently with the above DHE staining (**Figure 4)** using the same batch of oxLDL. Compared to the pattern of oxLDL-induced intracellular ROS production, the concentration-dependent increase in the mitochondrial superoxide generation caused by oxLDL appeared to be more linear. This means mitochondrial superoxide production could be a secondary event initiated by the excess ROS generated in the cytoplasm. These comparable effects of oxLDL on intracellular and mitochondrial superoxide production indicate that the oxidative damage on mitochondria caused by oxLDL could be a later event, and the increased oxidative stress was primarily raised from a source outside the mitochondria.

Figure 3.5 A)

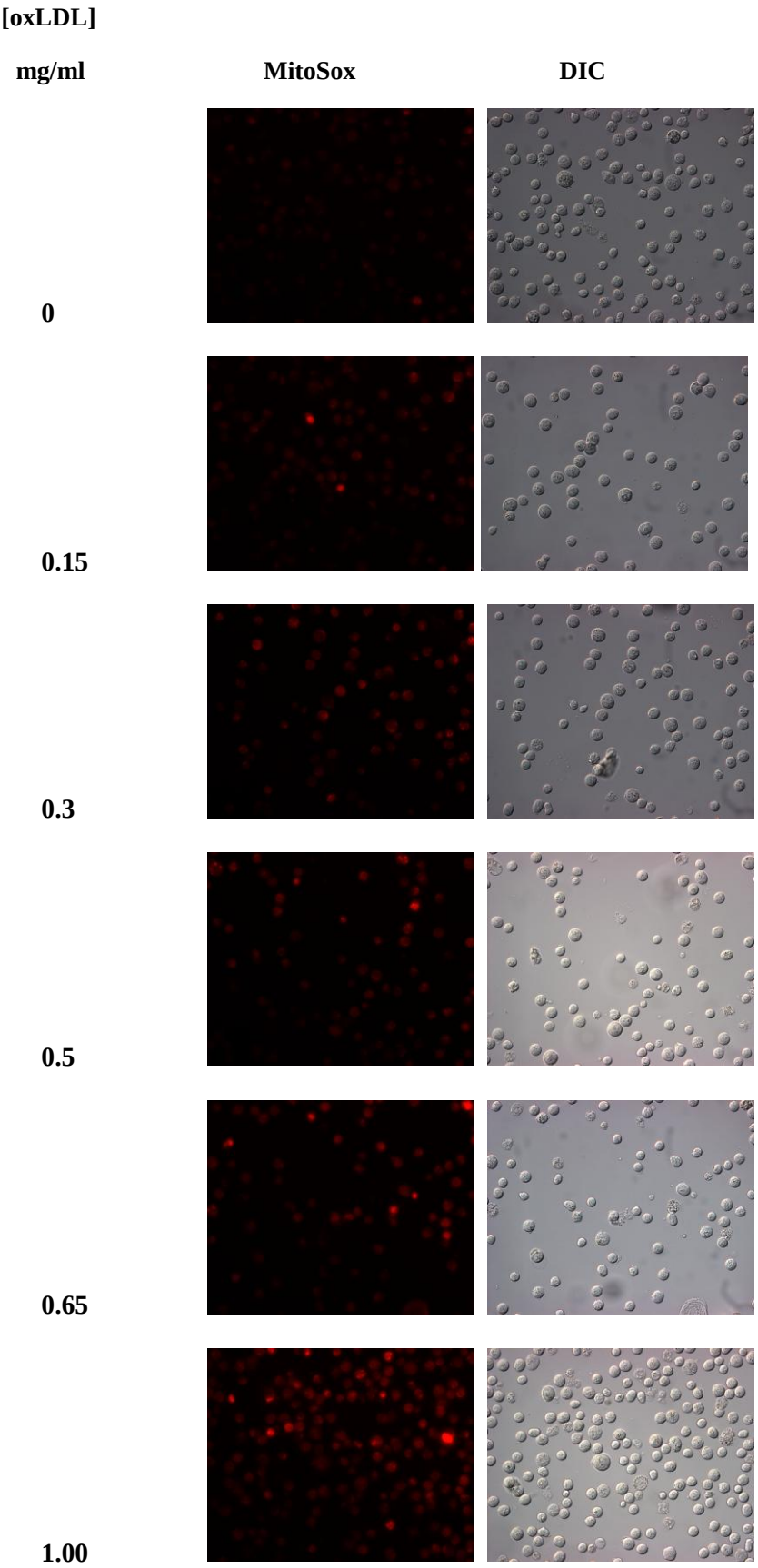

Figure 3.5 B)

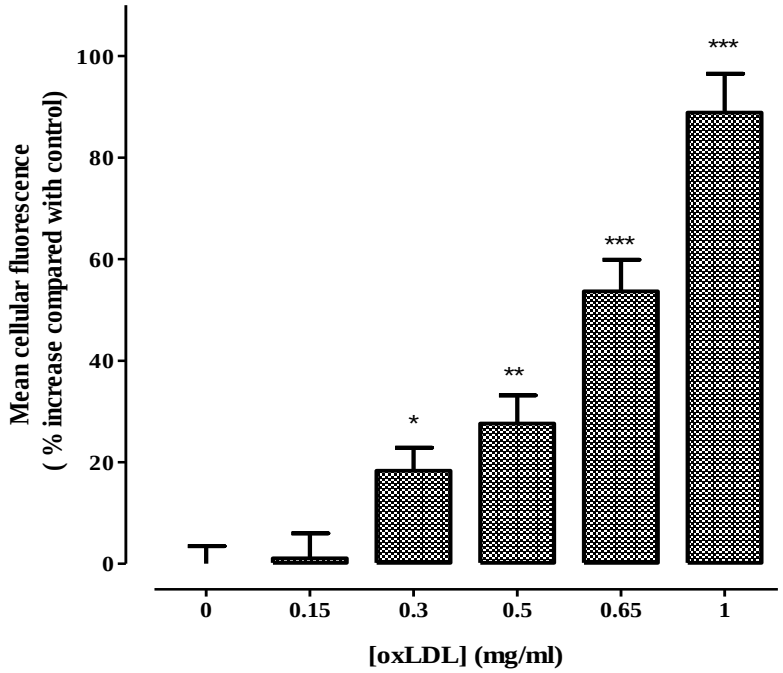

Figure 3.5 Effect of oxLDL on mitochondrial superoxide production in U937 cells.

U937 cells (0.5×10^6 cells/ml) were incubated in RPMI-1640 containing the increasing concentrations of oxLDL for 3 hours at 37 ^oC. A control with 0 mg/ml oxLDL added was also included. At the end of treatment, washed cells were stained with 5 μM MitoSox red for 10 minutes in dark for the fluorescence probing of mitochondrial superoxide. A) The cells were then viewed under a fluorescence microscope (λex/λem of 510 nm/580 nm). DIC photos for each of the respective fluorescence photos are shown. B) Cellular fluorescence intensities are converted to numerical values using Image J software, and results are presented as a percentage of the control value (0 mg/ml oxLDL added). Significance is indicated from this control. 500 cells in each treatment were collected for quantification, and results shown are mean fluorescence ± SEM of triplicate experiments.

3.2.3 The effect of oxLDL on intracellular GSH levels in U937 cells

GSH is the key component of intracellular antioxidant defence system controlling the redox-thiol state, and GSH depletion appears to be a potential indicator of oxidative stress within the cell (Gieseg et al., 2009b). The effect of oxLDL on cellular GSH levels in U937 cell was thus investigated by exposing cells to 0.5 mg/ml oxLDL, and the intracellular GSH levels were subsequently determined by HPLC analysis at various time points (**Figure 3.6**). At the 0 time point, the cellular GSH was measured as 4.12 nmol/10^6 cells, and it dropped rapidly by 20 % after 1 hour of incubation with oxLDL. Following a 3-hour

treatment, a 55% intracellular GSH loss was observed and this decrease continued until only 6 % cellular GSH was left after 9 hours of treatment.

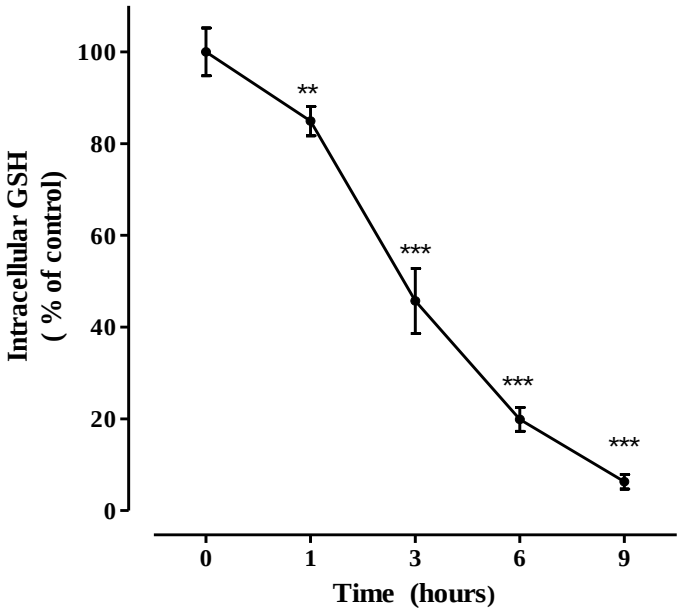

Figure 3.6 Time course study of oxLDL-induced GSH loss in U937 cells.

U937 cells (0.5×10^6 cells/ml) were incubated in RPMI-1640 containing 0.5 mg/ml oxLDL at 37 ^oC. At various times, the cells were removed and intracellular GSH was measured by HPLC analysis. Data are expressed as a percentage of the respective control value at 0 hour which was 4.12 nmol/10^6 cells, and significance is indicated from this control. Results displayed are the mean ± SEM of triplicates from a single experiment, representative of three separate experiments.

3.2.4 The effect of oxLDL on intracellular aconitase activity in U937 cells

Many studies have shown aconitase is prone to suffer from oxidative damage with a significant activity loss when exposed to superoxide (Yarian and Sohal, 2005, Cabiscol et al., 2000, Gardner et al., 1994). Therefore, the effect of oxLDL on intracellular aconitase was studied in order to further investigate the oxidative stress induced by oxLDL in U937 cells.

OxLDL-treated cells exhibited a concentration-dependent decrease in the intracellular aconitase activity after incubating with different concentrations of oxLDL for 24 hours (**Figure 3.7**). It should be noted that aconitase exists in both the mitochondria and cytoplasm, and this study measured the combined intracellular aconitase activity, rather than those in the isolated organelles. Depending on the various conditions of cells during the assay, the aconitase activity in non-treated cells was found to vary between 1.0 and 6.0

mU/mg protein. This result shown was a representative experiment of triplicate, and the total intracellular aconitase activity in the control cells was initially measured as 4.25 mU/mg protein. Cells incubated with 0.1 mg/ml oxLDL did not show any damage to aconitase possibly because the oxLDL at low concentration was insufficient to cause oxidative damage to cellular proteins. However, upon the addition of 0.2 and 0.5 mg/ml oxLDL, the intracellular aconitase loss reached 20 % and 25 % of the total activity respectively. Only 0.356 mU/mg protein of total aconitase activity (10 % of the respective control) was observed in cells exposed to 1 mg/ml oxLDL. These results clearly show that oxLDL-induced oxidants production caused oxidative modification on intracellular aconitase, resulting in the protein inactivation.

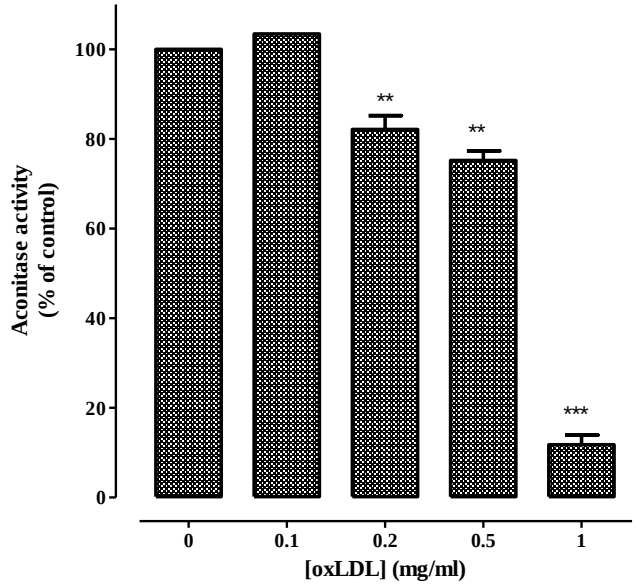

Figure 3.7 Effect of increasing concentrations of oxLDL on aconitase activity in U937 cells.

U937 cells (0.5×10^6 cells/ml) were treated with the increasing concentrations of oxLDL, followed by incubation at 37°C in RPMI-1640 for 24 hours. A control without oxLDL was also included. Intracellular aconitase activities were assayed after two PBS washes. Data are expressed as a percentage of the control value which was 4.25 mU/mg protein, and significance is indicated from this control. Results are displayed as mean ± SEM of triplicates from a single experiment, representative of three separate experiments.

To examine the progression of oxLDL-mediated aconitase activity loss in U937 cells, a time course study was also carried out by incubating cells with 0.5 mg/ml oxLDL and assaying the combined intracellular aconitase activity at various time points (**Figure 3.8**). The intracellular aconitase activity was assayed as 1.436 mU/mg protein prior to the addition of oxLDL, but it decreased rapidly by 50 % following a 3 hour incubation with

oxLDL and continuously dropped by 60 % after 6 hours. A further progressive decline was detected over the next 3 hours until only 9 % aconitase activity measured at 9 hours treatment, and there was no further change at 24 hours. It should note that oxLDL-induced aconitase activity loss occurred coincidently with the GSH loss (**Figure 3.6**) and ROS production (**Figure 3.3**) shown previously within 3 hours after oxLDL treatment, and these events were far more severe in the first 3 hours than the oxLDL-induced cell viability loss. These imply that oxLDL-induced cell death possibly occurs only after significant oxidative damage to cellular components and the cellular metabolism failure happens.

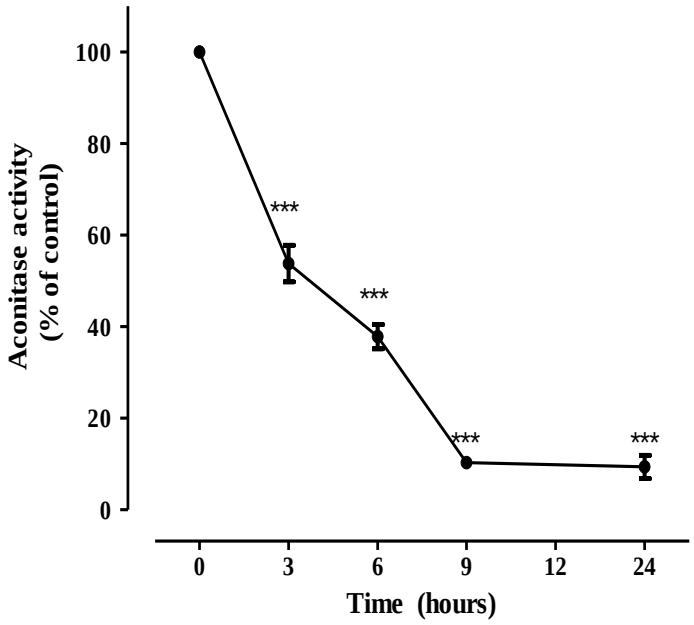

Figure 3.8 Time course study of oxLDL-induced aconitase activity loss in U937 cells.

U937 cells (0.5×10^6 cells/ml) were incubated in RPMI-1640 containing with 0.5 mg/ml oxLDL at 37 ^{o}C. At various times, the cells were removed and intracellular aconitase activity was assayed after two PBS washes. Data are expressed as a percentage of the respective control value at 0 hour which was assayed as 1.436 mU/mg protein, and significance is indicated from this control. Results are displayed as mean ± SEM of triplicates from a single experiment, representative of three separate experiments.

3.2.5 The effect of oxLDL on intracellular calcium levels in U937 cells

Free Ca^{2+} ions are key signalling molecules within cells with the concentration tightly regulated between 100 to 200 nM in both the mitochondria and cytosol, and the abnormal increase can lead to both the apoptotic and necrotic cell death (Halliwell and Gutteridge, 2007a). It was previously found that HOCl-induced oxidative stress in HMDM resulted in intracellular Ca^{2+} influx, which was responsible for the Ca^{2+}-dependent cell death (Yang et

al., 2012). With the aim of further investigating the correlation between the increased oxidative stress and the change in the intracellular Ca^{2+} levels, the effect of oxLDL on cytosolic Ca^{2+} level in U937 cells was therefore examined.

Cells were probed with the cell-permeable fluorescent indicator, fluo-3AM, for the detection of free cytosolic Ca^{2+} (see **section 2.2.8.3**). The cells were exposed to 0.5 mg/ml oxLDL in calcium-containing RPMI-1640 medium without phenol red, followed by examination of the fluorescence by fluorescence microscope (**Figure 3.9A**) and the fluorescence intensities were also quantified based on the fluorescence images (**Figure 3.9B**). An initial rise by 5-fold in the fluorescence intensity was observed in the first 2-hour incubation with oxLDL. Followed by a deep drop by 250 % at 3 hour time point, a secondary increase in the fluorescence intensity by approximately 3-fold was detected before reaching a maximum in the next hour. Apart from the fluctuation in the fluorescence intensity over the 6-hour treatment, it should be particularly noted that the detectable increase in the fluorescence occurred as early as 5 minute after treatment, suggesting oxLDL evoked intracellular Ca^{2+} influx very fast and much earlier than any other oxidative damage studied so far, such as superoxide production, GSH loss, and aconitase activity loss. Hence, cytosolic Ca^{2+} increase could be a secondary initiator of the subsequent oxidative damage in response to oxLDL.

In considering the fluctuation in the fluorescence intensities, the probed cells were also analysed by flow cytometry. **Figure 3.10A** shows the flow cytometry histogram plot of fluorescence intensity against the cell number in the presence of oxLDL. Cells displayed a time-dependent shifting in the fluorescence over the first 3 hour of incubation, indicating a continuous rise in the intracellular Ca^{2+} levels in the first 3 hours. The fluorescence intensities seemed to stay stable over the next 3 hour treatment. **Figure 3.10B** is the quantification of fluorescence intensity measured by flow cytometry over a 6-hour treatment. A slight increase by 30 % in the fluorescence intensity compared to the starting point was observed after a 5-minute incubation with oxLDL, which agreed with that found using the fluorescence microscope; though this was not statistically significant. The fluorescence intensity was then elevated dramatically by 4.5-fold within 3 hours incubation with oxLDL, followed by a slight increase in the next hour and then reaching a plateau. Surprisingly, the deep decrease in the fluorescence intensity observed by fluorescence

microscope at 3 hours time point was not observed by flow cytometry. This is hard to explain at this stage. The important information suggested from these results is that the cytosolic free Ca^{2+} increase occurred very fast and it appears to be the primary event upon exposure to oxLDL which may be responsible for the subsequent cellular oxidative modifications.

To confirm that the detected fluorescence was resulted from Ca^{2+} reacting with fluo-3AM dye, not from oxLDL reacting with the dye, a positive control using calcium ionophore A23187 (Br-A) was therefore performed. Calcium ionophore A23187 is a lipid soluble molecule that is highly selective for Ca^{2+} and greatly increase the ability of Ca^{2+} to cross cell membrane. The fluorescence images (**Figure 3.11A**) and the numerical values converted from the fluorescence intensity (**Figure 3.11B**) showed U937 cells exhibited a concentration-dependent increase in the fluorescence intensity by 40 % to 80 % compared to the control after 3-hour incubation with 1 to 8 μM of A23187.

Figure 3. 9 A)

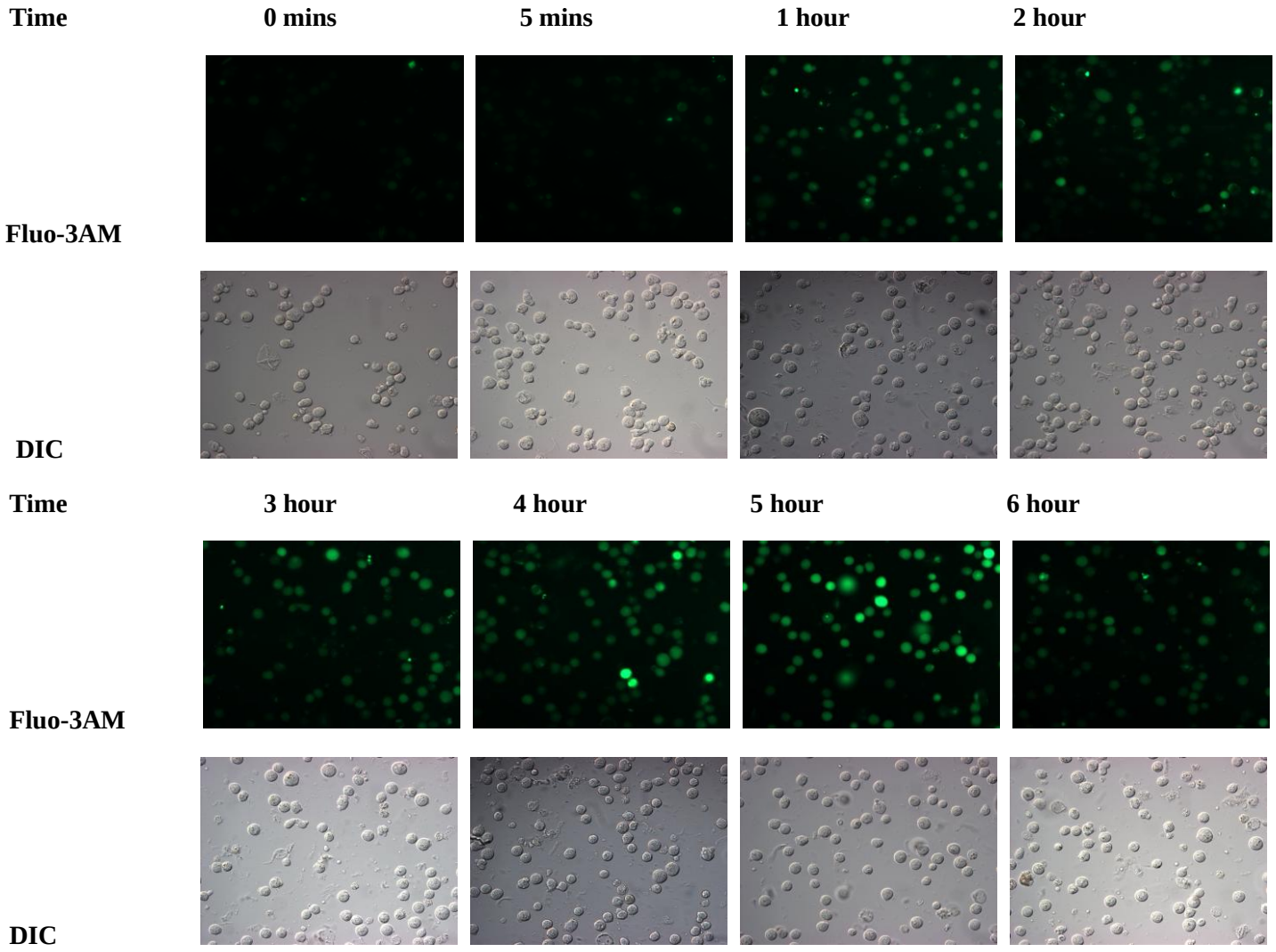
Time
0 mins
5 mins
1 hour
2 hour
Fluo-3AM
DIC
Time
3 hour
4 hour
5 hour
6 hour
Fluo-3AM
DIC

Figure 3. 9 B)

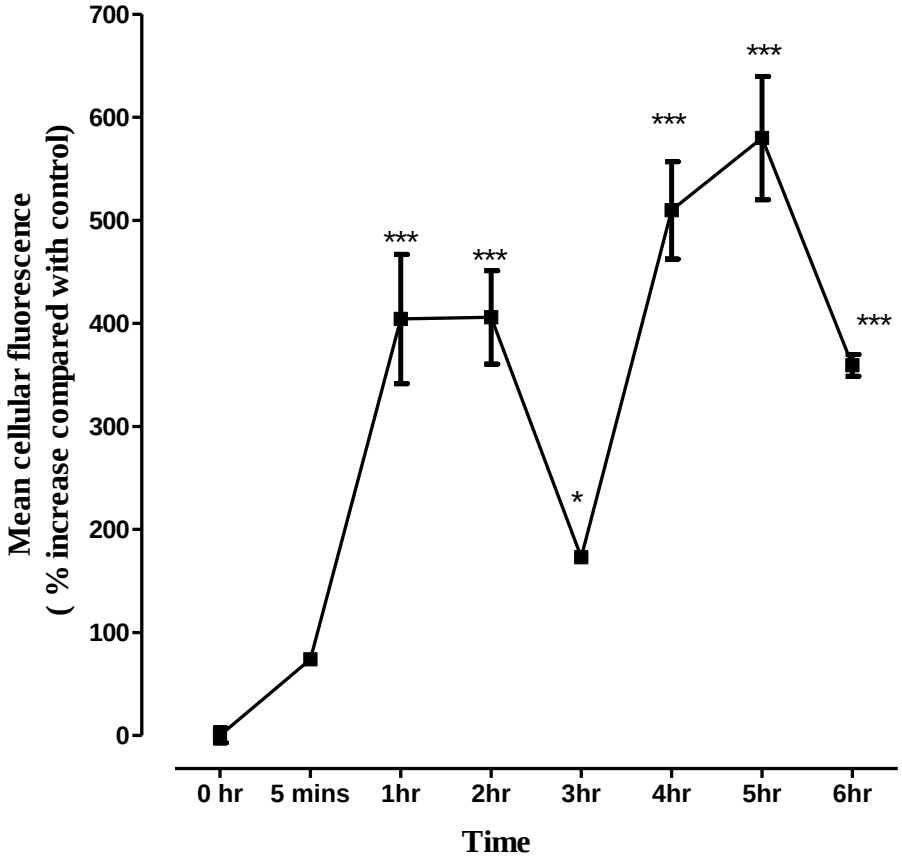

Figure 3.9 Effect of oxLDL on intracellular cytosolic Ca^{2+} levels in U937 cells (by fluorescence microscope).

U937 cells (0.5×10^6 cells/ml) were pre-incubated with 10 μM Fluro-3AM for 1 hour, followed by treatment with 0.5 mg/ml oxLDL in non-phenol red RPMI-1640 at 37 ^oC. A) At various times, cell samples were removed and viewed under a fluorescence microscope (λex/λem =488/530 nm). DIC photos for each of the respective fluorescence photos are shown. B) Cellular fluorescence intensities are converted to numerical values using Image J software, and results are presented as a percentage of the respective control value at 0 hour. Significance is indicated from this control. 500 cells in each treatment were collected for quantification, and results shown are mean fluorescence ± SEM of duplicate experiments.

Figure 3.10 A)

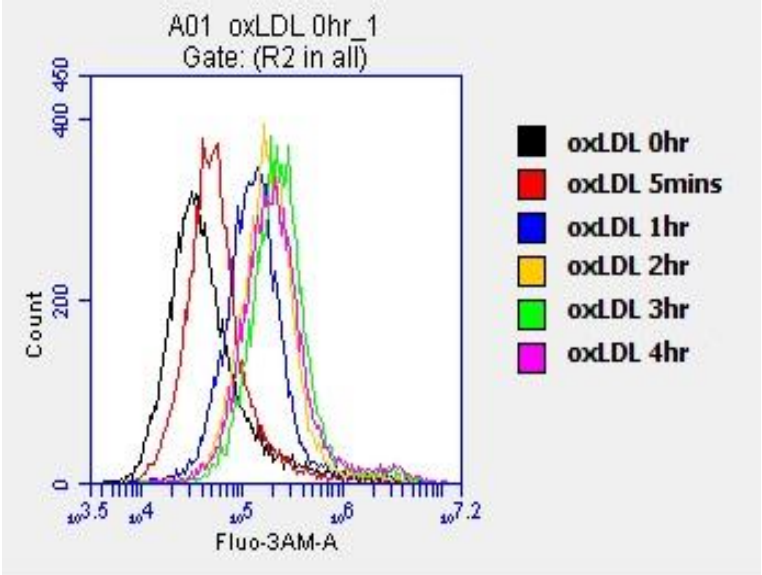

Figure 3.10 B)

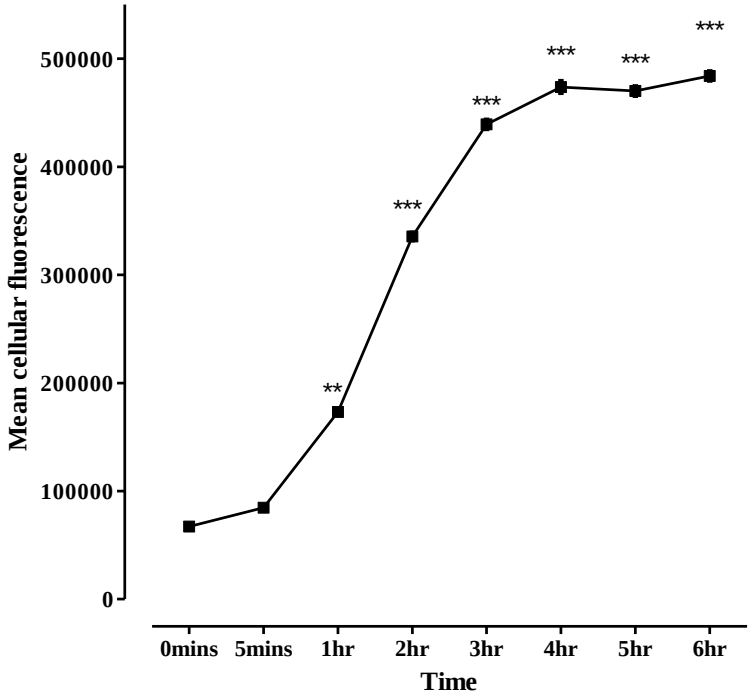

Figure 3.10 Effect of oxLDL on intracellular cytosolic Ca^{2+} levels in U937 cells (by flow cytometry).

U937 cells (0.5×10^6 cells/ml) were pre-incubated with 10μM Fluro-3AM for 1 hour, followed by treatment with 0.5mg/ml oxLDL in non-phenol red RPMI-1640 at 37°C. At various times, cell samples were removed and analysed by flow cytometry. A) shows the representative flow cytometry histogram plot of cell counts against Fluro-3AM fluorescence over 4 hours. B) shows the mean cellular fluorescence measured by flow cytometry over 6 hours. 10,000 cells were randomly collected for analysis. Significance is indicated from the 0 time point data. Results shown are mean fluorescence ± SEM of triplicate experiments.

Figure 3. 11 A)

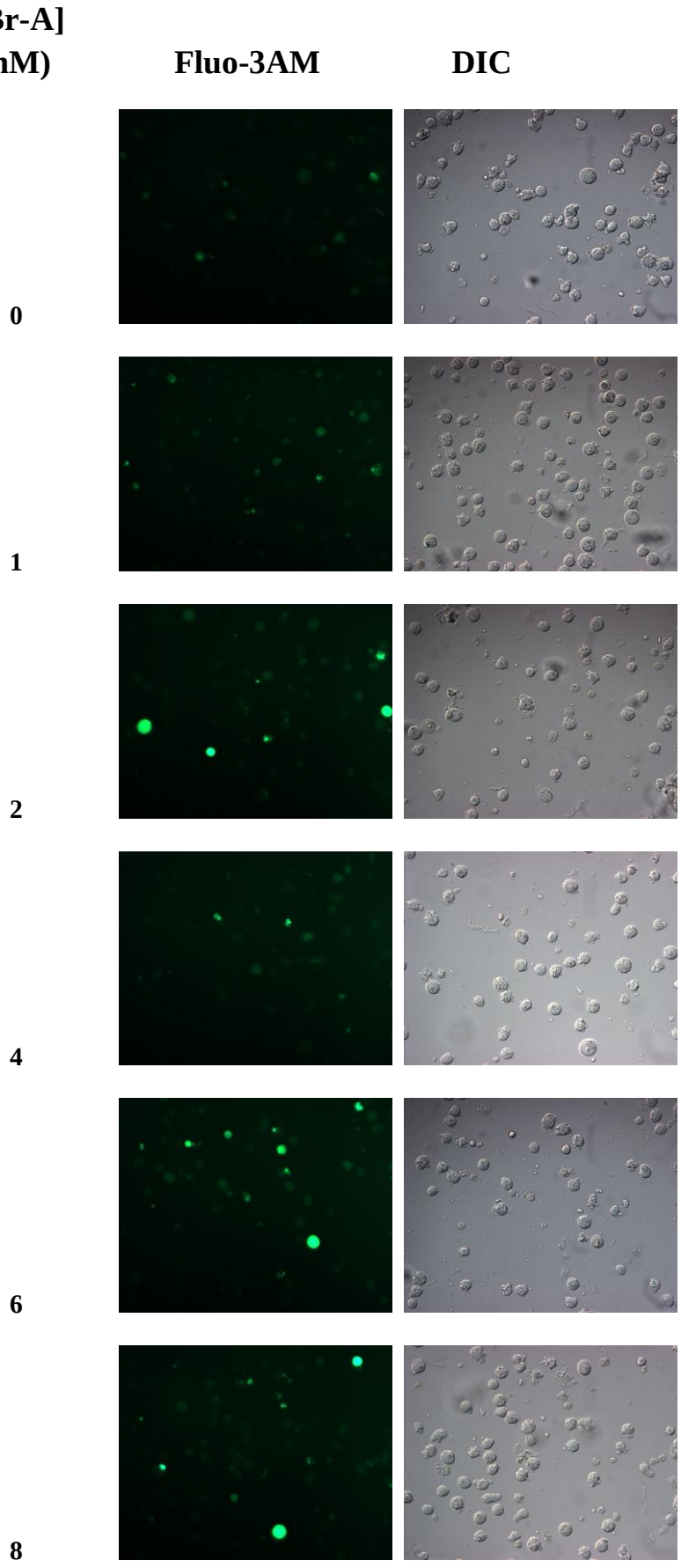

Figure 3. 11 B)

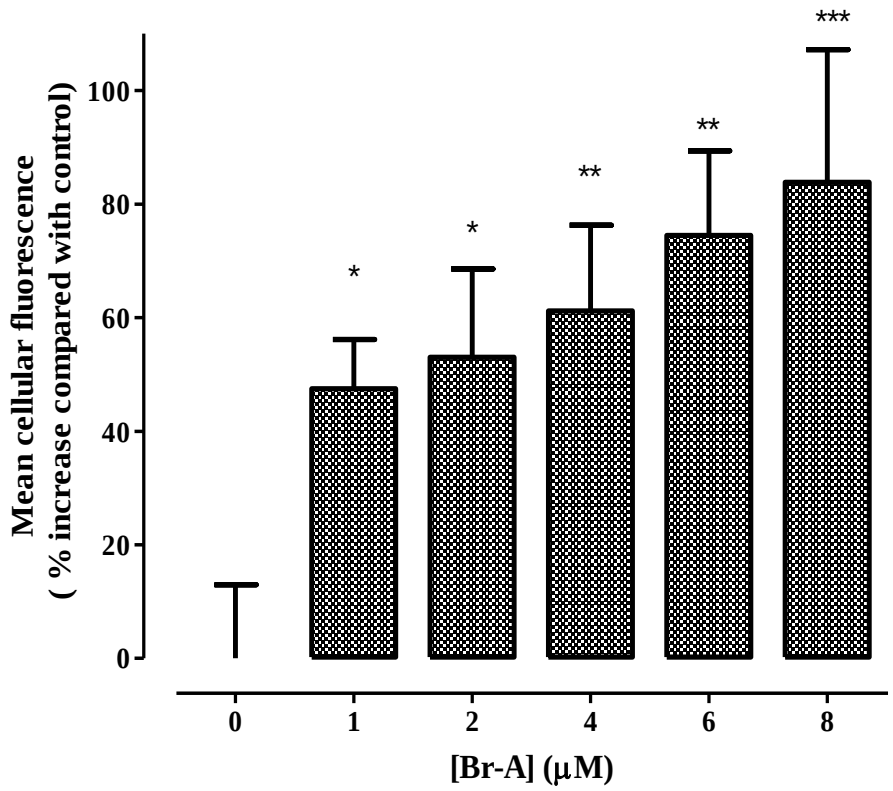

Figure 3.11 Ca^{2+} ionophore A23187 (Br-A) induced an increase in cytosolic Ca^{2+} in U937 cells.

U937 cells (0.5×10^6 cells/ml) were pre-incubated with 10 μM Fluo-3AM ester for 1 hour, followed by the treatment with the increasing concentrations of calcium ionophore A23187 (Br-A) in non-phenol red RPMI 1640 for 3 hours. A control with 0μM Br-A added was also included. A) The cells were then viewed under a fluorescence microscope (λex/λem = 488/530 nm). DIC photos for each of the respective fluorescence photos are shown. B**)** Cellular fluorescence intensities are converted to numerical values, which are presented as a percentage of the control (0μM Br-A added) and significance is indicated from this control value. 500 cells in each treatment were collected for quantification, and results shown are mean fluorescence ± SEM of triplicate experiments.

3.3 NADPH oxidase (NOX) is the major oxidative stress site

An increasing body of evidence suggests that oxidative stress caused by an excessive production of ROS is a major factor contributing to the progression of atherosclerosis. Yet the source of oxidative stress and how oxLDL triggers the oxidant production remains unclear. It is generally agreed that NOX is the predominant superoxide generating enzyme complex, so it was hypothesized that NOX may be a major source of oxidative stress in the atherosclerotic plaque. Therefore, the following studies aimed to investigate whether oxLDL activates NOX and the participating role of NOX in oxLDL-induced oxidative

stress via inhibitory studies. The effects of NOX inhibitor apocynin or diphenyleneiodonium (DPI) on oxLDL-induced cell viability loss, superoxide production, intracellular GSH loss, and aconitase activity loss in U937 cells will be examined. Cells were pre-treated with apocynin or DPI for 3 hours prior to the addition of oxLDL in the following experiments. The same experiments in the absence of oxLDL were also set up to determine the effects of apocynin or DPI itself on U937 cells.

3.3.1 Effect of apocynin and DPI on oxLDL-mediated cell death

In order to ensure that cell death was the result of oxLDL treatment, rather than apocynin or DPI, the cytotoxicity of apocynin or DPI itself on U937 cells were firstly examined by incubating cells with different concentrations of apocynin or DPI and measuring cell viability by the MTT reduction assay. There was only 10 % cell viability loss compared to the respective control after exposure to 10, 20, 50 and 100 μM apocynin for 24 hours, but no statistical significance was detected (**Figure 3.12A**), implying apocynin had no significant cytotoxic effect in the range of these dosages. By comparison, DPI-treated cells showed a concentration-dependent cell viability loss (**Figure 3.12B**). DPI at 1 μM did not affect the cell viability, but cells treated with 2 to 10 μM DPI had 10% cell death compared to the control, and the cell viability continued to decline by 20 % upon exposure to 20 and 100 μM DPI, suggesting that DPI was not significantly cytotoxic at low concentration (< 5 μM), but it could cause negative effects above 5 μM.

The effects of apocynin and DPI on oxLDL-mediated cell death were then assessed. Following a 24-hour treatment with oxLDL, 70 % of cell viability loss was observed compared to the cell-only control (**Figure 3.13A**). Pre-incubation with 10 – 100 μM of apocynin significantly elevated the cell viabilities by 10 – 20 % compared to oxLDL-treated cells. DPI at 1 μM prevented the oxLDL-mediated cell death by 10 %, but cells pre-treated with 2 – 5 μM DPI did not protect U937 cells against oxLDL-induced cell viability loss (**Figure 3.13B**). These two experiments were conducted concurrently using the same batch of oxLDL to ensure the oxLDL had the same toxicity.

Figure 3.12 A)

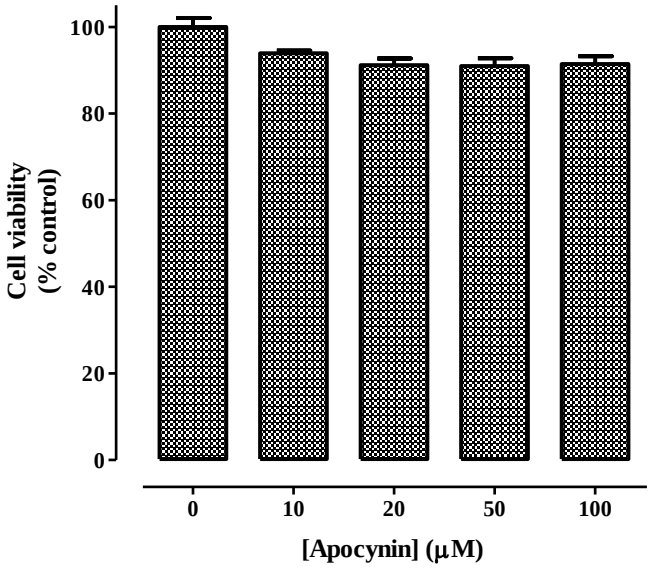

Figure 3.12 B)

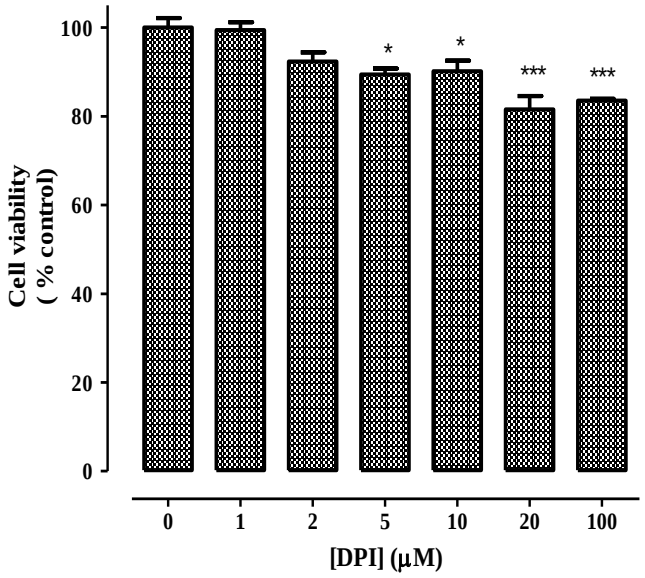

Figure 3.12 Effects of increasing concentrations of apocynin or DPI on cell viability in U937 cells.

U937 cells (0.5×10^6 cells/ml) were treated with the increasing concentrations of A) apocynin, or B) DPI, followed by incubation at 37 ^{o}C in non-phenol red RPMI-1640 for 24 hours. A control without apocynin or DPI was also included. Cell viability was subsequently analyzed using the MTT reduction assay. Data are expressed as a percentage of the respective control with the actual absorbance reading of 1.041 at 570nm. Significance is indicated from this value. Results are displayed as mean ± SEM of triplicates from a single experiment, representative of three separate experiments.

Figure 3.13 A)

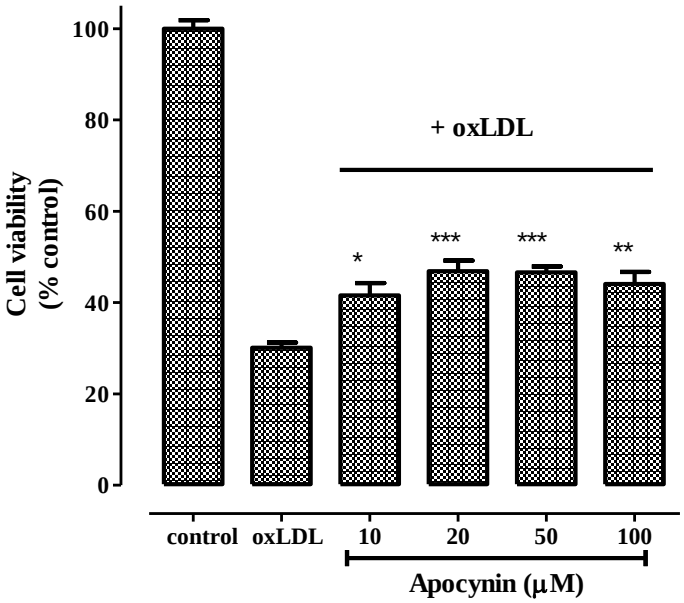

Figure 3.13 B)

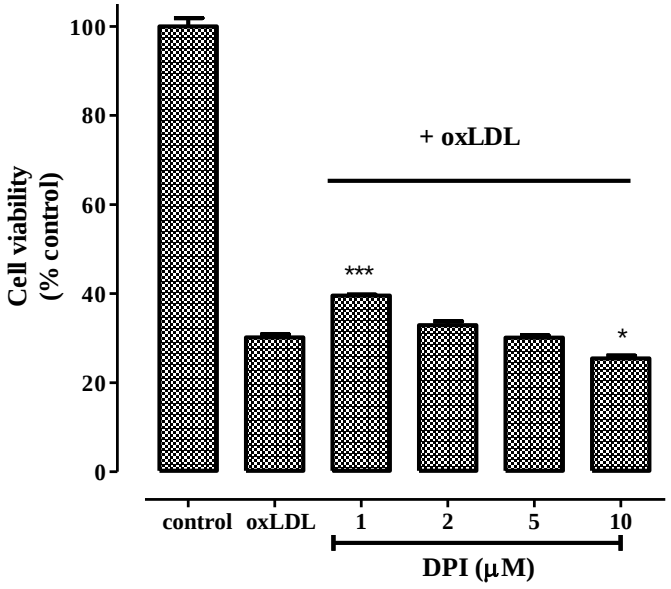

Figure 3.13 Effects of apocynin or DPI on oxLDL-mediated cell death in U937 cells.

U937 cells (0.5×10^6 cells/ml) were pre-incubated in RPMI-1640 containing the increasing concentrations of A) apocynin, or B) DPI for 3 hours at 37 ^{o}C, followed by treatment with 0.3 mg/ml oxLDL for 24 hours. A positive control without apocynin or DPI and a negative control with 0.3 mg/ml oxLDL but no apocynin or DPI were included. Cell viability was subsequently analyzed using the MTT reduction assay. Data are expressed as a percentage of the positive control with the actual absorbance reading of 1.041 at 570 nm.. Significance is indicated from the negative control. Results are displayed as mean ± SEM of triplicates from a single experiment, representative of three separate experiments.

7,8-Dihydroneopterin (7,8-NP) has been shown previously to efficiently prevent oxLDL-induced cell viability loss by scavenging radical flux and reduce oxidative stress (Gieseg et al., 2009a, Baird et al., 2005a). In order to have a clear insight into the contribution of NOX-derived oxidative stress to oxLDL-induced cell death, another MTT experiment which included the effects of 7,8-NP, apocynin and DPI on oxLDL-induced cell death all together were performed (**Figure 3.14**). Higher dosages of apocynin and DPI were used in this experiment in order to define their optimal concentrations should be used in U937 cells. Cells treated with apocynin and DPI in the absence of oxLDL were also included. In consistent with the above results **(Figure 3. 12)**, 100 μM apocynin did not affect the cell viability in the absence of oxLDL, while DPI at 10 μM decreased the cell viability by 10 % compared to the cell-only control. Cells treated with 0.5 mg/ml oxLDL remained 40 % viable after 24 hours, and pre-incubation with 200 μM 7,8-NP significantly brought back the cell viability back to 85 %. Treatments of cells with 50, 100 and 300 μM apocynin before incubation with oxLDL resulted in the increase in the oxLDL-induced cell viability loss by 15 %, 20 % and 10 %, respectively. These results agreed with what was shown in the previous figure, and they also indicated that the optimal concentration of apocynin protection against oxLDL appeared to be around 100 μM. Pre-incubation with 5 and 10 μM DPI protected the U937 cells from oxLDL-induced cell death by 20 % and 15 %, respectively. Yet DPI at 50 μM did not protect cells against oxLDL-induced cell viability loss, and in fact, caused a further decrease in viability by 20 % compared to oxLDL-treated cells, further confirming that DPI was only protective from oxLDL damages at low concentration (< 5 μM). There results implied that oxLDL stimulated NOX, and the activate NOX accounted for the resulting cell death. The data also indicate that DPI has other negative effects on the cells which place them in a considerable amount at stress.

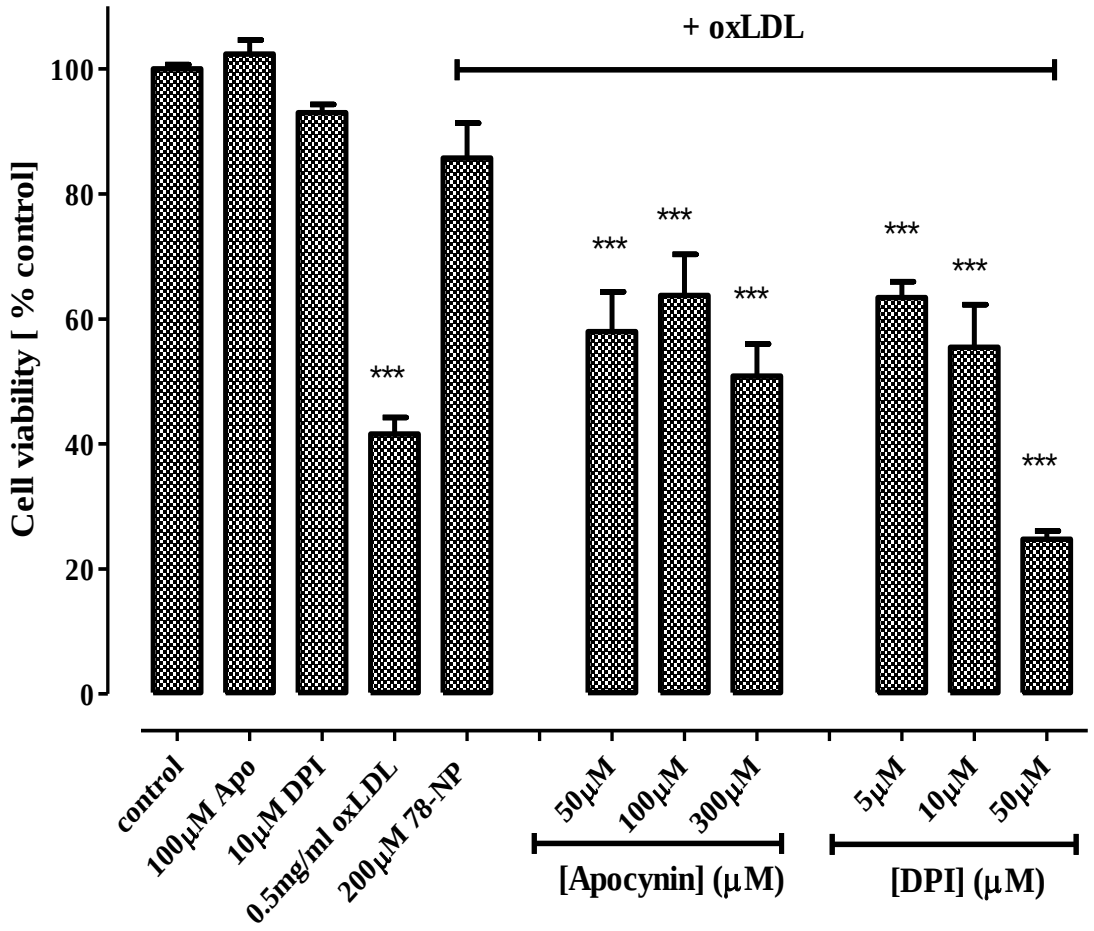

Figure 3.14 Effects of 78-NP, apocynin and DPI on oxLDL-mediated cell death in U937 cells.

U937 cells (0.5×10^6 cells/ml) were treated with 0.5mg/ml oxLDL after pre-incubation in RPMI-1640 containing either 200μM of 7,8-NP for 10 minutes or with the increasing concentrations of apocynin or DPI for 3 hours. Cells treated with 100μM and 10μM of apocynin and DPI, respectively, were also included. A positive control of cell-only treatment and a negative control with 0.5mg/ml oxLDL (no 7,8-NP ,apocynin or DPI added) were included. After 24 hours, cell viability was subsequently analyzed using the MTT reduction assay. Data are expressed as a percentage of the positive control with the actual absorbance reading of 0.641 at 570nm., and significance is indicated from the negative control (oxLDL-treated cells). Results are displayed as mean ± SEM of triplicates from a single experiment, representative of three separate experiments.

3.3.2 Effect of apocynin and DPI on oxLDL-mediated ROS production

Without oxLDL, apocynin within the concentration range of 10 – 100 μM did not cause much change in the DHE fluorescence intensity after 3 hours (**Figure 3.15**), implying apocynin itself did not induce ROS production in U937 cells. However, cells treated with DPI without oxLDL for 3 hours exhibited a dose-dependent increase in the fluorescence intensity (**Figure 3.16A**). DPI at 1 and 2 μM promoted the fluorescence intensities to increase by 40 % compared to the respective control, and 5 μM DPI significantly elevated the fluorescence intensity by 60 % (**Figure 3.16B**). 10 μM DPI caused a further fluorescence intensity rise by 90 % compared to the control. These result suggested that DPI itself induced superoxide generation in U937 cells, which could be responsible for the resulting cell death shown in **Figure 3.13**. Alternatively, it suggested that ROS scavenging is reduced by DPI.

The effect of apocynin and DPI on oxLDL-induced ROS generation in U937 cells was then examined. There was an immense fluorescence burst in cells treated with 0.3 mg/ml oxLDL after 3 hours (**Figure 3.17A**), and the fluorescence intensities was lifted by 60 % compared to the control (**Figure 3.17B**). Treatments of cells with 10 – 100 μM apocynin prior to oxLDL incubation significantly weakened the oxLDL-induced fluorescence increase, and the fluorescence intensities were lowered by 40 – 60 % compared to the oxLDL-treated cells, indicating apocynin efficiently inhibited oxLDL-mediated ROS generation. However, the similar pattern of protection was not seen in cells pre-treated with DPI. The oxLDL-promoted fluorescence increase was reduced to the control level (no oxLDL added cells) by DPI only at low concentration (< 5 μM) (**Figure 3.18A**). Pre-treatment of cells with 1 and 2 μM DPI significantly reduced the fluorescence intensities by 40 % and 60 % relative to the cells treated only with oxLDL (**Figure 3.18B**). The fluorescence intensities were slightly raised following the 5 μM DPI pre-treatment, but it was still 40 % less than oxLDL-treated cells. Yet cells pre-incubated with 10 μM DPI showed the same amount of fluorescence intensity with the oxLDL-treated cells, suggesting that DPI at 10 μM did not prevent oxLDL-induced ROS production at all. This agrees with the previous results that DPI only at the concentrations lower than 5 μM was protective against oxLDL-induced damage. These results also suggested that NOX was a key site for the intracellular ROS generation in response to oxLDL activation as the inhibition of NOX activity significantly suppressed oxLDL-induced ROS production.

Figure 3.15 A)

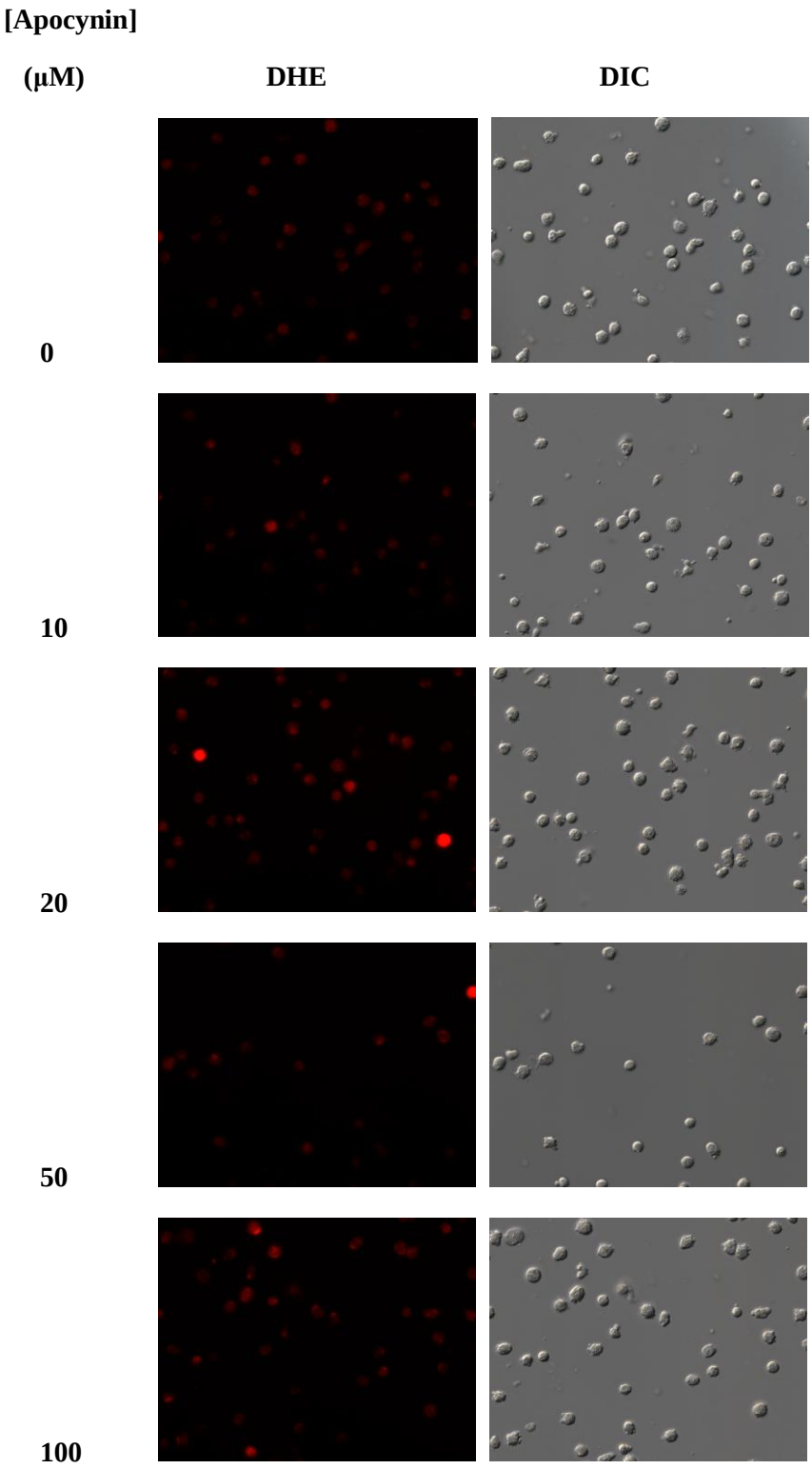

Figure 3. 15 B)

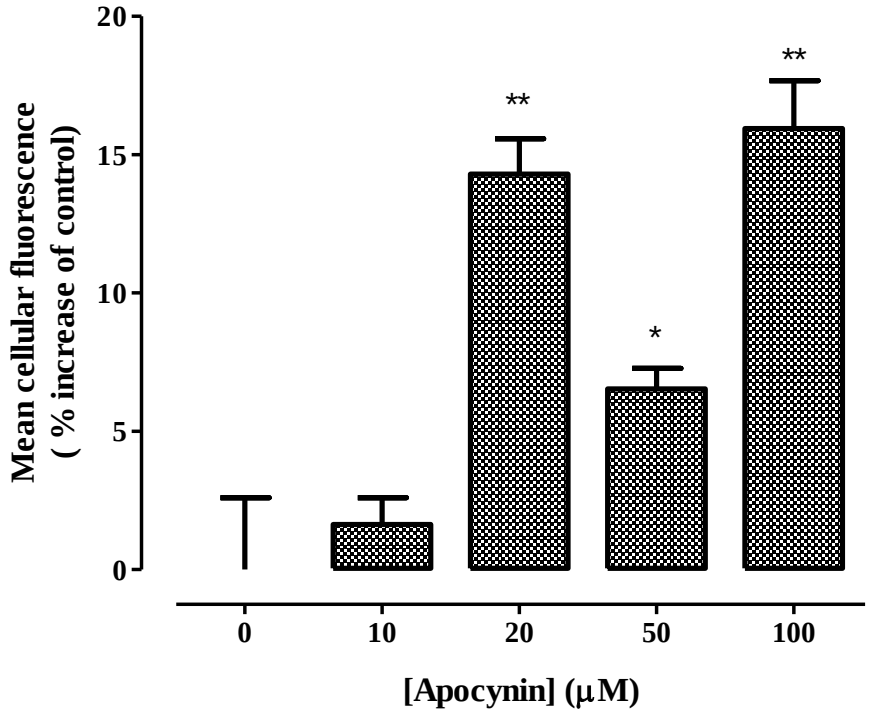

Figure 3.15 Effect of apocynin on ROS productions in U937 cells.

U937 cells (0.5×10^6 cells/ml) were incubated in RPMI-1640 containing the increasing concentrations of apocynin for 3 hours at 37°C. At the end of treatment, washed cells were stained with 10μM DHE for 20 minutes in dark for the fluorescence probing of intracellular superoxide. A) The cells were then viewed under a fluorescence microscope (λex/λem of 500-530nm/590-620nm). DIC photos for each of the respective fluorescence photos are shown. B) Cellular fluorescence intensities are converted to numerical values using Image J software, and results are presented as a percentage of the control (0μM apocynin added). No significance is detected from this control. 500 cells in each treatment were collected for quantification, and results shown are mean fluorescence ± SEM of triplicate experiments.

Figure 3. 16 A)

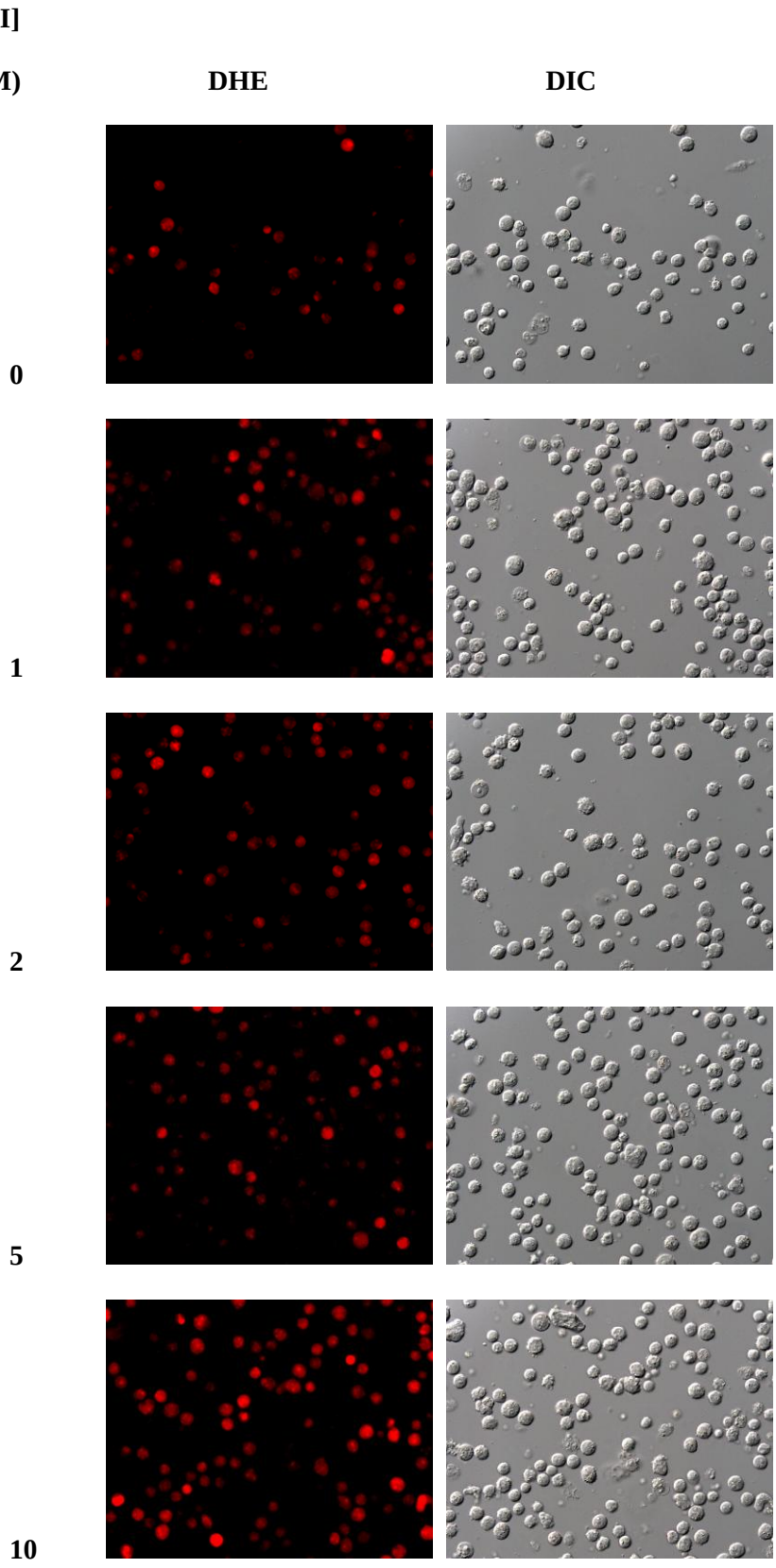

Figure 3.16 B)

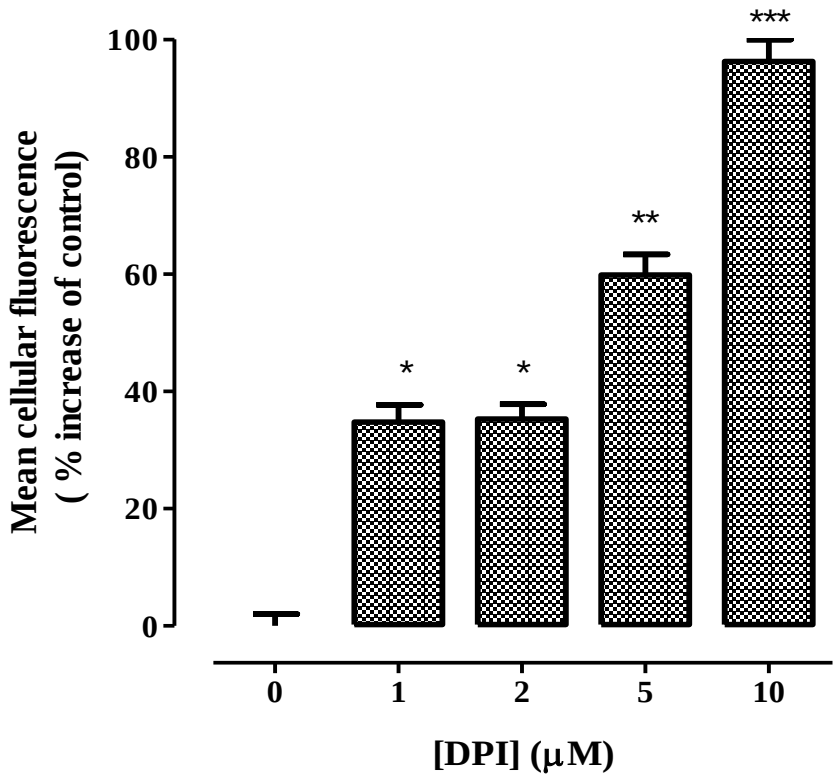

Figure 3.16 Effect of DPI on ROS productions in U937 cells.

U937 cells (0.5×10^6 cells/ml) were incubated in RPMI-1640 containing the increasing concentrations of DPI for 3 hours at 37°C . At the end of treatment, washed cells were stained with 10μM DHE for 20 minutes in dark for the fluorescence probing of intracellular superoxide. A) The cells were then viewed under a fluorescence microscope (λex/λem of 500-530nm/590-620nm). DIC photos for each of the respective fluorescence photos are shown. B) Cellular fluorescence intensities are converted to numerical values using Image J software, and results are presented as a percentage of the control (0μM DPI added). Significance is indicated from this control. 500 cells in each treatment were collected for quantification, and results shown are mean fluorescence ± SEM of triplicate experiments.

Figure 3. 17 A)

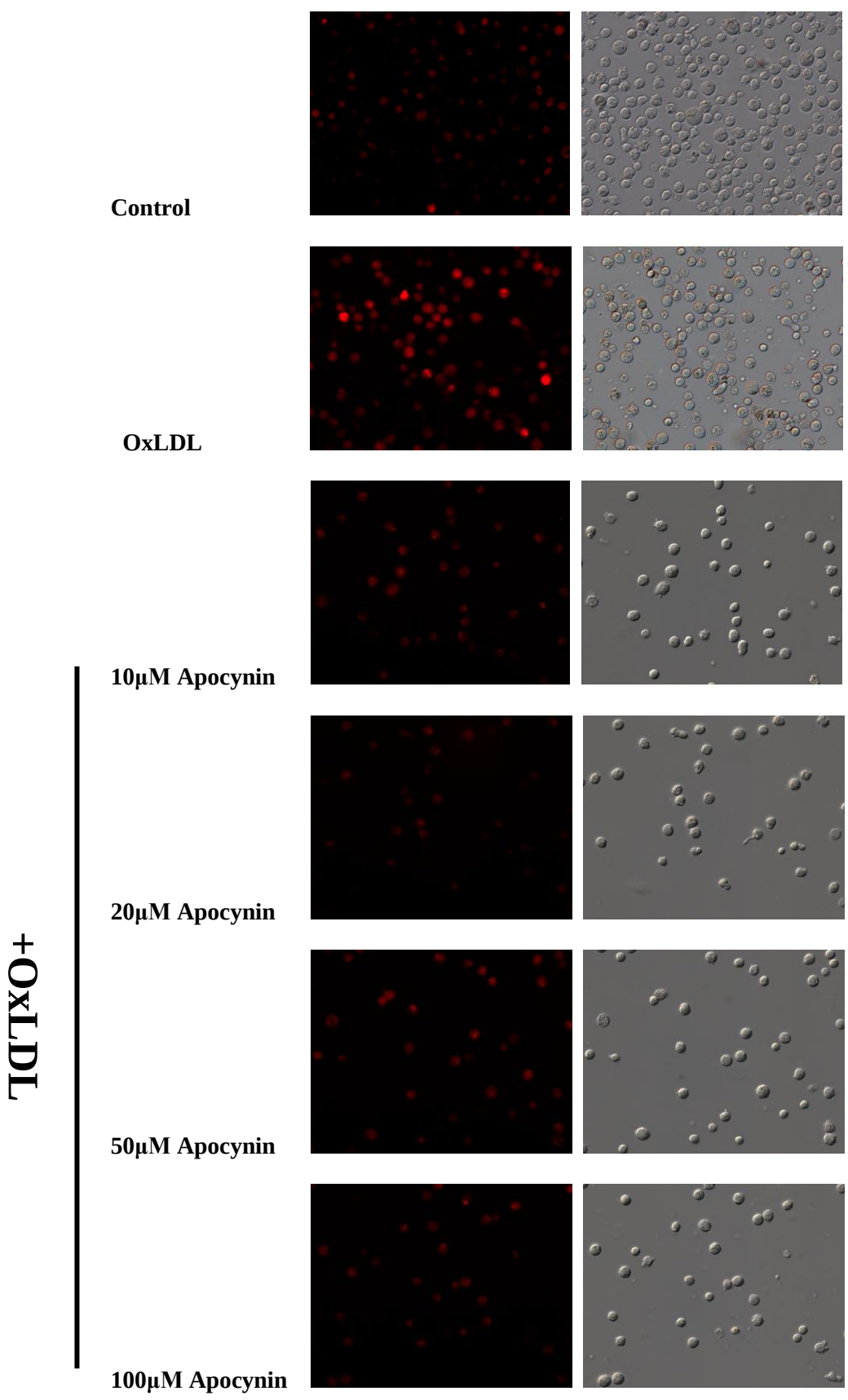
DHE
DIC
Control
OxLDL
10µM Apocynin
20µM Apocynin
50µM Apocynin
100µM Apocynin
+OxLDL

Figure 3.17 B)

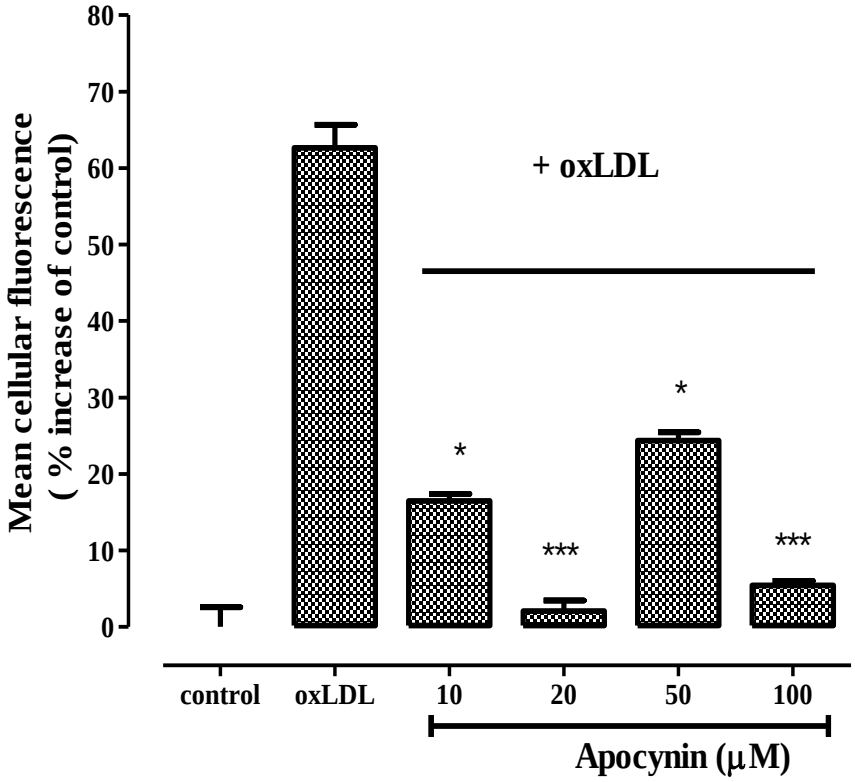

Figure 3.17 Effect of apocynin on oxLDL-induced ROS productions in U937 cells.

U937 cells (0.5×10^6 cells/ml) were pre-incubated in RPMI-1640 containing the increasing concentrations of apocynin for 3 hours at 37^oC , followed by treatment with 0.3 mg/ml oxLDL for another 3 hours. A positive control with cell-only treatment and a negative control with 0.3mg/ml oxLDL but no apocynin were also included. At the end of treatment, washed cells were incubated with 10μM DHE for 20 minutes in dark for the fluorescence probing of intracellular superoxide. A) The cells were then viewed under a fluorescence microscope (λex/λem of 500-530nm/590-620nm). DIC photos for each of the respective fluorescence photos are shown. B) Cellular fluorescence intensities are converted to numerical values using Image J software, and results are presented as a percentage of the positive control. Significance is detected from the negative control (oxLDL added only). 500 cells in each treatment were collected for quantification, and results shown are mean fluorescence ± SEM of triplicate experiments.

Figure 3. 18 A)

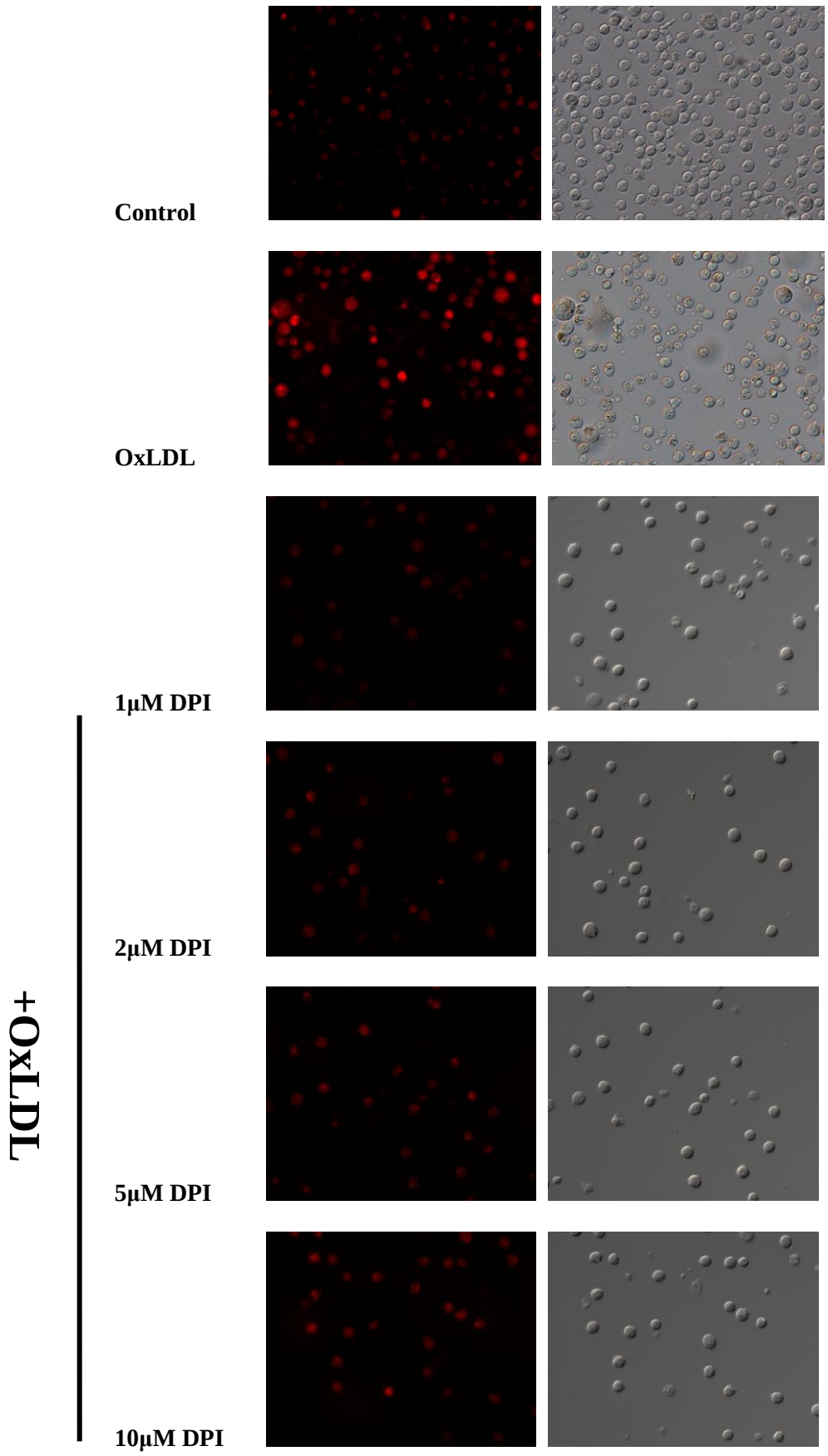

Figure 3. 18 B)

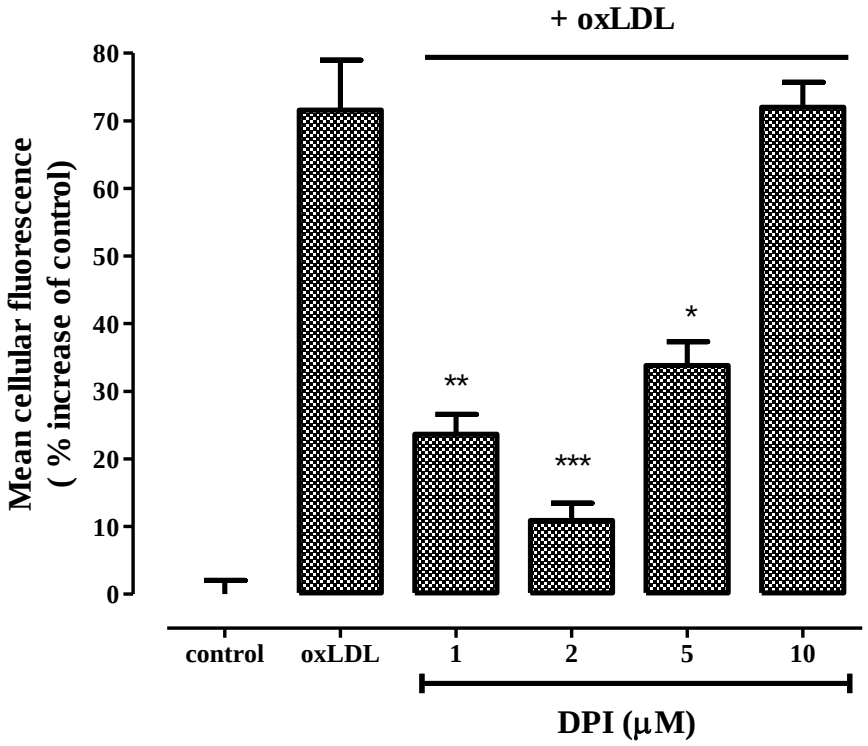

Figure 3.18 Effect of DPI on oxLDL-induced ROS productions in U937 cells.

U937 cells (0.5×10^6 cells/ml) were pre-incubated in RPMI-1640 containing the increasing concentrations of DPI for 3 hours at 37°C , followed by treatment with 0.3 mg/ml oxLDL for another 3 hours. A positive control with cell-only treatment and a negative control with 0.3 mg/ml oxLDL but no DPI were also included. At the end of treatment, washed cells were incubated with 10μM DHE for 20 minutes in dark for the fluorescence probing of intracellular superoxide. A) The cells were then viewed under a fluorescence microscope (λex/λem of 500-530nm/590-620nm). DIC photos for each of the respective fluorescence photos are shown. B) Cellular fluorescence intensities are converted to numerical values using Image J software, and results are presented as a percentage of the positive control. Significance is detected from the negative control (oxLDL added only). 500 cells in each treatment were collected for quantification, and results shown are mean fluorescence ± SEM of triplicate experiments.

3.3.3 Effect of apocynin and DPI on oxLDL-mediated GSH loss

Cells were treated with different concentrations of apocynin or DPI without oxLDL for 3 hours , followed by determination of intracellular GSH concentrations to examine whether apocynin or DPI itself affects intracellular GSH levels. Apocynin at 10 – 100 μM and DPI at 1 – 10 μM slightly caused fluctuations in the intracellular GSH levels, but none of them had a significant effect (**Figure 3.19**).

Figure 3.19 A)

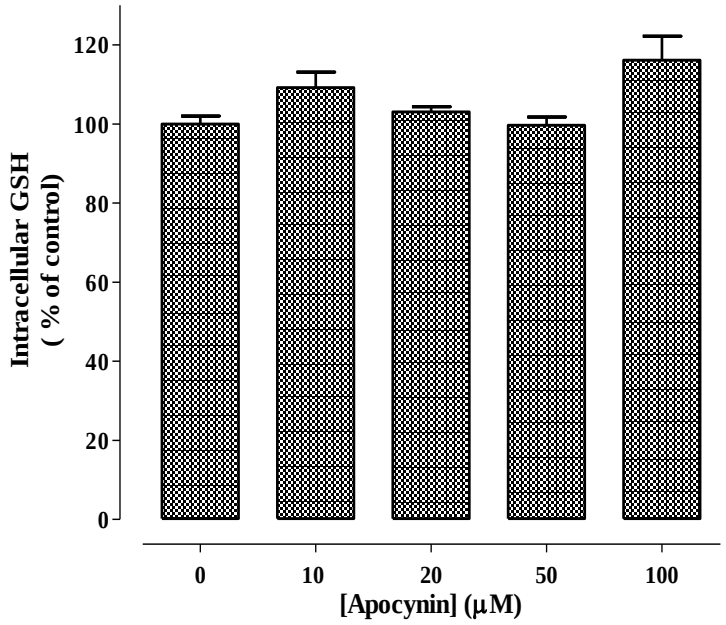

Figure 3.19 B)

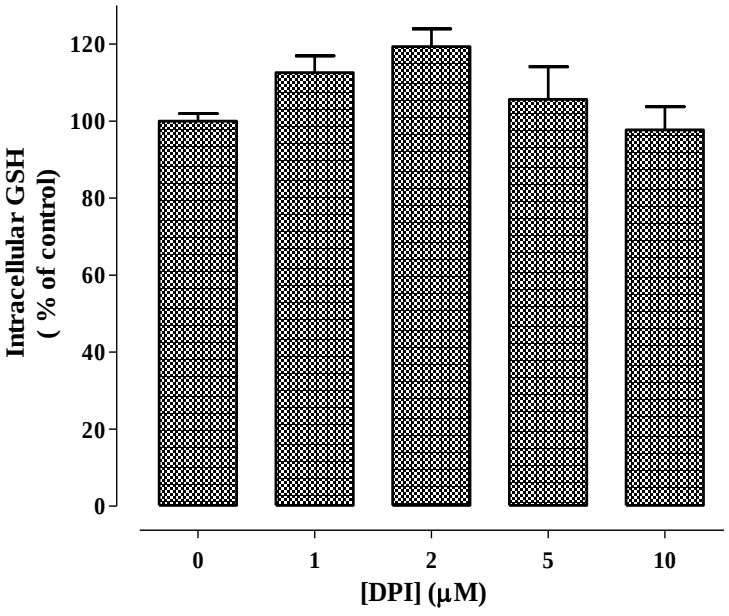

Figure 3.19 Effects of apocynin or DPI on intracellular GSH level in U937 cells.

U937 cells (0.5×10^6 cells/ml) were incubated in RPMI-1640 with the increasing concentrations of A) apocynin, or B) DPI for 3 hours at 37°C. A control with 0 μM apocynin or DPI added was included. Intracellular GSH was measured by HPLC analysis. Data are expressed as a percentage of the respective control value which is 3.53 nmol/10^6 cells. No significance is detected from this control. Results are displayed as mean ± SEM of triplicates from a single experiment, representative of three separate experiments.

Cells treated with 0.3 mg/ml oxLDL only for 3 hours caused a 40 % decrease in the intracellular GSH level compared to the respective control (**Figure 3.20A**). Pre-incubation of cells with apocynin before adding oxLDL completely prevented oxLDL-induced GSH loss, and in fact, the intracellular GSH levels were gradually elevated with the increasing concentration of apocynin. In the presence of oxLDL, 10 μM apocynin abolished the oxLDL-mediated GSH loss and brought it back to the control level. Apocynin at 20, 50 and 100 μM also prevented oxLDL-induced GSH loss, and the intracellular GSH levels were elevated by 20 %, 40 % and 60 % compared to the control, respectively. The examination of DPI on oxLDL-induced GSH loss were also performed concurrently using the same batch of oxLDL (**Figure 3.20B**). Similarly, pre-treatments of DPI also removed oxLDL-induced GSH loss, but different from the concentration-dependent increase caused by apocynin, the intracellular GSH levels in cells pre-incubated with 1 – 10 μM DPI were all increased by 60 % compared to the oxLDL-treated cells. This different pattern of the effect of DPI on oxLDL-induced GSH loss from that of apocynin could rise from the side effects of DPI itself on cells. These data implied that inhibition of NOX significantly prevented oxLDL-mediated GSH loss, and restored the intracellular redox environment.

Figure 3.20 A)

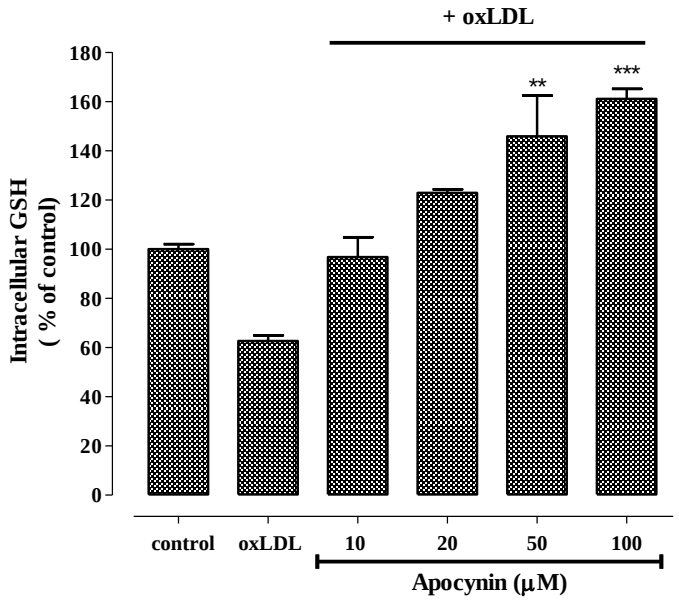

Figure 3.20 B)

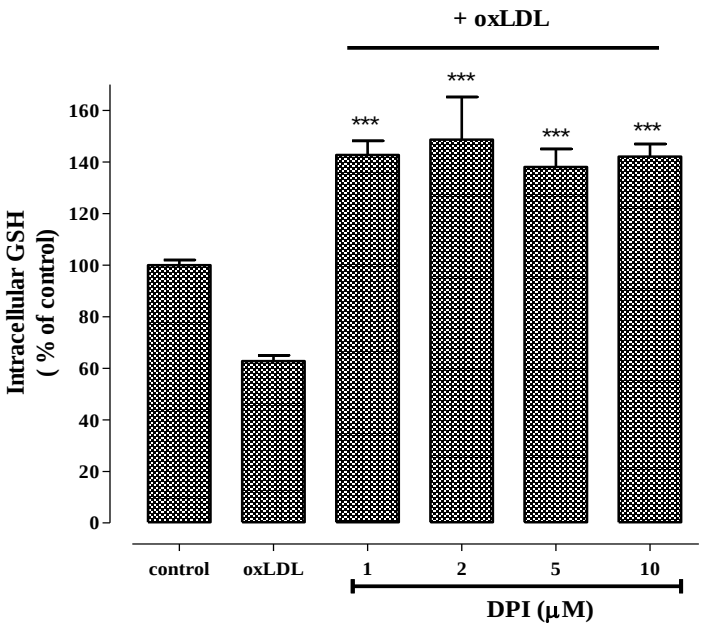

Figure 3.20 Effects of apocynin or DPI on oxLDL-induced intracellular GSH loss in U937 cells.

U937 cells (0.5×10^6 cells/ml) were pre-incubated in phenol-red RPMI-1640 containing the increasing concentrations of A) apocynin, or B) DPI for 3 hours at 37°C, followed by treatment with 0.3 mg/ml oxLDL for another 3 hours. A positive control with cell-only treatment and a negative control with 0.3 mg/ml oxLDL (no apocynin or DPI added) were included. Intracellular GSH was measured by HPLC analysis. Data are expressed as a percentage of the positive control value which is 3.53 nmol/10^6 cells. Significance is indicated from the negative control (oxLDL-treated cell only). Results are displayed as mean ± SEM of triplicates from a single experiment, representative of three separate experiments.

3.3.4 Effect of apocynin and DPI on oxLDL-mediated aconitase activity loss

Intracellular combined aconitase activity was assayed after exposing cells with increasing concentrations of apocynin or DPI in the absence of oxLDL for 24 hours. Apocynin in the range of 10 – 100 μM caused approximately ±10 % fluctuations in the aconitase activity, but no significance was observed against the respective control (**Figure 3.21A**). In contrast, DPI appeared to induce a more significant effect on intracellular aconitase (**Figure 3.21B**). Following a 24-hour incubation with 1 μM DPI, cells had a 20 % increase in the aconitase activity compared to the respective control. However, the intracellular aconitase activity then displayed a gradual decrease with increasing concentration of DPI. DPI at 2 and 5 μM caused the aconitase activity to reduce by 20 % and 40 % compared to the control, respectively, followed by a further dramatic decline in the cells treated with 10 μM DPI until only 10 % of aconitase activity was observed. These result imply that DPI itself generated oxidative stress resulting in the oxidative damage on the intracellular aconitase.

The devastating damage of DPI on aconitase could possibly due to the direct damage of DPI on the protein. In order to examine this assumption, the positive aconitase control protein was treated with different concentrations of DPI and subsequently determined its activity (**Figure 3.22**). 200 μg aconitase protein without treatment of DPI was measured to obtain the activity of 0.9 mU/mg protein. Treatments of aconitase with 1 – 10 μM caused approximately 20 % activity loss, suggesting that the aconitase activity loss caused by DPI *in vitro* could be also because of the direct damages from DPI in addition to the DPI-induce oxidative stress.

Figure 3.21 A)

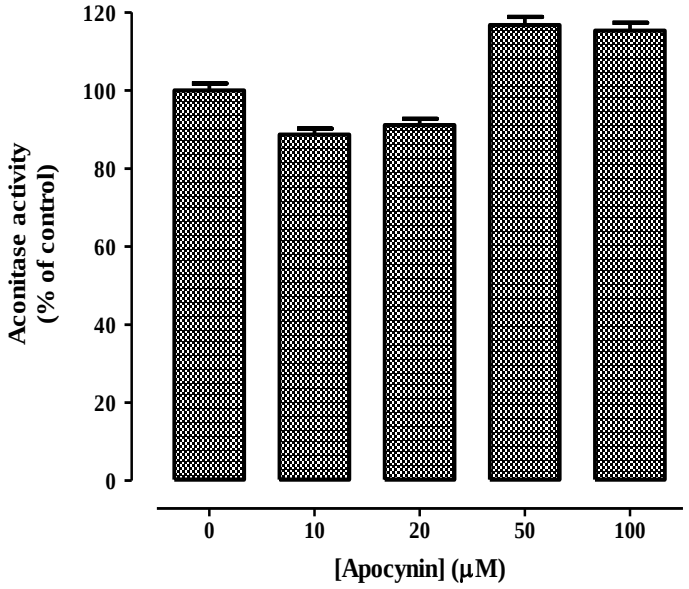

Figure 3.21 B)

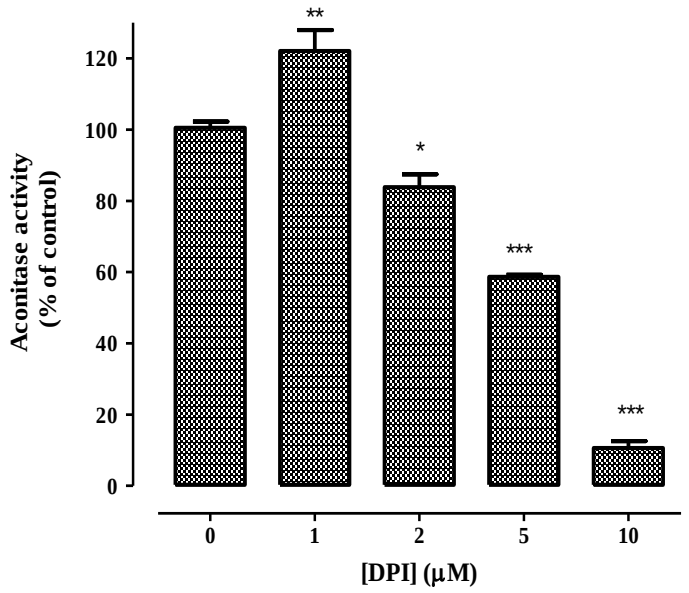

Figure 3.21 Effect of increasing concentrations of apocynin or DPI on aconitase activity in U937 cells.

U937 cells (0.5×10^6 cells/ml) were treated with increasing concentrations of A) apocynin, or B) DPI, followed by incubation at 37 ^{o}C in RPMI-1640 for 24 hours. A control without apocynin or DPI was included. Intracellular aconitase activities (mU/mg protein) were subsequently assayed after two PBS washes. Data are expressed as a percentage of the respective control which was measured as 6.19 mU/mg protein, and significance is indicated from this value. Results are displayed as mean ± SEM of triplicates from a single experiment, representative of three separate experiments.

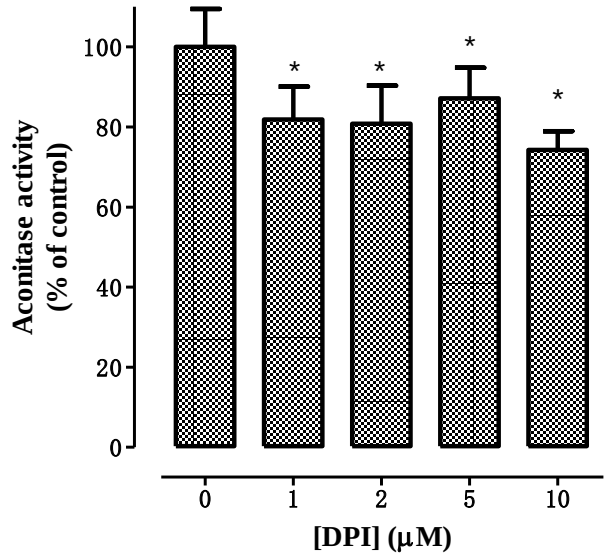

Figure 3.22 Effect of increasing concentrations of DPI on aconitase positive control protein activity.

200μg positive aconitase was treated with the increasing concentrations of DPI, and the activity was subsequently assayed at 37 ^{o}C. Results are presented as a percentage of control (0μM DPI added) which is 0.9 mU/mg protein and no significance is detected from this value. Results are displayed as mean ± SEM of triplicates from a single experiment.

To further confirm that oxLDL-activated NOX is the main site for oxidative stress, aconitase activities were also measured in cells pre-treated with apocynin or DPI before incubation with oxLDL (**Figure 3.23**). Another treatment of pre-incubation with 7,8-dihydroneopterin (7,8-NP) was also included in this experiment to assess the 7,8-NP protection of oxLDL-induced aconitase activity loss. After a 3-hour incubation, there was 4.12 mU/mg protein of intracellular combined aconitase activity in the cell-only control, and 0.5 mg/ml oxLDL decreased the aconitase activity by 50 % compared to the respective control. The presence of 200 μM 7,8-NP restored the aconitase activity by 20 % compared to the oxLDL-treated cells, and 100 μM apocynin also increased it by 30 %. Pre-treatment of cells with 10 μM DPI did not protect the aconitase activity loss from oxLDL-induced damage, and in fact, it caused a further 7 % decline in the oxLDL-induced aconitase activity loss, which is consistent with the DPI toxicity already described in the above findings. It should be noted that the degree of 7,8-NP and apocynin protection against oxLDL-induced aconitase activity loss appeared to be dependent on the toxicity of oxLDL used. It varied in the range of 5 – 30 % protection from oxLDL-induced aconitase activity

loss with the oxLDL killing rate between 20 % to 50 %. The more toxic oxLDL was to cells, the less amount of protection of 7,8-NP and apocynin displayed. These results further support that inhibition of NOX significantly reduced oxLDL-induced oxidative stress and prevented oxLDL-induced aconitase inactivation, thereby protecting the subsequent cell viability loss. The protection of 7,8-NP against oxLDL-induced aconitase inactivation also support that 7,8-NP was protective against oxLDL-induced oxidative damages via its ability to scavenge intracellular oxidants. Moreover, it implies DPI was not a specific NOX inhibitor as it could cause some side effects and induce oxidative damages to cellular components.

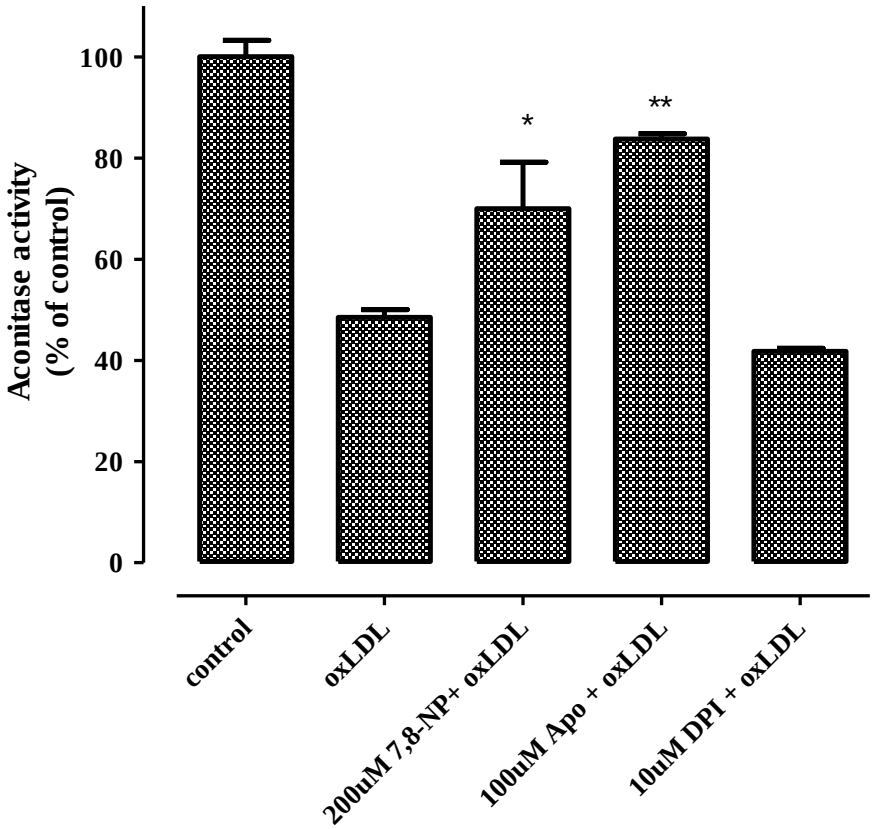

Figure 3.23 Effects of 7,8-NP, apocynin and DPI on oxLDL-induced aconitase activity loss in U937 cells.

U937 cells (0.5×10^6 cells/ml) were pre-incubated with 200μM 7,8-NP for 10 minutes in dark, 100μM apocynin or 10μM DPI in RPMI-1640 at 37°C for 3 hours, followed by incubation with 0.5mg/ml oxLDL for 24 hours. A positive control with cell-only treatment and a negative control with 0.5mg/ml oxLDL only were also included. Intracellular aconitase activities were subsequently assayed after two PBS washes. Data are expressed as a percentage of the positive control which is 4.12 mU/mg protein, Significance is indicated from the negative control level. Results are displayed as mean ± SEM of triplicates from a single experiment, representative of three separate experiments.

Knowing that aconitase exists in the mitochondria matrix too, not only in the cytoplasm, isolation of mitochondria from cytosol and determination of aconitase activity in both compartments, therefore, enable a better understanding of where exactly oxLDL could cause oxidative damages intracellularly. Hence, the following study examined the effects of 7,8-NP and apocynin on the aconitase activities with addition of oxLDL in both cytoplasmic and mitochondrial fractions. To ensure the separation process of mitochondria from cytosol (see **section 2.2.11.2**) was effective, the succinate dehydrogenase assay (see **section 2.2.12**) was performed on the cytoplasmic and mitochondrial samples after treatments. The change of the amount in 2,6-dichlorophenolindophenol (DCIP), an artificial electron acceptor in the assay, was resulted from the reduction of its oxidized form via the electron transfer process catalyzed by succinate dehydrogenase, which is only present in the inner mitochondrial membrane. Thus, the greater change in the amount of DCIP in 30 minutes means the more succinate dehydrogenase was present, and consequently more mitochondria component. The result showed that the change in the DCIP levels in the mitochondrial fraction of the cell-only control was approximately 9-fold greater than that in the control cytoplasm sample (**Figure 3.24A**), suggesting there was only a small amount of mitochondria ending up on the cytoplasm fraction. There were also greater changes in the DCIP levels observed in the mitochondria fractions of the other three treatments, indicating that mitochondria was successfully separated from the cytoplasm. On the other hand, these data also showed a dramatic decrease in the change of the DCIP levels in the mitochondrial fractions where oxLDL was added, and the presence of 7,8-NP and apocynin seemed to have some protective effects, although they were not very significant. These also provided evidence that oxLDL caused oxidative damage in the mitochondria and therefore resulted in the succinate dehydrogenase activity loss. This is beyond the scope of this research programme, so it will not be investigated further.

Aconitase activities were also assayed in both mitochondrial and cytoplasmic fractions in this experiment (**Figure 3.24B**). DPI was not used in this experiment, since it has already been shown that DPI had no protection on oxLDL-induced aconitase activity loss. At the end of the treatments, the cell-only control had 80 and 100 $\mu U/10^6$ cells of aconitase activities in the cytosol and mitochondria, respectively. 0.5 mg/ml oxLDL caused a significant decrease in the aconitase activity by 20 % in the cytosol and 60 % in the mitochondria. Cells pre-treated with 200 μM 7,8-NP and 100 μM apocynin prevented

oxLDL-induced aconitase activity loss in the cytosol by 20 %. The mitochondrial aconitase activity was increased by 10 % in the presence of 7,8-NP compared to the oxLDL-treated mitochondrial sample, but this appeared not to be significant enough. By comparison, apocynin had no effect on the oxLDL-induced aconitase activity loss in the mitochondria at all. These results suggest that oxLDL caused oxidative stress in both mitochondria and cytosol, and it seemed to cause more damages in the mitochondria. 7,8-NP was protective against oxLDL-induced oxidative stress intracellularly, but mainly in the cytoplasm rather than mitochondria. Inhibition of NOX only reduced oxLDL-induced oxidative stress in the cytosol, but not in the mitochondria. This could be because oxLDL-activated NOX initiates a cascade of oxidative events in the cytosol, which subsequently cause oxidative stress in the mitochondria. Once this cascade has been activated to fire up mitochondrial radical-generating system, inhibiting NOX activity could not be sufficient to reduce mitochondrial damage.

Figure 3.24 A)

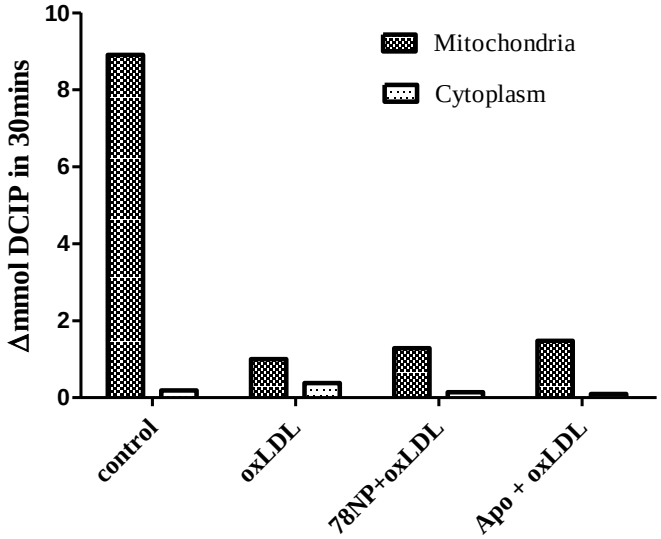

Figure 3.24 B)

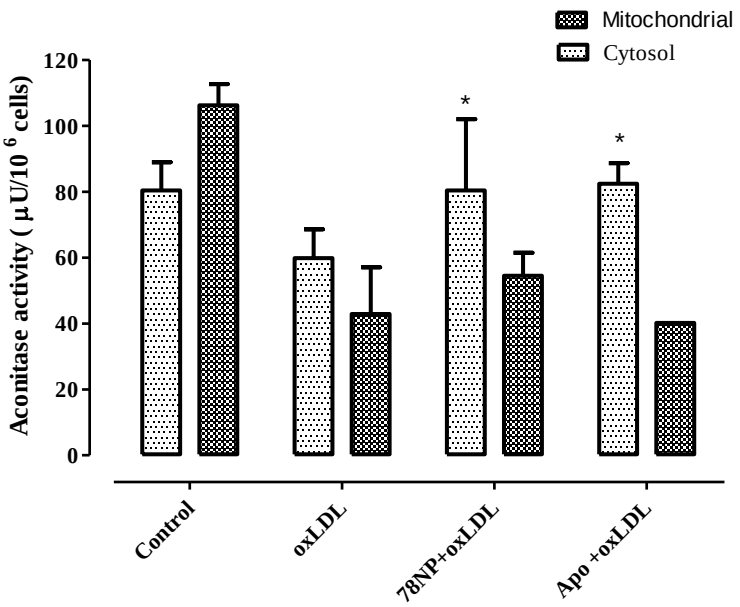

Figure 3.24 Effects of 7,8-NP and apocynin on oxLDL-induced aconitase activity loss in cytoplasmic and mitochondrial fractions.

U937 cells (0.5×10^6 cells/ml) were pretreated with 200μM 7,8-NP for 10 minutes in dark or 100μM apocynin in RPMI-1640 at 37°C for 3 hours, followed by incubation with 0.5mg/ml oxLDL for 24 hours. A positive control with cell-only treatment and a negative control with 0.5mg/ml oxLDL only were also included. A) After 24 hours, mitochondria were separated from cytosol, and succinate dehydrogenase assay were performed in both fractions to determine the amount of isolated mitochondria in each fraction. B) Mitochondrial and cytosolic aconitase activities ($\mu U/10^6$ cells) were subsequently assayed after two PBS washes. Significance is indicated from negative control level. Results are displayed as mean ± SEM of triplicates from a single experiment, representative of three separate experiments.

3.3.5 Effect of 7,8-NP and apocynin on oxLDL-mediated intracellular calcium influx

Both ROS production and Ca^{2+} influx to the cytosol have been found to be early oxLDL-triggered events. The following study, therefore, investigated whether ROS was responsible for the abnormal cytoplasmic Ca^{2+} rise. OxLDL-induced intracellular Ca^{2+} level increase was studied here using both fluorescence microscope and flow cytometry. Following a 6-hour treatment, 200 μM 7,8-NP and 100 μM apocynin themselves did not change the Fluo-3AM fluorescence intensities compared to the cell-only control (**Figure 3.25A**), but cells treated with 0.5 mg/ml oxLDL caused a significant increase in the fluorescence intensities, which was notably suppressed by the pre-treatment of 200 μM 7,8-NP. Pre-incubation of 100 μM apocynin appeared to slightly decrease the oxLDL-induced fluorescence intensity increase. The histogram plot of flow cytometry showed a large fluorescence intensity shifting in the oxLDL-treated cells from the respective control (**Figure 3.25B**), which was observed to move back towards the control in the cells pre-treated with 200 μM 7,8-NP. 100 μM apocynin had little effect on the oxLDL-induced fluorescence intensity shifting, which was consistent with the observations on the fluorescence microscope.

A time course of the effect of 7,8-NP and apocynin on the oxLDL-induced Ca^{2+} increase was studied by flow cytometry over 6 hours (**Figure 3.25C**). In the absence of oxLDL, cells treated with 200 μM 7,8-NP or 100 μM apocynin showed the same fluorescence intensities with the respective cell-only control. OxLDL triggered a rapid fluorescence increase by 4.5 fold in the first 3 hours, followed by a slight rise over the next 3 hours. The oxLDL-induced fluorescence intensities increase were slightly reduced in the presence of 7,8-NP at each time point in the first 3 hours. Instead of continuing to rise in the oxLDL-treated cells over the next 3 hours, 7,8-NP significantly decreased the oxLDL-induced fluorescence intensities by approximately 25 – 30 % at each time point. The patterns of fluorescence intensity in the cells pre-incubated with apocynin appeared to be similar to the 7,8NP pre-treated cells. The exception was the oxLDL-induced fluorescence intensity rise was slightly elevated at 3 hours by apocynin, but this was not statistically significant. After 3 hours, apocynin caused only about a 10 % decrease in the fluorescence intensity at each time point compared to oxLDL-treated cells. These results indicated that 7,8-NP inhibited oxLDL-induced intracellular Ca^{2+} influx, but this protection appeared to occur

after 3 hours. Inhibition of NOX with apocynin also prevented oxLDL-induced intracellular Ca^{2+} increase, but this was a much less significant effect than shown with 7,8-NP.

Figure 3.25 A)

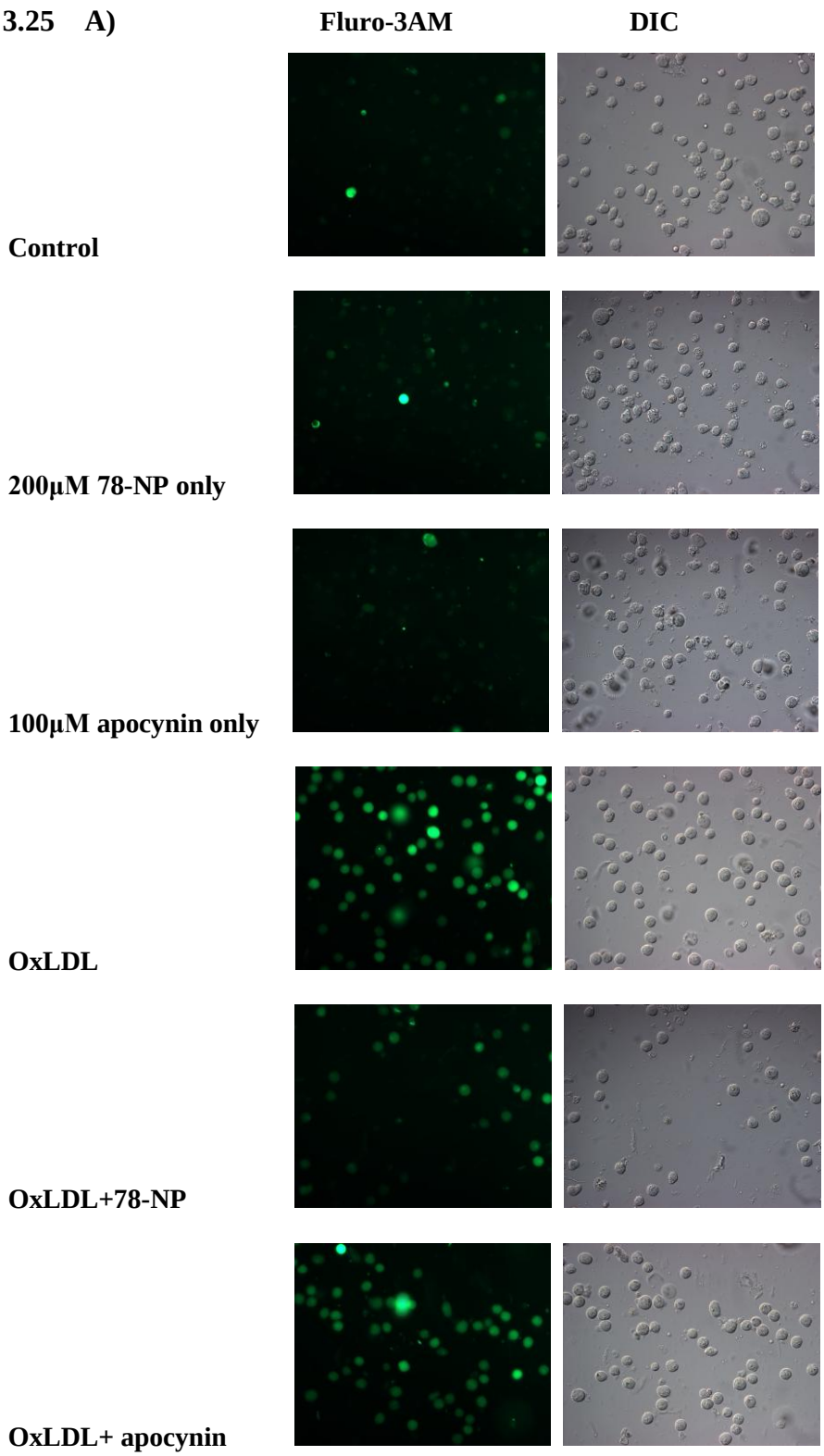

Figure 3.25 B)

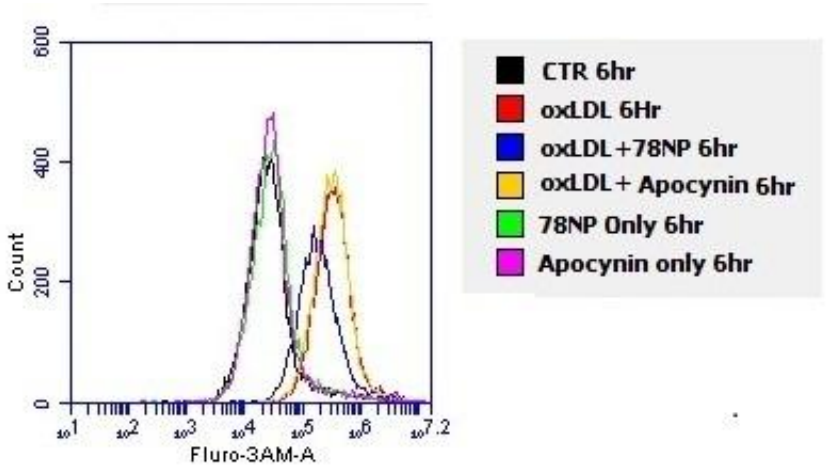

Figure 3.25 C)

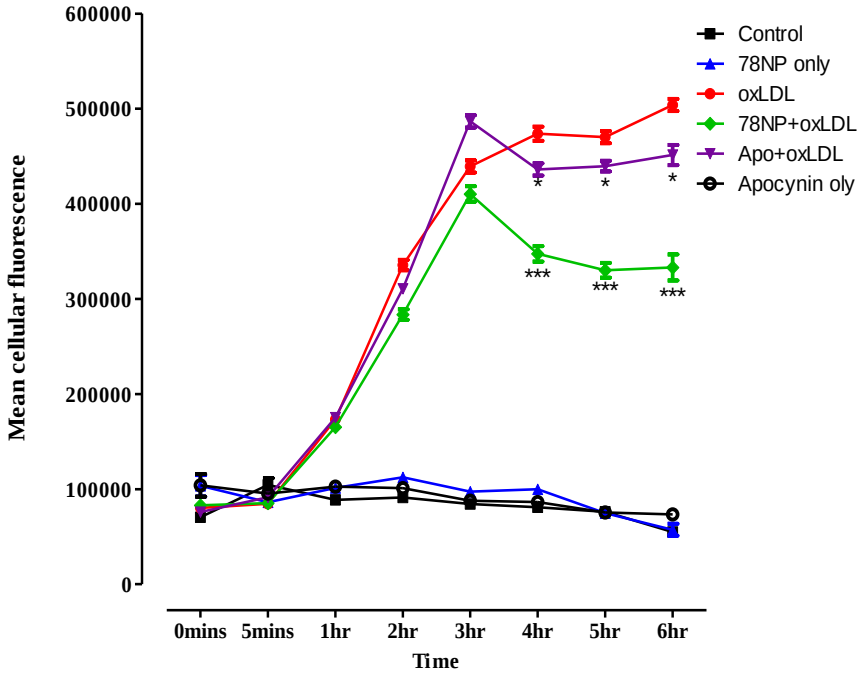

Figure 3.25 Effects of 78-NP and apocynin on oxLDL-induced intracellular Ca^{2+} influx

U937 cells (0.5×10^6 cells/ml) were pre-incubated with 10μM of Fluro-3AM with or without 200μM 7,8-NP /100μM apocynin for 1 hour, followed by treatment with 0.5mg/ml oxLDL in non-phenol red RPMI-1640 at 37°C. At various times, cell samples were removed and viewed under the fluorescence microscope (λex/λem =488/530nm) and analyzed by flow cytometry as well. A) shows the DIC photos and the respective fluorescence photos taken by fluorescence microscope at 5 hours. B) shows the representative flow cytometry histogram plot of cell counts against Fluro-3AM fluorescence at 5 hours. C) shows the mean cellular fluorescence measured by flow cytometry over 6 hours. Results shown are mean fluorescence ± SEM of triplicate experiments. At each time point, intracellular Ca^{2+} levels were significantly elevated with the addition of oxLDL ($p<0.05$). Significance indicated in the graph was detected from the treatment of cells with oxLDL-only at each time point.

3.3.6 Mechanism of NOX activation

The data presented so far have suggested that NOX was activated in response to oxLDL, contributing to the increased oxidative stress. It is known that upon activation, the cytosolic subunit of NOX, $p47^{phox}$, is extensively phosphorylated, resulting in the subsequent assembly and translocation of the other cytosolic subunits $p67^{phox}$ and $p20^{phox}$ with the cyto558 subunit on the plasma membrane. In order to directly prove that oxLDL activated NOX, a time course study of $p47^{phox}$ protein expression upon exposure to oxLDL was studied over 6 hours by western blot (**Figure 3.26**). Phosphorylated $p47^{phox}$ was notably increased after 1 hour incubation (**Figure 3.26A**). The protein band intensities were then quantified and corrected with β-actin (**Figure 3.26B**). Following an initial sharp increase in $p47^{phox}$ protein expression by 90 % after a 2-hour treatment with oxLDL, the amount of expressed $p47^{pho}$x protein reached a maximum by 3-fold after 3 hours. There was then a gradual decrease in $p47^{phox}$ protein by 60 % at 4 and 5 hours until a continuous decline by 90 % at 6 hours compared to the 3-hour point. These results suggested that oxLDL-induced NOX activation took place after 1 hour upon exposure to oxLDL, and it achieved the maximum at 3 hours. It is also noted that the progression of NOX activation by oxLDL coincided with the oxLDL-induced intracellular ROS production (**Figure 3.3**).

Figure 3.26 A)

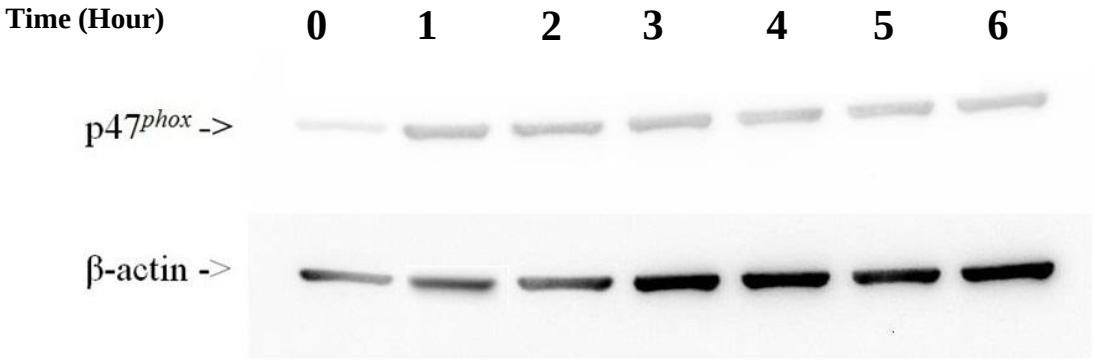

Figure 3.26 B)

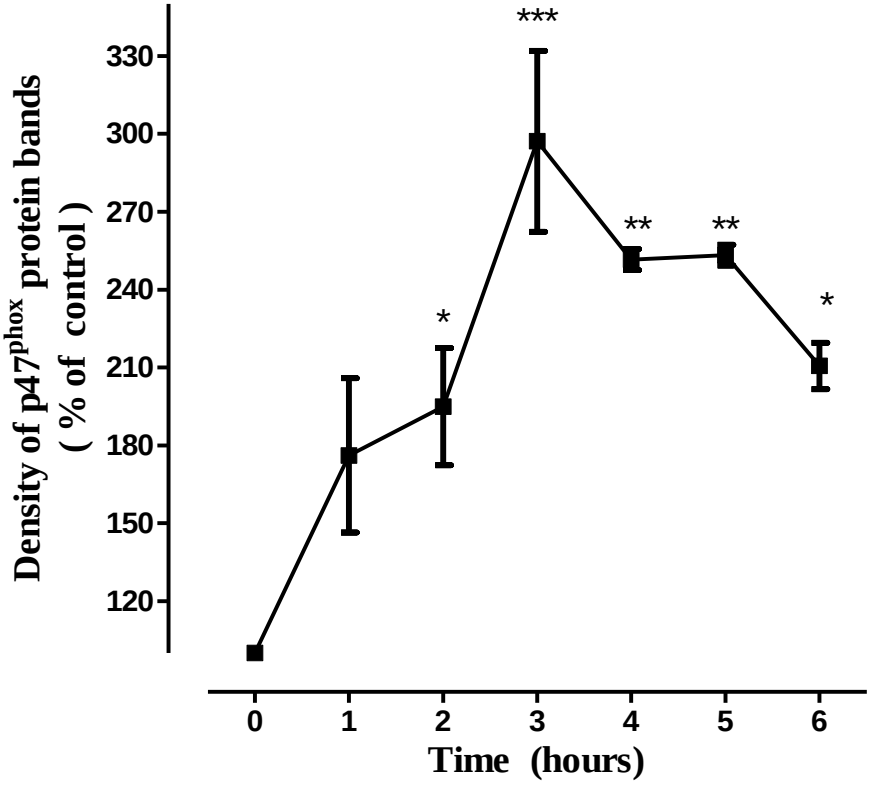

Figure 3. 26 Time course study of p47^{phox} activation by oxLDL in U937 cells.

U937 cells (0.5×10^6 cells/ml) were treated with RPMI-1640 containing 0.5mg/ml oxLDL. At various times, **A)** cell samples were removed and the presence of activated p47^{phox} in the whole cell lysate was examined by western blotting. The western blot photo was modified using Photoshop. **B)** The protein band intensities were quantified using Image J software, and corrected with β-actin. Data are expressed as a percentage of the 0 hour control and significance is indicated from this control. Results are displayed as mean ± SEM of four separate experiments.

The effect of 7,8-NP and apocynin on NOX activation was also examined by measuring $p47^{phox}$ protein expression. Cells treated with PMA were included as a positive control, as it is already known that PMA activates NOX (Li et al., 2002). **Figure 3.27A** was a representative western blot of $p47^{phox}$ protein expression after different treatments. Without any stimulant, there was no $p47^{phox}$ expression observed in the cell-only control. Following a 3-hour incubation with PMA, $p47^{phox}$ phosphorylation occurred, which was also detected in the cells treated with 0.5 mg/ml oxLDL. Cells pre-treated with 200 μM 7,8-NP also showed $p47^{phox}$ expression, but this was not observed in the cells with pre-treatment of 100 μM apocynin. Quantitative analysis showed that phosphorylated $p47^{phox}$ was notably increased by 40 % upon exposure to both PMA and oxLDL, compared to cell-only control (**Figure 3.27B**). 7,8-NP did not prevent oxLDL-activated $p47^{phox}$ phosphorylation, but apocynin significantly abolished the increase in the treatment of oxLDL by 30 %. These results provided direct evidence that oxLDL activated NOX, which is believed to account for the consequent increase in oxidative stress. Apocynin inhibited oxLDL-induced NOX activation by suppressing $p47^{phox}$ phosphorylation, and therefore protected against oxLDL-induced oxidative stress. Additionally, 7,8-NP did not inhibit oxLDL-activated $p47^{phox}$ expression suggested that 7,8-NP must protect against oxLDL-induced oxidative stress via the other pathway, most likely ROS scavenging.

Figure 3.27 A)

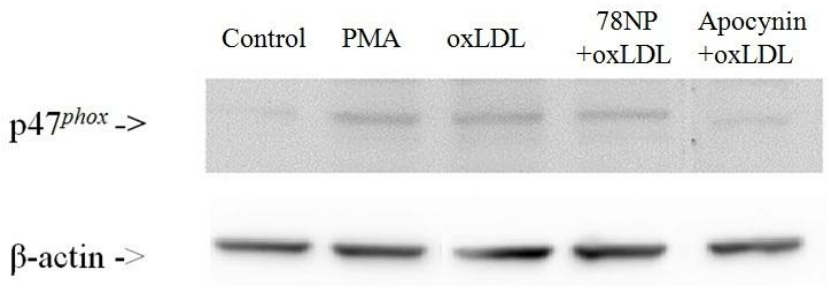

Figure 3.27 B)

Figure 3.27 Effects of 78-NP and apocynin on NADPH oxidase subunit $p47^{phox}$ protein expression in U937 cells.

U937 cells (0.5×10^6 cells/ml) were pre-treated with 200 μM 7,8-NP for 10 minutes in dark or 100 μM apocynin in RPMI-1640 at 37 ^oC for 3 hours, followed by incubation with 0.5 mg/ml oxLDL for 3 hours. A positive control with 40 μM PMA treatment and a negative control with 0.5 mg/ml oxLDL only treatment were also included. **A)** At the end of treatment, the presence of activated $p47^{phox}$ in the whole cell lysate was examined by western blotting. A representative western blot of $p47^{phox}$ was shown. The western blot photo was modified using Photoshop. **B)** The protein band intensities were quantified using Image J software, and corrected with β-actin. Data are expressed as a percentage of the positive control data (PMA-treated cells). Significance is indicated as shown. Results are displayed as mean ± SEM of four separate experiments.

3.4 7,8-Dihydroneopterin (7,8-NP) protection against oxLDL-induced oxidative stress

It has been shown previously by this laboratory that the water-soluble antioxidant 7,8-dihydroneopterin (7,8-NP) provides protection to U937 cells against oxLDL-induced cell death, and it also prevents oxLDL-induced intracellular GSH loss by scavenging oxLDL-mediated ROS, independently of other antioxidants, such as GSH and α-tocopherol (Baird et al., 2004a, Baird et al., 2005a). Therefore, 7,8-NP is key factor to maintain the intracellular redox environment. The following experiments were designed to further examine 7,8-NP protection against oxLDL-induced ROS production in U937 cells to supplement the results shown in the previous sections.

Cells were pre-treated with different concentrations of 7,8-NP for 10 minutes before the incubation with oxLDL, followed by the DHE staining and analysis by fluorescence microscope and flow cytometry. Cells treated with 0.3 mg/ml oxLDL for 3 hours showed an immense increase in the DHE fluorescence compared to the respective control, but this oxLDL-induced fluorescence increase was dramatically suppressed in the presence of 7,8-NP (**Figure 3.28A**). Similarly, the flow cytometry histogram plot displayed a one-fold shift in the fluorescence intensity in cells treated with oxLDL only, which was prevented by the addition of 7,8-NP (**Figure 3.28B**). **Figure 3.28C** showed a more accurate quantification of cellular mean fluorescence intensities detected by flow cytometry, indicating that the fluorescence intensity was significantly elevated by 150 % when cells were exposed to oxLDL, which was resulted from the excessive ROS production induced by oxLDL. The oxLDL-induced fluorescence intensity increase was dramatically decreased by 50 %, reaching the cell-only control level when cells were pre-treated with 50 – 200 μM 7,8-NP, suggesting oxLDL-mediated superoxide was scavenged by 7,8-NP.

The effect of 7,8-NP on oxLDL-induced mitochondrial superoxide production was also examined in order to investigate the protective effect of 7,8-NP in the mitochondria. Cells treated with oxLDL only showed a very high fluorescence intensity increase by 150 % compared to the cell-only control (**Figure 3.29**), which was due to the oxLDL-induced superoxide generation in mitochondria. 7,8-NP at 50 μM significantly prevented oxLDL-induced mitochondrial superoxide production by 60 %. The presence of 100 – 200 μM 7,8-

NP reduced the oxLDL-mediated fluorescence rise by 30 – 40 %, but there was no statistical significance observed, suggesting 7,8-NP protection from oxLDL-induced mitochondrial superoxide generation may be very limited.

Figure 3.28 A)

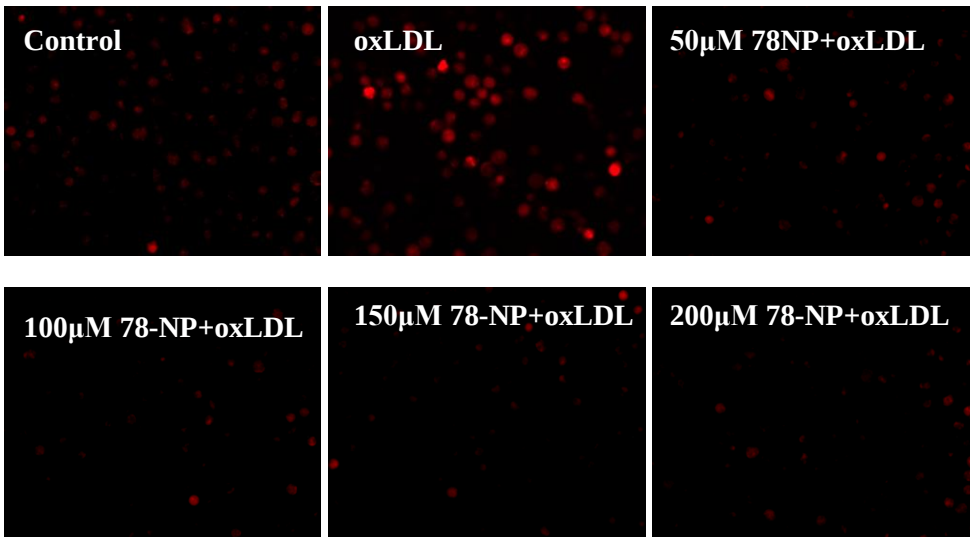

Figure 3.28 B)

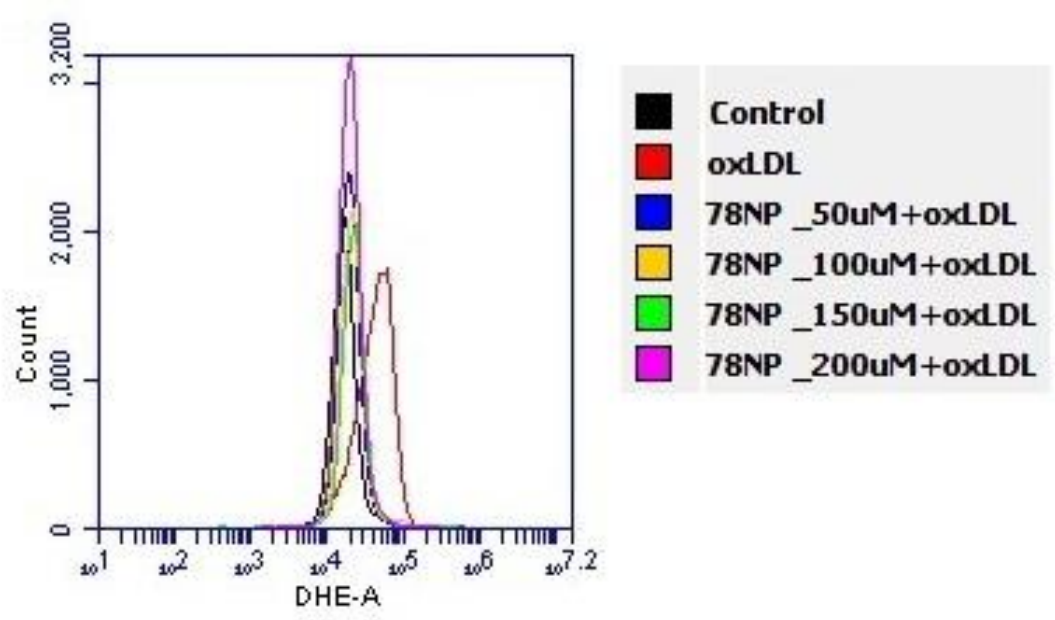

Figure 3.28 C)

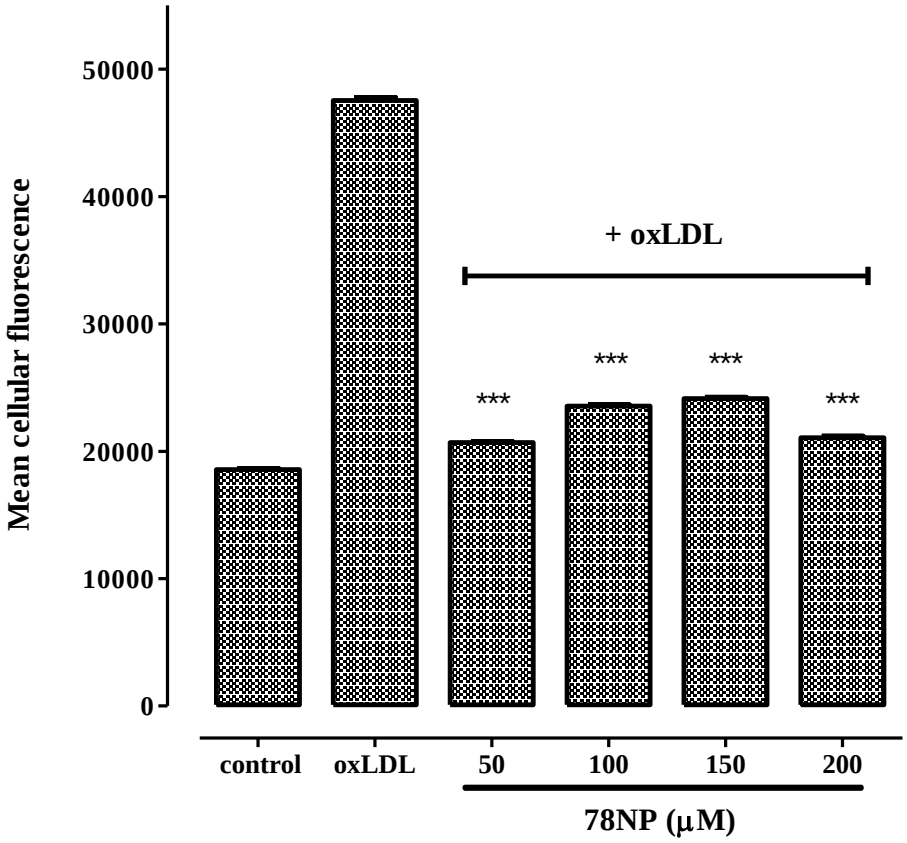

Figure 3.28 Effect of 78-NP on oxLDL-induced ROS productions in U937 cells.

U937 cells (0.5×10^6 cells/ml) were pre-incubated in RPMI-1640 containing the increasing concentrations of 78-NP for 10 minutes at 37°C , followed by treatment with 0.3mg/ml oxLDL for another 3hours. A positive control with cell-only treatment and a negative control with 0.3mg/ml oxLDL but no 78-NP were also included. At the end of treatment, washed cells were incubated with 10μM DHE for 20 minutes in dark for the fluorescence probing of intracellular superoxide. A) The cells were then viewed under a fluorescence microscope (λex/λem of 500-530nm/590-620nm). DHE fluorescent photos are shown. B) shows the flow cytometry histogram plot of cell counts against DHE fluorescence. C) shows the mean cellular fluorescence intensities measured by flow cytometry and significance is indicated from the negative control value (oxLDL treated cells). Results shown are mean fluorescence ± SEM of triplicate experiments.

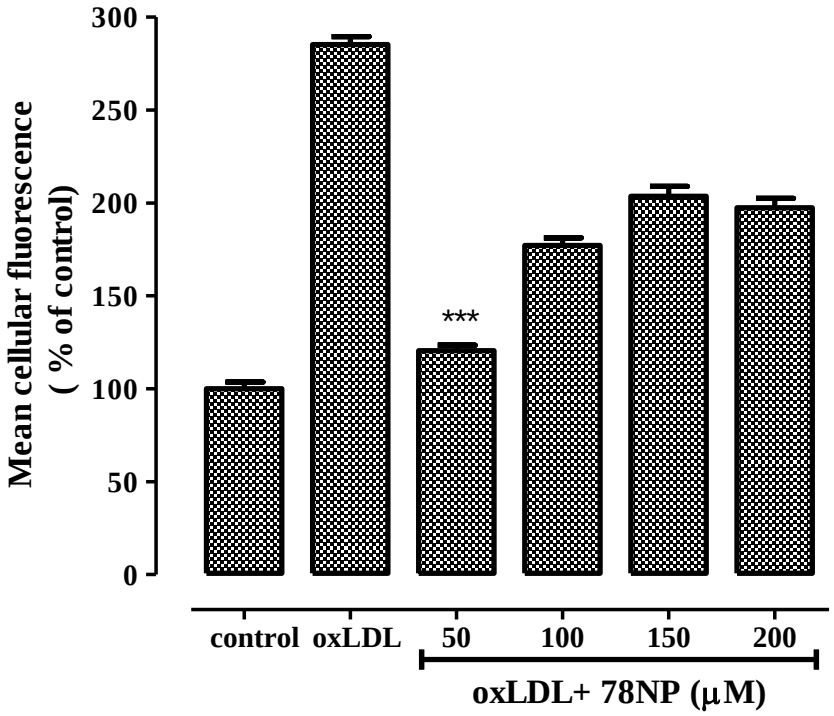

Figure 3.29 Effect of 7,8-NP on oxLDL-induced mitochondrial ROS productions in U937 cells.

U937 cells (0.5×10^6 cells/ml) were pre-treated with the increasing concentrations of 78-NP for 10 minutes in dark, followed by incubation with 0.3mg/ml oxLDL for 3hours at 37°C. A positive control with cell-only treatment and a negative control with 0.3mg/ml oxLDL but no 78-NP were also included. At the end of treatment, washed cells were incubated with 5μM MitoSox red for 10 minutes in dark for the fluorescence probing of intracellular superoxide. The cells were then viewed under a fluorescence microscope (λex/λem of 510nm/580nm). Cellular fluorescence intensities are converted to numerical values, which are presented as a percentage of the cell-only control (0μM oxLDL added). Significance is indicated from the negative control. 500 cells in each treatment were collected for quantification, and results shown are mean fluorescence ± SEM of triplicate experiments.

In order to ensure the diminished rise in the oxLDL-induced fluorescence rise was because of 7,8-NP scavenging ROS, not the interaction between 7,8-NP and the fluorescent dyes, cells treated with different concentrations of 7,8-NP without the presence of oxLDL were probed with DHE and MitoSox to examine the effect of 7,8-NP itself on intracellular ROS production. Upon exposure to 50 – 200 μM 7,8-NP, there was no significant change in the DHE fluorescence intensity observed using flow cytometry (**Figure 3.30**), suggesting 7,8-NP did not mediate intracellular ROS production. Yet the mitochondrial fluorescence appeared to decrease by 20 – 40 % with the increasing concentration of 7,8-NP compared to the respective control, not statistically significant, though (**Figure 3.31**). This effect of

7,8NP seemed to account for the limited protection on oxLDL-induced mitochondrial superoxide production shown above.

Figure 3.30 A)

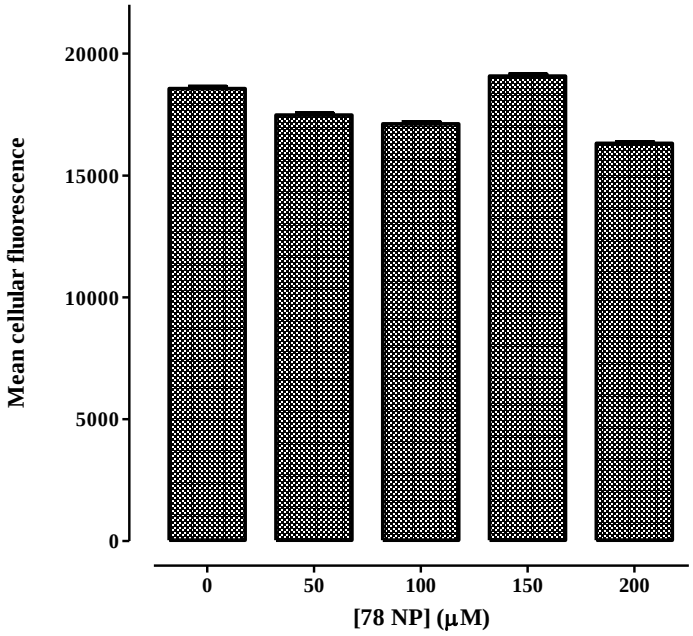

Figure 3.30 B)

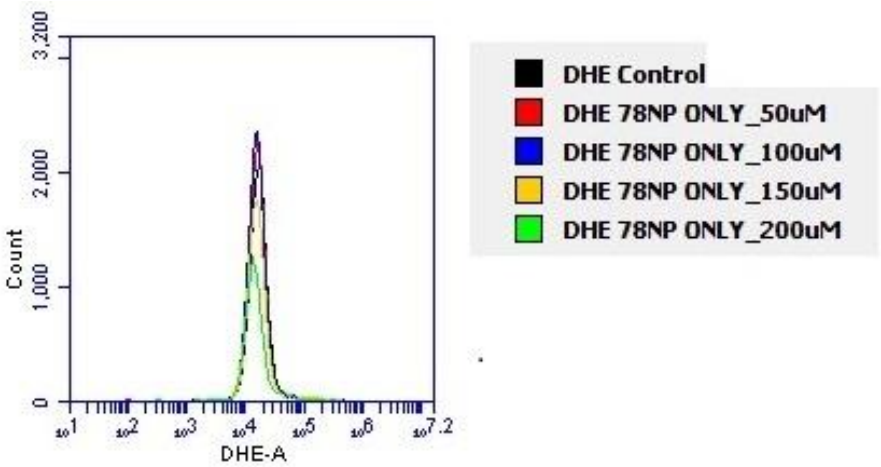

Figure 3.30 Effects of 78-NP on intracellular ROS productions in U937 cells.

U937 cells (0.5 $\times 10^6$ cells/ml) were incubated in RPMI-1640 containing the increasing concentrations of 78-NP for 3hours at 37^{o}C . At the end of treatment, the cells were washed and stained with 10µM DHE for 20 minutes in dark before analysis by flow cytometry. A control with 0µM 78-NP added was also included. A) shows the mean cellular fluorescence intensities measured by flow cytometry and no significance is detected from the control value (0µM 78-NP added). Results shown are mean fluorescence ± SEM of triplicate experiments. B) shows the flow cytometry histogram plot of cell counts against DHE fluorescence.

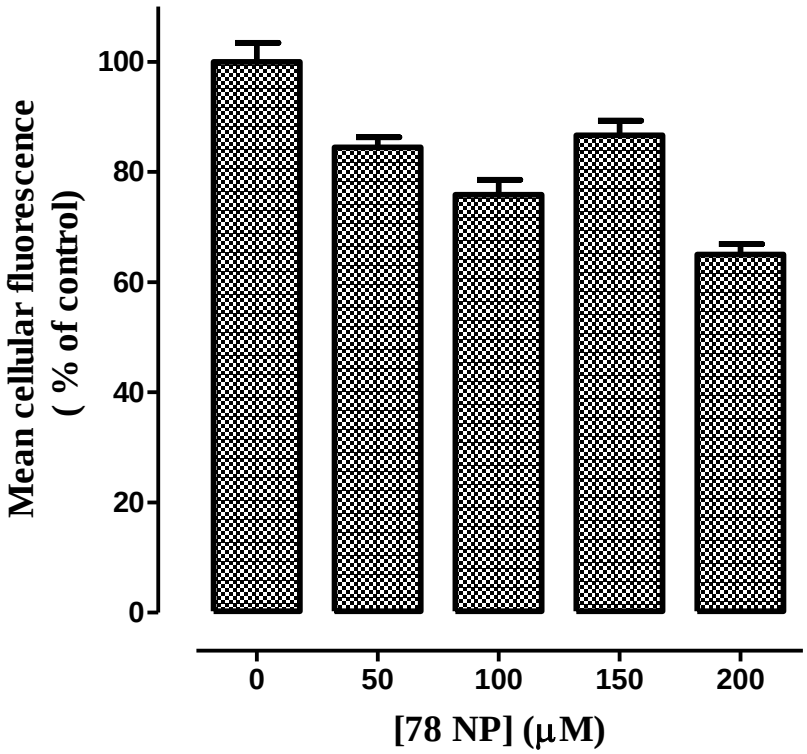

Figure 3.31 Effect of 78-NP on mitochondrial ROS productions in U937 cells.

U937 cells (0.5×10^6 cells/ml) were incubated in RPMI-1640 containing increasing concentrations of 78-NP for 3hours at 37^oC . At the end of treatment, washed cells were stained with 5μM MitoSox red for 10 minutes in dark for the fluorescence probing of mitochondrial superoxide. The cells were then viewed under a fluorescence microscope (λex/λem of 510nm/580nm).). Cellular fluorescence intensities are converted to numerical values, which are presented as percentage of the cell-only control (0μM 78-NP added). No significance is detected from this control. 500 cells in each treatment were collected for quantification, and results shown are mean fluorescence ± SEM of triplicate experiments.

4. DISCUSSION

4.1 OxLDL-induced cell death in U937 cells

This research programme examined the cytotoxic effects of oxLDL on U937 cells. The U937 cells monocyte-like cell line was selected for use in this study since monocytes are involved in the primary and ongoing interaction with oxLDL within the artery wall and lipid-filled foam cells arise from monocyte-derived macrophage cell (Lusis, 2000). U937 cells are commonly used as an atherosclerotic model since they are relatively easy to maintain, and they grow rapidly with a doubling time of between 3-4 days. They are relatively homogeneous, compared to the more heterogeneous nature of comparatively small quantities of human monocyte-derived macrophages (HMDMs) isolated from human blood samples. More importantly, U937 cells seem to share the same oxLDL-induced cell death mechanism with HMDMs (Baird et al., 2004a). In both cell types, oxLDL causes increased oxidative stress with overproduction of ROS, loss of cellular glutathione (GSH) and oxidative loss of metabolic enzymes, such as glyceraldehydes-3-phosphoate dehydrogenase (GAPDH), triggering caspase-independent necrosis (Gieseg et al., 2009a).

This study began by examining the effect of oxLDL on U937 cell viability to confirm the previous findings. The cell viability loss in U937 cells was analyzed via the MTT reduction assay. The MTT assay measures cell viability in terms of metabolism and energy levels. MTT compound is reduced by mitochondrial NADH dehydrogenases to formazan only in living and metabolically active cells, and formazan production is directly proportionally to cell numbers (Mosmann, 1983). Another method commonly used to measure cell viability is trypan blue exclusion assay, which measures the integrity of the cell membrane and indicates the occurrence of necrosis or secondary necrosis. This assay usually gives more biased results due to the cell counting errors under the microscope. Previous studies from this laboratory have demonstrated that cell viability obtained by MTT assay was strongly correlated with that measured by trypan blue assay (Baird et al., 2004a). Therefore, the MTT reduction assay was chosen over the trypan blue assay to measure cell viabilities in this research.

In this study, oxLDL showed a high degree of toxicity to U937 cells, and the loss of cell viability was dependent on the oxLDL concentration (**Figure 3.1**), as shown in previous studies (Baird, 2003, Rutherford, 2010). The median lethal dose (LD_{50}) of oxLDL was found to vary between 0.2 and 0.5 mg/ml to U937 cells, depending on the individual oxLDL preparation, although the exact cause is still unknown (Gieseg et al., 2009a). It appears that there are significant differences between the oxLDL preparations in different laboratories also. The concentration of the LDL when oxidized, the oxidant and its concentration, the length of oxidation, the temperature of oxidation and transition metal will affect the finished product (Lougheed and Steinbrecher, 1996).

The oxLDL caused the rapid loss of U937 cell viability with the first 6 hours of incubation (**Figure 3.2**). Depending on different oxLDL preparations, a lag time before cell viability decrease could occur after 3 hours incubation with oxLDL. This has also been observed by other members from this laboratory. The lag phase suggests that oxLDL is not immediately toxic to U937 cells, but triggers cellular events that cause cells to die, such as metabolic dysfunctions and cellular glutathione (GSH) loss (Baird et al., 2005a). OxLDL could cause cell death either via necrosis or apoptosis depending on the different cell types (Gieseg et al., 2009a, Baird et al., 2004a). An examination of U937 cell morphology during incubation with oxLDL revealed that oxLDL caused necrotic cell death with characteristics of cell swelling, disrupted cell membrane and loss of cellular contents. Previous studies showed that oxLDL-induced necrosis in U937 cells with a rapid loss of intracellular GSH, resulting in caspase-3 inactivation due to the oxidation of essential free thiol groups in the active site. The failure of caspase-3 activation leads to the necrotic cell death with cell swelling and lysis with no phophatidylserine (PS) exposure on the cell membrane (Baird et al., 2004a). In contrast, oxLDL caused apoptosis in THP-1 cells with the appearance of annexin V staining morphology due to the flipping of PS to the outer surface of the cell membrane, caspase-3 activation, cell shrinkage and a small amount of reduction in cellular GSH level (Baird et al., 2004a). The difference in oxLDL-induced cell death could be related to the varying mechanisms of oxLDL uptake. Unlike native LDL, oxLDL is readily bound by scavenger receptors. Of these scavenger receptors, scavenger receptor-A (SR-A) and CD36 are best known to be involved in foam cell formation and oxLDL-mediate cell death (Gieseg et al., 2009a). The expression of CD36 in U937 cells has been found to be

four-fold higher than that in THP-1 cells (Nguyen-Khoa et al., 1999), which may result in an initial burst of oxLDL uptake and the resultant oxidative stress in the U937 cells.

4.2 OxLDL-induced oxidative stress in U937 cells

A detailed investigation into the influence of oxLDL in U937 cells was followed by examining the effect of oxLDL on intracellular reactive oxygen species (ROS) production, GSH level and aconitase activity.

ROS production

Examinations of intracellular ROS generations using fluorescence probes showed oxLDL triggered a high level of intracellular and intra-mitochondrial superoxide productions within 3 hours (**Figure 3.3 – 3.5**). The excessive generation of ROS within cells appears to be the key feature of oxLDL cytotoxicity. How exactly oxLDL triggers ROS production remains unknown. Treatment of oxLDL with various antioxidants before addition to cells did not reduce oxLDL toxicity or ROS productions suggests that oxLDL may activate cells' own oxidant generating system, such as mitochondrial respiration chain, NADPH oxidase (NOX), xanthine oxidase and etc., by inducing a shift in redox balance and subsequent initiation of downstream signalling cascades (Gieseg et al., 2009b, Gieseg et al., 2009a). Interestingly, the pattern of the effect of increasing concentrations of oxLDL on intracellular superoxide production in **Figure 3.4** is different from that on mitochondrial superoxide production in **Figure 3.5**. Low dose of oxLDL promoted superoxide generation to increase by 80 % compared to the control, followed by a slight and gradual rise by up to 20 % with the increased oxLDL concentration. In comparison, significantly increased mitochondrial superoxide generation was observed with an oxLDL dosage of 0.65 mg/ml, suggesting the amount of oxLDL has to reach the lethal dose to induce mitochondrial dysfunctions. This also implies that mitochondrial dysfunction could be a secondary event initiated by the oxLDL-mediated ROS overproduction and other cellular oxidative damage in the cytoplasm. Overload of cytosolic Ca^{2+} appears to be a key factor triggering mitochondrial ROS production and destabilisation in macrophages, leading to mitochondrial permeability pore (MPT) opening, loss of mitochondrial membrane potential,

and subsequently calpain activation, lysosomal destabilization, and eventually cell death (Yang et al., 2012). The relationship between mitochondrial damage and Ca^{2+} influx will be discussed later.

GSH

In parallel with the increased superoxide production, intracellular GSH levels were also found to decrease upon the addition of oxLDL (**Figure 3.6**), which was in consistent with early studies (Baird, 2003, Rutherford, 2010). GSH is the major intracellular antioxidant which is synthesized and regenerated intracellularly at the expense of NADPH. It reacts rapidly with a range of oxidants including $OH^{\bullet}$, HOCl, $ONOO^{-}$, $RO^{\bullet}$, $NO_2^{\bullet}$ and less efficiently with $O_2^{\bullet-}$ (Halliwell and Gutteridge, 2007b). GSH regeneration from GSSH enables cells to withstand a certain level of oxidative stress. The overwhelming of this protection through complete oxidation of GSH or inhibition of GSH regeneration through oxidative damage to metabolic enzymes results in further increased susceptibility to oxidative stress (Ballatori et al., 2009) and cell death (Boggs et al., 1998). Protein oxidation and cell death in THP-1 cells treated with peroxyl radicals were previously found to become significant only once GSH levels had almost been depleted (Kappler et al., 2007). Thus, GSH depletion provides a direct measure of the cellular antioxidant status. Reduced GSH level correlated with the increased intracellular ROS production disrupts the oxidant/antioxidant balance, clearly showing that oxLDL induced an increased oxidative stress in U937 cells.

Aconitase

Intracellular aconitase activity has also been found to decrease with the increased oxLDL concentration (**Figure 3.7**), and both cytosolic and mitochondrial aconitase activity were affected by oxLDL (**Figure 3.29**). A rapid decrease in intracellular aconitase activity occurred within 6 hours upon exposure to oxLDL (**Figure 3.8**), which was coincident with superoxide production and GSH loss, suggesting oxLDL-induced oxidative stress was responsible for the intracellular aconitase damage. Aconitase has been previously found to be very sensitive to oxidative damage due to the presence of the [4Fe-4S] cluster in the aconitase enzymatic centre (Murakami and Yoshino, 1997). ROS, in particular superoxide,

can readily attack the [4Fe-4S] cluster by distracting one labile iron to form an inactive [3Fe-4S] cluster, resulting in the inactivation of aconitase (Castro et al., 1994, Hausladen and Fridovich, 1994). Aconitase has been found to be the only enzyme undergoing the significant oxidative modification in the citric acid cycle during aging (Yarian and Sohal, 2005, Yarian et al., 2006). More importantly, a causal relationship between decreased aconitase activity and shortened life-span was reported in the aging houseflies (Yan et al., 1997). Inactivation of aconitase is contributed to a decline in the overall efficiency of mitochondrial bio-energetics by blocking electron flow to oxygen and results in an accumulation of reduced metabolites, such as NADH, leading to 'reductive stress' (Yan et al., 1997). It is likely that the increased reductive stress causes an increased production of ROS through autoxidation of the reduced metabolites, thus further increasing oxidative damage to macromolecules. Besides, the free iron released from the [4Fe-4S] cluster upon oxidant attack could also contributes to further ROS production via the Fenton reaction. Therefore, aconitase inactivation is not only the consequence of oxLDL-induced oxidative damages, it may also initiate the cascade with the potential to cause a dramatic increase in the cellular burden of oxidative damage, resulting in metabolism failure and eventually cell death.

The current results have clearly shown that oxLDL mediates significant oxidative stress in U937 cells. The progression of cell viability loss was very closely correlated with cellular and mitochondrial superoxide burst, loss of cellular GSH content and intracellular aconitase activity loss. These findings support the current oxidative hypothesis for oxLDL cytotoxicity that oxLDL is internalised by cells via scavenger receptors and evokes high levels of intracellular oxidative stress. It is suggested that the formation of highly reactive oxidised lipid and protein species in response to oxLDL overwhelms the cells' antioxidant capacity, which results in imbalances in the intracellular redox environment, changes in various signalling pathways and gene expression, leading to cell death via caspase-independent necrosis (Baird et al., 2004a).

4.3 OxLDL-induced in calcium influx in U937 cells

The effect of oxLDL on cytosolic calcium (Ca^{2+}) levels were studied using both fluorescence microscope and flow cytometry. The result obtained using the flow cytometer was different from that using the fluorescence microscope. Instead of a continuous rise in the intracellular Ca^{2+} levels within the 6 hours after oxLDL treatment shown by the flow cytometer (**Figure 3.11**), a deep drop was detected after an initial rise at 3 hours upon oxLDL treatment on the fluorescence microscope, followed by a second rise in the next 3 hours (**Figure 3.10**). The exact reason for the difference is unexplained. It is possible that some errors during the manual data quantification process from the fluorescence imagings could occur, but this should not be significant enough. Considering that there was a half an hour for cell processing before examination on fluorescence microscope, something may happen during this time, in particular at 3-hour time point, for example, Ca^{2+} leakage out of cells, so that the fluorescent signal detected was less. However, flow cytometry is a rapid method. It can measure the cellular fluorescence immediately after collecting cells, without any extra processing, so reducing the possible post experimental loss of signal using the flow cytometer. If the initial rise measured by fluorescence microscopy is real, it may indicate the cytosolic Ca^{2+} increase occurring within the first 3 hours, and the excessive cytosolic Ca^{2+} can be uptake into mitochondria, resulting in the second rise after 3hours which may correspond to the Ca^{2+} accumulated in the mitochondria. Why the flow cytometry did not see this is uncertain, and suggests it may be an artifact of the sample processing for microscopy.

Ignoring the drop, the results obtained using both instruments demonstrated that oxLDL evoked a quick and large rise in cytosolic Ca^{2+}. The Ca^{2+} inonphore A23187 caused a concentration-dependent increase in cytosolic calcium level after 5 hours (**Figure 3.11**), indicating that the observed increase in the fluorescence intensity in oxLDL-treated U937 cells was most likely due to the cytosolic Ca^{2+} reacting with the fluo-3AM ester dye, not oxLDL reacting with the dye.

The elevation in cytosolic Ca^{2+} could be attributed to both Ca^{2+} influx from the extracellular media via L- or T-type Ca^{2+} channels on cell membranes and/or Ca^{2+} release from ER via ryanodine receptors (RyRs) in the ER membrane (Negre-Salvayre et al., 1992,

Deng et al., 2005, Yang, 2009, Yang et al., 2012). The opening of Ca^{2+} channels in the plasma membrane could occur via plasma membrane depolarization. It was previously hypothesized that plasma membrane depolarization in cardiocytes caused by voltage-gated Na^{+}-channel activation resulted in inward Na^{+}-current, facilitating L-type Ca^{2+}-channels on the plasma membrane (Maack and O'Rourke, 2007). The activity of voltage-gated Na^{+}-channels and plasma membrane potential in U937 cells after oxLDL treatment can be examined to validate this hypothesis in the future. A more likely possibility is that oxLDL-induced ROS production regulates the plasma membrane Ca^{2+} channels through thiol modulation within the protein complex (Inoue et al., 2008). This could be supported by the early finding that the thiol oxidizing agent 5,5'-Dithiobis (2-nitrobenzoic acid) (DTNB) up-regulated L-type Ca^{2+} channels at the extracellular face of the cell membrane (Campbell et al., 1996). It appears that an allosteric thiol-containing 'redox switch' is present on the L-type Ca^{2+} channel subunit complex. The major superoxide-generating complex NADPH oxidase (NOX) on the plasma membrane could be a key regulator in the opening of the L- or T-type Ca^{2+} channels upon cells exposure to oxLDL. A recent study showed that inhibition of NOX by apocynin or DPI suppressed the L-type Ca^{2+} channel expression and blocked the influx of extracellular calcium (Wang et al., 2010).

Maack and O' Rourke previously suggested a 'Ca^{2+}-induced Ca^{2+} release', a process in which Ca^{2+} release from intracellular ER could be resulted from the influx of extracellular Ca^{2+} which triggers the opening of the RyRs on the ER membrane (Maack and O'Rourke, 2007). However, the other studies demonstrated oxLDL induced a gradual rise in cytosolic calcium with time in the absence of external calcium source (Deng et al., 2009, Deng et al., 2005), implying that mobilization of calcium from intracellular ER store occurred in the absence of external Ca^{2+} and the opening of RyR on the ER membrane did not have to be initiated by the extracellular Ca^{2+} influx. It is likely that the critical thiol groups within the RyR protein are targeted by ROS in responses to oxLDL, leading to ER-Ca^{2+} release. Previous finding of HOCl interacting with the essential thiols leading to RyR activity suggests that RyR receptors on ER membrane could be activated via thiol oxidation by oxidants (Sun et al., 2001, Anzai et al., 1998). It is hard to distinguish from current results that whether Ca^{2+} released from intracellular store or influx of extracellular Ca^{2+} happens first, or whether these two events happen at the same time. This can be investigated via the

spatiotemporal examination of cytosolic Ca^{2+} rise using L- or T- type Ca^{2+} channel blockers or RyR inhibitors.

Cytosolic Ca^{2+} increase could also occur via other non-specific pathway (Deng et al., 2005). This is supported by previous study in this laboratory that HOCl-promoted intracellular Ca^{2+} increase was never completely prevented using any of the Ca^{2+} channel blockers or Ca^{2+} chelator (Yang, 2009).

OxLDL-elicited overload of cytosolic Ca^{2+} due to either extracellular Ca^{2+} influx or depletion of ER Ca^{2+} has been found to be a key event triggering calcium-dependent necrosis or apoptosis (Nicotera and Orrenius, 1998, Gieseg et al., 2009a, Porn-Ares et al., 1998). Little is known about the precise mechanism of how the increased intracellular Ca^{2+} are involved in the oxLDL-toxicity effect. It is very possible that cytosolic Ca^{2+} accumulation triggers mitochondrial dysfunction leading to cell death. A recent study described a significant increase in mitochondrial Ca^{2+} was correlated with the cytosolic Ca^{2+} influx mediated by oxLDL in PMA-stimulated U937 cells, suggesting the oxLDL-induced cytosolic Ca^{2+} rise triggered the Ca^{2+} mobilization from the cytoplasm to mitochondria via Ca^{2+} uniporter on inner mitochondrial membrane, resulting in the MTP pore opening and mitochondrial transmembrane potential loss (Deng et al., 2009). The similar findings were also described in HOCl-treated HMDM cells (Yang et al., 2012).

OxLDL-induced cytosolic Ca^{2+} overload may contribute to mitochondrial destabilization by inducing mitochondrial ROS production as a result of Ca^{2+} influx into mitochondria. Grijalba *et al.* showed that Ca^{2+} alters the lipid organization of the inner mitochondrial membrane by interacting with the anionic head of cardiolipin molecules, suggesting that increased Ca^{2+} may affect the mitochondrial respiratory chain function and favour superoxide radical production at intermediate steps of the respiratory chain (Grijalba et al., 1999). The mitochondrial ROS production can serve as the oxidizing agent for MPT pore activation (Inoue et al., 2008). The excess oxidants possibly involves the oxidation of thiols on the pore complex in cooperation with Ca^{2+} (Petronilli et al., 1994). The sensitivity of MPT pore can be increased by oxidation or cross-linking of critical dithiols in membrane proteins, promoting the subsequent MPT pore opening (Chernyak et al., 1995). Alternatively, Ca^{2+} can bind to the matrix side of inner mitochondrial membrane and

promotes extensive conformational changes of membrane proteins which causes the thiol groups more susceptible to oxidation (Kowaltowski et al., 1997).

Excessive mitochondrial Ca^{2+} can also induce MPT pore opening by activating Ca^{2+}-dependent calpains (Gores et al., 1998). Active calpain 10 has been demonstrated in the outer membrane, intermembrane and mostly matrix fractions of isolated mitochondria. Early study showed mitochondrial matrix calpain 10 triggered MPT pore and caused damage to mitochondrial complex I (Arrington et al., 2006). It is likely that mitochondrial calpain activates MPT pore opening by cleaving proteins to generate positively charged peptides which may allosterically modulate pore opening by binding at a site that normally binds cations (Aguilar et al., 1996).

Mitochondrial Ca^{2+} released from MPT pore can subsequently activate cytosolic calpain. The inhibition of mitochondrial calpain activation prevented cytosolic calpain activation in HOCl-treated HMDM, indicating that cytosolic calpain activation occurs after MPT pore opening (Yang, 2009). Why cytosolic calpain is activated after mitochondrial Ca^{2+}-triggered MPT opening rather than upstream of mitochondrial dysfunction is not fully understood. Activated calpains have been shown to cause bleb formation and necrotic cell death by proteolytically cleaving cytoskeletal proteins (Miyoshi et al., 1996, Weber et al., 2005). Calpain activation can also cause lysosomal destabilization and the release of cathepsin, a protease responsible for degradation of cellular components, leading to necrotic or apoptotic cell death (Yap et al., 2006). In addition, there are also other apoptotic factors released from mitochondria via the opened MPT pore, such as cytochrome c, leading to caspase activation and subsequent apoptotic cell death (Nicotera and Orrenius, 1998).

Resting cells tightly regulate free Ca^{2+} in the range of 100 to 200 nM in both the cytosol and the mitochondria (Halliwell and Gutteridge, 2007b). A rise in cytosolic Ca^{2+} seems to be a key event in oxLDL-induced oxidative stress and cell death. OxLDL may activate NADPH oxidase (NOX) on plasma membrane, and NOX-mediated ROS triggers cytosolic Ca^{2+} increase via Ca^{2+} channels on plasma and ER membrane. The Ca^{2+} overload activates calpain, along with the elevated Ca^{2+} triggers mitochondrial ROS production and MPT

pore formation, leading to mitochondrial membrane potential loss, subsequently lysosome destabilization and eventually cell death (**Figure 4.1**).

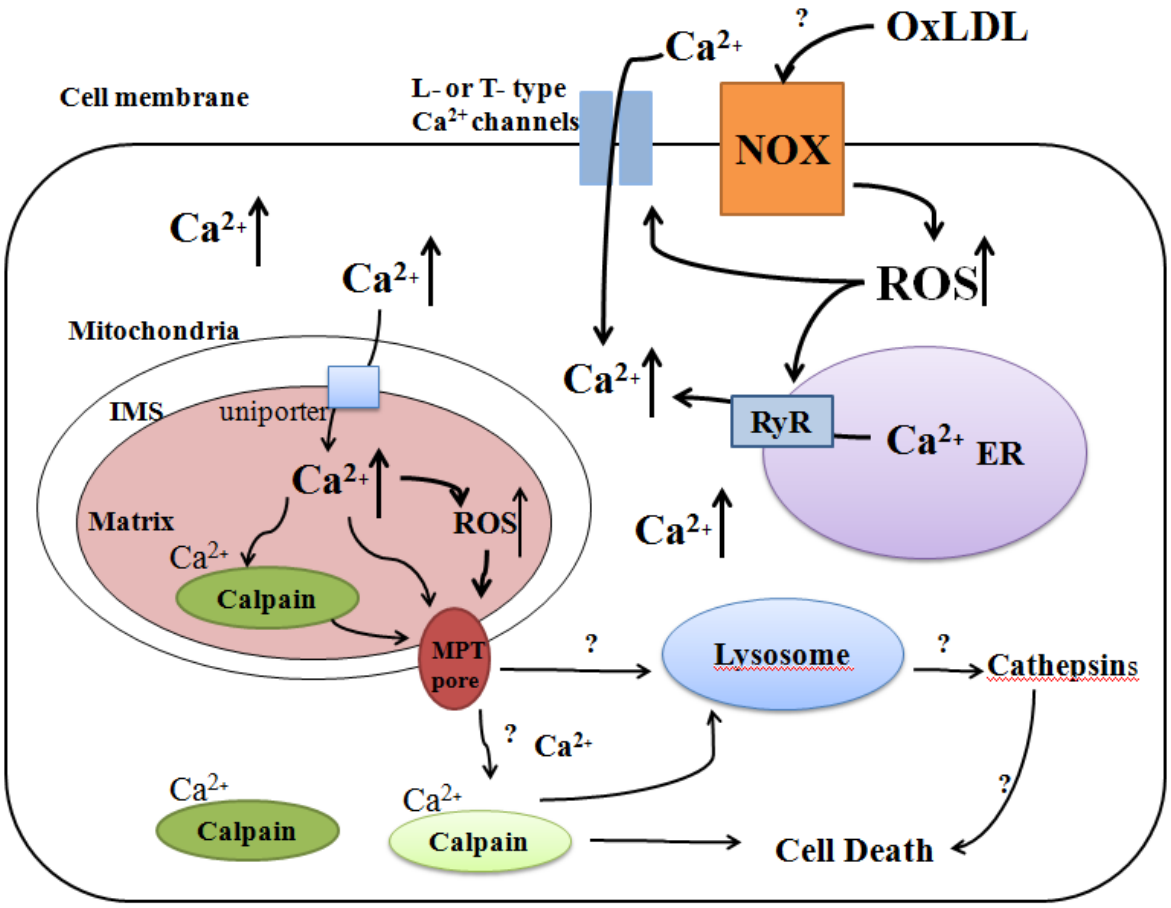

Figure 4.1 Proposed involvement of Ca^{2+} in oxLDL cytotoxicity to U937 cells
OxLDL activates plasma membrane superoxide generating system NADPH oxidase (NOX). NOX-derived ROS triggers the voltage-dependent L- and T-type Ca^{2+} channels on cell membrane and ryanodine receptors (RyRs) on endoplasmic reticulum (ER), resulting in the influx of extracellular Ca^{2+} and release of Ca^{2+} from ER to cytosol. Both events lead to cytosolic Ca^{2+} increase. The excess cytosolic Ca^{2+} can be taken up into mitochondria via Ca^{2+} uniporter on the inner mitochondrial membrane. Ca^{2+} accumulation in mitochondria matrix possibly activates calpain, facilitating mitochondrial permeability transition (MPT) pore to open. Ca^{2+} also triggers increased mitochondrial ROS production, which also contributes to MPT pore opening. MPT pore activation leads to mitochondrial membrane potential loss, along with the release of activated mitochondrial matrix calpain (dark green), Ca^{2+} and other apoptotic factors, such as cytochrome c. The released Ca^{2+} also activate cytosolic calpain (light green). Together with the matrix calpain, they may lead to necrotic cell death by degrading cytoskeletal proteins, leading to cell membrane blebbing and rupture. They can also destabilize lysosomes ,resulting in the release of cathepsin protease that may degrade cellular components, causing cell death. The arrows with "?" indicates that either the pathways are a hypothesis or are not investigated in this research.

4.4 NADPH oxidase (NOX) and oxidative stress

Current results have clearly shown that oxLDL induces increased oxidative stress in U937 cells. The source of oxidative stress and how oxLDL triggers oxidant production is not exactly clear. This study hypothesized that NOX is the major source of ROS production and oxidative stress, and this was investigated via the inhibitory studies by examining the effects of NOX inhibitors apocynin and DPI on oxLDL-mediated cell death, ROS production, intracellular GSH content, aconitase activity and cytosolic Ca^{2+} influx. Both apocynin and DPI are the most commonly used, and have shown inhibitory effects of ROS production in monocytes, macrophages and neutrophils in the past with IC_{50} around 1-10 μM (Gerber et al., 2002, Barbieri et al., 2004, Qin et al., 2006). However, neither of them are very specific NOX inhibitors, and there are some studies suggesting both of them may actually induce oxidative stress in nonphagocytic cells or monocytes where NOX is not completely activated (Riganti et al., 2004, Vejrazka et al., 2005, Riganti et al., 2006). In particular, DPI can inhibit many other flavoproteins and cause complex changes in the cell functions.

In consideration of the potential side effects apocynin and DPI may have on U937 cells, the preliminary experiments were performed to examine their cytotoxicity without adding oxLDL. Studies of the effects of apocynin on cell viability, intracellular superoxide production, GSH level, aconitase activity and cytosolic Ca^{2+} level without the addition of oxLDL revealed that apocynin was not cytotoxic and did not cause any significant oxidative damages in U937 cells. In comparison, DPI was only inert to cells at 1 μM in the absence of oxLDL. DPI above 5 μM caused 20 % cell death and 10-20% increase in intracellular superoxide production, indicating DPI itself was capable of inducing oxidative stress in U937 cells. DPI reduced intracellular aconitase activity in a concentration-dependent manner, and it also directly damaged the aconitase positive control protein, suggesting DPI had other negative effects on cells which places them in a considerable amount of stress due to its non-specificity to a range of flavoproteins. DPI may exert toxicity by affecting the activity of central metabolic pathways such as pentose phosphate pathway (PPP) and the TCA cycle. Riganti *et al.* have observed that DPI inhibited a few NAD(P)H-dependent enzymes in PPP and TCA cycle, including glucose 6-phosphage

dehydrogenase (G6PD), GAPDH and lactate dehydrogenase (LDH), resulting in the increased ROS production and intracellular GSH depletion (Riganti et al., 2004).

Further studies showed that the oxLDL-mediated cell death was prevented by apocynin and 1 μM DPI, implying oxLDL induced U937 cell death via NOX activation. Both apocynin and DPI reduced oxLDL-induced ROS production and completely prevented intracellular GSH loss, suggesting oxLDL-activated NOX is the key factor in oxLDL-induced oxidative stress and subsequent cell death. More importantly, apocynin and DPI elevated GSH levels by 60% compared to cell-only control, showing inhibition of NOX not only reduced intracellular radical flux, also enhanced antioxidant capability. The decreased loss of GSH could be due to the inhibition of NOX activity. Reduction in NOX activity led to the increased availability of NADPH, which can be utilized to regenerate GSH from GSSG, resulting in the elevations in intracellular GSH level. Another possibility is the increased conversion of cysteine to glutathione, as cysteine is part of the cell culture media. The disappearance of the concentration-dependent increase in GSH with the increasing DPI could be because of utilization of GSH in the neutralization of the DPI-mediated side effects.

Moreover, oxLDL-induced intracellular aconitase activity loss was prevented by apocynin, but not by DPI. This is not surprising since it has been shown above that DPI itself caused damages on aconitase. The further examination in the aconitase activity in cytoplasmic and mitochondrial fractions showed apocynin protected the decrease in aconitase activity caused by oxLDL in the cytoplasm, but not in the mitochondria, implying that inhibition of NOX did not stop oxidative damage in mitochondria once mitochondria uncoupling was triggered. This agrees with the above discussion of calcium-dependent mitochondrial oxidative stress.

Inhibition of NOX activity by apocynin reduced the oxLDL-mediated intracellular Ca^{2+} increase, suggesting that the perturbation of intracellular Ca^{2+} is related to oxLDL-mediated NOX activation. How oxLDL-mediated Ca^{2+} influx and NOX-mediated ROS production affect each other is not understood. It is very likely that oxLDL activates NOX, and NOX-caused ROS production triggers the plasma membrane Ca^{2+} channel to open

through thiol alterations on the protein complex, resulting in the influx of extracellular Ca^{2+}, which in turn stimulates mitochondrial Ca^{2+} uptake and ROS production in mitochondria (Inoue et al., 2008). This can be supported by a recent study that inhibition of NOX by apocynin, DPI and gp91ds-tat suppressed the L-type Ca^{2+} channel expression and blocked the influx of extracellular calcium (Wang et al., 2010). In plants, NOX-derived ROS activate plasma membrane Ca^{2+} channels, thereby regulating root hair outgrowth (Foreman et al., 2003). Similarly, the Ca^{2+} release from intracellular store can also be modulated by NOX-derived ROS. An early report revealed that the RyRs on the ER membrane were activated in response to NOX-derived ROS due to the oxidation of the reactive cysteine residues on RyR (Liu and Pessah, 1994). The activation of NOX could also affect the intracellular Ca^{2+} signaling by increasing the sensitivity of intracellular Ca^{2+} in endothelial cells (Zweier et al., 2000). On the other hand, Ca^{2+} influx may also down-regulate NOX by activating Ca^{2+}-dependent protein kinase C. Early study showed that inhibition of protein kinase C by EGTA, a Ca^{2+} chelator, inhibited NOX activation in neutrophils (Cox et al., 1985). Similar observation was also reported in plants, where Ca^{2+} influx activated the NOX, and in turn led to an increase in cytosolic Ca^{2+} (Lecourieux et al., 2002). Therefore, it is possible that oxLDL-activated NOX triggers the cytosolic Ca^{2+} rise, which further supports NOX activity and promotes more ROS production, initiating the down-stream cascade damage to mitochondria. In order to better understand the relationship between Ca^{2+} influx and NOX activation in response to oxLDL, future investigation can be followed up by examining the effects of L- or T-type Ca^{2+} channel blockers, ER RyRs blockers or mitochondrial Ca^{2+} uniporter inhibitors on NOX activation and ROS production.

Mechanism of NOX activation by oxLDL

The detailed immunoblotting study showed that oxLDL activated NOX and increased NOX subunit $p47^{phox}$ protein levels. The progression of NOX activation by oxLDL coincided with ROS generation and both reached the peak levels after 3 hours, implying that oxLDL-activated NOX is the major source of ROS production. Indeed, increased NOX subunit protein levels may contribute to further enhanced NOX activity (Cifuentes et al., 2000). How oxLDL stimulates NOX activation is not exactly known. The lipid peroxide species generated by oxLDL may be involved in the NOX activation. Early research has revealed that lysophosphatidylcholine, one of the active molecules present in

oxLDL, can activate protein kinase C (PKC) upon oxLDL uptake (Kugiyama et al., 1992, Ohgushi et al., 1993). This initial PKC activation is the driving force for $p47^{phox}$ phosphorylation and the subsequent NOX activation. The other studies, on the other hand, suggested the crucial role of oxLDL-protein moiety in NOX activation, in particular apoliproptein B (apoB), though this has not yet been extensively investigated (Nguyen-Khoa et al., 1999). Scavenger receptor CD36 appears to be a key activator of NOX, involving in the binding of lipid and protein components of oxLDL (Nguyen-Khoa et al., 1999, Young et al., 2009). Nguyen-Khoa *et al.* showed that oxLDL-induced NOX activation level in U937 cells was 10 times higher than that in THP-1 cells, which was attributed to the higher CD36 expression levels in U937 cells (Nguyen-Khoa et al., 1999). However, CD36 has been recently shown to be down-regulated by 7,8-NP (Gieseg et al., 2010b), and current study demonstrated the failure of 7,8-NP to prevent oxLDL-induced NOX activation. These together imply that other receptors other than CD36 may be involved in the oxLDL-induced NOX activation mechanism.

4.5 7,8-NP protection against oxLDL-induced oxidative stress

7,8-NP is a redox active compound synthesized intracellularly in human macrophages upon IFN-γ induction. It can act as either a pro-oxidant or antioxidant depending on the chemical environment. This laboratory has shown that 7,8-NP at low micromolar concentrations is a very potent antioxidant (Gieseg et al., 2009c, Gieseg et al., 2008). A maximum protection against oxLDL damage in U937 cells and HMDM was established with 200 μM 7,8-NP (Baird, 2003). The present study showed that 7,8-NP prevented U937 cells from oxLDL-induced cell death, ROS production and intracellular aconitase activity loss. 7,8-NP also decreased Ca^{2+} rise after 3 hours oxLDL treatment. These results are in consistent with the previous studies which showed that 7,8-NP provides protection for U937 cells (Baird et al., 2005b) and for HMDM cells (Amit, 2008) against the toxic effects of oxLDL. This study also showed 7,8-NP above 50 μM did not significantly reduce oxLDL-induced mitochondrial ROS production, indicating 7,8-NP may have no or limited protection against oxidative damage in mitochondria. This may explain the finding that 7,8-NP protected oxLDL-induced aconitase activity loss in cytoplasm, but not in

mitochondria. Moreover, he cytosolic Ca^{2+} increase induced by oxLDL was also reduced by the addition of 7,8-NP, in particular after 3 hours. This suggests that 7,8-NP scavenges ROS, in turn reducing the cytosolic Ca^{2+} rise. The failure of 7,8-NP inhibition of oxLDL-stimulated NOX activation indicates that 7,8-NP did not protect cells by directly preventing NOX activity, but by scavenging NOX-derived radicals.

Current findings are in consistent with previous studies that 7,8-NP can protect cells from oxLDL-induced oxidative stress by scavenging radicals, such as peroxyl radicals, superoxide, hypochlorite and hydroxylradicals (Duggan *et al.*, 2002, Oettl *et al.*, 1997). On a larger scale, the radical scavenging ability of 7,8-NP may explain the inhibition of radical-induced damages to a variety of cellular substrates and cells in the presence of 7,8-NP (Duggan *et al.*, 2001, Duggan *et al.*, 2002). 7,8-NP also inhibits copper-, peroxyl radical- and cell-mediated LDL oxidation (Gieseg *et al.*, 2003, Gieseg *et al.*, 1995). In addition, 7,8-NP has also been shown to prevent oxLDL-induced intracellular GSH loss in both U937 cells and HMDM by scavenging oxLDL-induced intracellular oxidants, which in turn maintained the intracellular redox environment and hence prevented cell viability loss (Baird et al., 2004b, Baird et al., 2005a, Gieseg et al., 2010b).

7,8-NP may also protect cells from oxLDL-induced damage by down-regulating oxLDL scavenge receptor CD36. This is supported by a recent research that 7,8-NP induced a down-regulation of the 100-kDa plasma membrane glycoform of CD36 in HMDM (Gieseg et al., 2010a). A strong link exists between CD36-meidated LDL uptake and ROS production. It has been showed that inhibition of CD36 by anti-CD36 antibodies has greatly reduced levels of ROS production, caspase activation and cell death (Sukhanov et al., 2006, Wintergerst et al., 2000). It is also reported that oxLDL binding to CD36 in HMDM generated large amounts of hydrogen peroxide (Maxeiner et al., 1998). Therefore, 7,8-downregulation of CD36 may also reduce ROS generation and the resulting oxidative stress. This is currently under investigation in this laboratory.

The protective effect of 7,8-NP appears to depend on the nature of the cell. 7,8-NP protects HMDM and U937 cells from oxLDL cytotoxicity and prevents the loss of intracellular

GSH, but it is unable to protect THP-1 cells and restore the THP-1 cellular thiol content though the thiol loss was only 20% (Baird et al., 2005b). THP-1 cells have significantly lower levels of CD36 expression on the plasma membrane compared with U937 cells (Alessio et al., 1996). This may explain the failure of 7,8-NP protection in THP-1 cells in response oxLDL.

4.6 Summery

This study showed that oxLDL causes the cell viability loss in U937 cells, triggers excess ROS production and intracellular GSH loss, which are consistent with previous findings. It also showed oxLDL induced intracellular aconitase activity decrease and cytosolic Ca^{2+} rise, further confirming oxLDL promoted increased oxidative stress in U937 cells.

It was hypothesized that oxLDL activates plasma membrane superoxide generating system NOX, which is a major source of oxidative stress. The inhibitory studies using NOX inhibitors apocynin or DPI showed that inhibition of NOX prevented oxLDL-induced cell death, ROS production, GSH loss and aconitase activity loss. OxLDL-mediated Ca^{2+} elevation was also inhibited by apocynin, indicating a link exists between NOX activation and Ca^{2+} influx in response to oxLDL. It is suspected that NOX is activated by oxLDL, and NOX-derived ROS production triggers both plasma membrane Ca^{2+} channels and RyRs on the ER membrane to open through thiol alterations on the protein complex, leading to extracellular Ca^{2+} influx and ER Ca^{2+} release. The accumulation of cytosolic Ca^{2+} mediates the mitochondrial Ca^{2+} uptake via mitochondrial Ca^{2+} uniporter and the subsequent oxidative stress in mitochondria, resulting in calpain activation, MPT pore opening and mitochondrial membrane potential loss. This notion can be further investigated in future by examining the effects of L- or T-type Ca^{2+} channel blockers, ER RyRs blockers or mitochondrial Ca^{2+} uniporter inhibitors on NOX activation and ROS production. Furthermore, the immunoblotting studies directly showed oxLDL stimulated NOX subunit $p47^{phox}$ expression and activated NOX, and the progression of NOX activation was strongly correlated to oxLDL-induced ROS production. These results suggest NOX generates a burst of superoxide in response to oxLDL, resulting in the increased oxidative stress and cell death.

This study also examined the protective effect of 7,8-NP on oxLDL-mediate damage in U937 cells. It showed that 7,8-NP prevented U937 cells from oxLDL-induced cell death, ROS production and intracellular aconitase activity loss. 7,8-NP also decreased Ca^{2+} rise after 3 hours oxLDL treatment. These findings suggest that 7,8-NP reduces oxLDL-mediated oxidative stress and protects cells from oxLDL damage by scavenging radical flux. The failure of 7,8-NP to inhibit oxLDL-activation of NOX via $p47^{phox}$ suggests that 7,8-NP scavenges NOX-derived ROS rather than directly interfering NOX activity.

In conclusion, this research demonstrates that NOX plays a key role in oxLDL-induced cell death. It clearly shows that oxLDL activated NOX in U937 cells, and oxLDL-activated NOX triggers oxidative stress via ROS overproduction and GSH depletion, causing aconitase inactivation. NOX activation also triggers cytosolic Ca^{2+} increase, which could lead to mitochondria dysfunction and ROS production, causing further damage to aconitase. The inactivation of metabolic enzyme, such as GAPDH and aconitase, will subsequently result in cellular metabolism failure, and eventually cell death. 7,8-NP can protected oxLDL-induced cell death by scavenging NOX-mediated radicals. This studies also leads to the further investigation on the potential relationship between Ca^{2+} influx and NOX in order to better understand the mechanism of oxLDL-induced cell death and the crucial role of oxidative stress in the development of atherosclerosis.

ACKNOWLEDGEMENTS

I would like to thank my research supervisor, Assoc. Professor Steven Gieseg, for his guidance and advice throughout the course of this research, and for being an active and available supervisor. I am also grateful for the input and advice of my co-supervisor, Dr. Ashley Garrill. I am very grateful to our technician, Maggie Tisch, for looking after the running of the laboratory and for her always cheerful nature; to Ela Sawicka for her great assistant throughout this research; to Jan Mackenzie for assistance with the fluorescence microscope; to Jackie Healy for her help using the ultracentrifuge and micro-tip sonicator; and to John Scott for solving computer problems.

Thank you very much to all of the generous people who donated blood that was used for the isolation of LDL, as this was a crucial part of my work. Also, to the nurses from the Student Health Centre who helped us with blood-letting; I would like to mention The Haematology Research Group (University of Otago) for gifting us the U937 cell line that I used throughout my research. A huge thank you to Assoc. Professor Sally McCormick from University of Otago to provide ultracentrifuge for us to make LDL preparation after Christchurch earthquakes. I would also like to acknowledge the National Heart Foundation of New Zealand supplying the funding for this research.

I would like to give special thanks to all of the members of the Free Radical Biochemistry Laboratory, in particular Hannah, Laura, Anastasia, Raj, Hanadi for their support, sharing of ideas, sharing of feelings and encouragements during the most difficult time after the Christchurch earthquakes, and also the delicious food for lab meetings. Special thanks to Hanadi and Lucy for being patient teachers during my first couple of months; to Raj for helping me with HPLC; to Hannah for proof-reading my thesis; and to Izani and Nathan for being lovely person to share the office. In particular, I would like to express a big thanks to Anastasia for her help in Western blot analysis and all the problems I had throughout my research, and thank you for going down to Dunedin to make LDL for all of us after the earthquakes. This work would have been difficult without all of you.

I also want to express love and thanks to my family in China for their support and encouragement, to my friends for providing entrainment, and especially to my husband Ricky for his endless support, patience and love through my study.

REFERENCES

Abo, A., Pick, E., Hall, A., Totty, N., Teahan, C. G. & Segal, A. W. (1991) Activation of the nadph oxidase involves the small gtp-binding protein p21(rac1). *Nature,* 353**,** 668-670.

Abo, A., Webb, M. R., Grogan, A. & Segal, A. W. (1994) Activation of nadph oxidase involves the dissociation of p21(rac) from its inhibitory gdp/gtp exchange protein (rhogdi) followed by its translocation to the plasma membrane. *Biochemical Journal,* 298**,** 585-591.

Aguilar, H. I., Botla, R., Arora, A. S., Bronk, S. F. & Gores, G. J. (1996) Induction of the mitochondrial permeability transition by protease activity in rats: A mechanism of hepatocyte necrosis. *Gastroenterology,* 110**,** 558-566.

Aldieri, E., Riganti, C., Polimeni, M., Gazzano, E., Lussiana, C., Campia, I. & Ghigo, D. (2008) Classical inhibitors of nox nad(p)h oxidases are not specific. *Current Drug Metabolism,* 9**,** 686-696.

Alessio, M., Demonte, L., Scirea, A., Gruarin, P., Tandon, N. N. & Sitia, R. (1996) Synthesis, processing, and intracellular transport of cd36 during monocytic differentiation. *Journal of Biological Chemistry,* 271**,** 1770-1775.

Amit, Z. (2008) A modle of complex plaque formation: 7,8-dihydroneopterin protects human monocyte-derived macrophages from oxidised low density lipoprotein-induced death. University of Canterbury, Christchurch, New Zealand.

Anderson, F., Game, B. A., Atchley, D., Xu, M., Lopes-Virella, M. F. & Huang, Y. (2002) Ifn-gamma pretreatment augments immune complex-induced matrix metalloproteinase-1 expression in u937 histiocytes. *Clinical Immunology,* 102**,** 200-207.

Anzai, K., Ogawa, K., Kuniyasu, A., Ozawa, T., Yamamoto, H. & Nakayama, H. (1998) Effects of hydroxyl radical and sulfhydryl reagents on the open probability of the purified cardiac ryanodine receptor channel incorporated into planar lipid bilayers. *Biochemical and Biophysical Research Communications,* 249**,** 938-942.

Arosio, B., Santambrogio, D., Gagliano, N., Ryan, A., Biasi, F., Vergani, C. & Annoni, G. (1997) Glutathione pretreatment lessens the acute liver injury induced by carbon tetrachloride. *Pharmacology and Toxicology,* 81**,** 164-168.

Arrington, D. D., Van Vleet, T. R. & Schnellmann, R. G. (2006) Calpain 10: A mitochondrial calpain and its role in calcium-induced mitochondrial dysfunction. *American Journal of Physiology - Cell Physiology,* 291**,** C1159-C1171.

Aviram, M. & Rosenblat, M. (2003) Macrophage nadph oxidase activation under oxidative stress increases cell-mediated oxidation of ldl and accelerates atherosclerosis development. *Atherosclerosis Supplements,* 4**,** 283-1.

Babior, B. M. (1999) Nadph oxidase: An update. *Blood,* 93**,** 1464-1476.

Baird, S. (2003) 7,8-dihydroneopterin inhibition of oxidised low density lipoprotein-induced cellular death. *PhD Thesis,* Universtiy of Canterbury, New Zealand.

Baird, S. K., Hampton, M. & Gieseg, S. P. (2004a) Oxidised ldl triggers phosphatidylserine exposure in human monocyte cell lines by both caspase-dependent and independent mechanisms. *FEBS Letters,* 578**,** 169-174.

Baird, S. K., Hampton, M. B. & Gieseg, S. P. (2004b) Oxidized ldl triggers phosphatidylserine exposure in human monocyte cell lines by both caspase-dependent and -independent mechanisms. *FEBS Letters,* 578**,** 169-174.

Baird, S. K., Reid, L., Hampton, M. & Gieseg, S. P. (2005a) Oxldl induced cell death is inhibited by the macrophage synthesised pterin, 7,8-dihydroneopterin, in u937 cells but not thp-1 cells. *Biochimica et Biophysica Acta,* 1745**,** 361-369.

Baird, S. K., Reid, L., Hampton, M. B. & Gieseg, S. P. (2005b) Oxldl induced cell death is inhibited by the macrophage synthesised pterin, 7,8-dihydroneopterin, in u937 cells but not thp-1 cells. *Biochimica et Biophysica Acta (BBA) - Molecular Cell Research,* 1745**,** 361-369.

Ball, R. Y., Stowers, E. C., Burton, J. H., Cary, N. R. B., Skepper, J. N. & Mitchinson, M. J. (1995) Evidence that the death of macrophage foam cells contributes to the lipid core of atheroma. *Atherosclerosis,* 114**,** 45-54.

Ballatori, N., Krance, S. M., Notenboom, S., Shi, S., Tieu, K. & Hammond, C. L. (2009) Glutathione dysregulation and the etiology and progression of human diseases. *Biological Chemistry,* 390**,** 191-214.

Banfi, B., Molnar, G., Maturana, A., Steger, K., Hegedus, B., Demaurex, N. & Krause, K. H. (2001) A ca2+-activated nadph oxidase in testis, spleen, and lymph nodes. *Journal of Biological Chemistry,* 276**,** 37594-37601.

Barbieri, S. S., Cavalca, V., Eligini, S., Brambilla, M., Caiani, A., Tremoli, E. & Colli, S. (2004) Apocynin prevents cyclooxygenase 2 expression in human monocytes through nadph oxidase and glutathione redox-dependent mechanisms. *Free Radical Biology and Medicine,* 37**,** 156-165.

Barry-Lane, P. A., Patterson, C., Van Der Merwe, M., Hu, Z., Holland, S. M., Yeh, E. T. H. & Runge, M. S. (2001) P47phox is required for atherosclerotic lesion progression in apoe-/- mice. *Journal of Clinical Investigation,* 108**,** 1513-1522.

Bayraktutan, U., Blayney, L. & Shah, A. M. (2000) Molecular characterization and localization of the nad(p)h oxidase components gp91-phox and p22-phox in endothelial cells. *Arteriosclerosis, Thrombosis, and Vascular Biology,* 20**,** 1903-1911.

Bayraktutan, U., Draper, N., Lang, D. & Shah M, A. (1998) Expression of a functional neutrophil-type nadph oxidase in cultured rat coronary microvascular endothelial cells. *Cardiovascular Research,* 38**,** 256-262.

Bedard, K. & Krause, K. H. (2007) The nox family of ros-generating nadph oxidases: Physiology and pathophysiology. *Physiological Reviews,* 87**,** 245-313.

Beinert, H. & Kennedy, M. C. (1993) Aconitase, a two-faced protein: Enzyme and iron regulatory factor. *FASEB Journal,* 7**,** 1442-1449.

Beinert, H., Kennedy, M. C. & Stout, C. D. (1996) Aconitase as iron-sulfur protein, enzyme, and iron-regulatory protein. *Chemical Reviews,* 96**,** 2335-2373.

Berliner, J. A. & Heinecke, J. W. (1996) The role of oxidised lipoproteins in atherosclerosis. *Free Radical Biology and Medicine,* 20**,** 707-727.

Berthier, A., Lemaire-Ewing, S., Prunet, C., Monier, S., Athias, A., Bessede, G., De Barros, J. P. P., Laubriet, A., Gambert, P., Lizard, G. & Neel, D. (2004) Involvement of a calcium-dependent dephosphorylation of bad associated with the localization of trpc-1 within lipid rafts in 7-ketocholesterol-induced thp-1 cell apoptosis. *Cell Death and Differentiation,* 11**,** 897-905.

Bjorkerud, B. & Bjorkerud, S. (1996) Contrary effects of light and strongly oxidised ldl with promotion of growth verus apoptosis on artery smooth muscle cells, macrophages and fibroblasts. *Atherosclerosis, Thrombosis and Vascular Biology,* 16**,** 416-424.

Boggs, S. E., Mccormick, T. S. & Lapetina, E. G. (1998) Glutathione levels determine apoptosis in macrophages. *Biochemical and Biophysical Research Communications,* 247**,** 229-233.

Brandes, R. P. & Kreuzer, J. (2005) Vascular nadph oxidases: Molecular mechanisms of activation. *Cardiovascular Research,* 65**,** 16-12.

Brown, M. S. & Goldstein, J. L. (1984) How ldl receptors influence cholesterol and atherosclerosis. *Scientific American,* Nov**,** 52-60.

Bulteau, A. L., Ikeda-Saito, M. & Szweda, L. I. (2003) Redox-dependent modulation of aconitase activity in intact mitochondria. *Biochemistry,* 42**,** 14846-14855.

Cabiscol, E., Piulats, E., Echave, P., Herrero, E. & Ros, J. (2000) Oxidative stress promotes specific protein damage in saccharomyces cerevisiae. *Journal of Biological Chemistry,* 275**,** 27393-27398.

Cai, H. & Harrison, D. G. (2000) Endothelial dysfunction in cardiovascular diseases: The role of oxidant stress. *Circulation Research,* 87**,** 840-844.

Campbell, D. L., Stamler, J. S. & Strauss, H. C. (1996) Redox modulation of l-type calcium channels in ferret ventricular myocytes: Dual mechanism regulation by nitric oxide and s-nitrosothiols. *Journal of General Physiology,* 108**,** 277-293.

Carafoli, E. (1987) Intracellular calcium homeostasis. *Annual Review of Biochemistry,* 56**,** 395-433.

Cassatella, M. A., Dellabianca, V., Berton, G. & Rossi, F. (1985) Activation by gamma-interferon of human macrophage capability to produce toxic oxygen molecules is accompanied by decreased km of the superoxide-generating nadph oxidase. *Biochemical and Biophysical Research Communications,* 132**,** 908-914.

Castor, L. R. G., Locatelli, K. A. & Ximenes, V. F. (2010) Pro-oxidant activity of apocynin radical. *Free Radical Biology and Medicine,* 48**,** 1636-1643.

Castro, L., Rodriguez, M. & Radi, R. (1994) Aconitase is readily inactivated by peroxynitrite, but not by its precursor, nitric oxide. *Journal of Biological Chemistry,* 269**,** 29409-29415.

Cathcart, M. K. (2004) Regulation of superoxide anion production by nadph oxidase in monocytes/macrophages: Contributions to atherosclerosis. *Arteriosclerosis, Thrombosis, and Vascular Biology,* 24**,** 23-28.

Cathcart, M. K., Mcnally, A. K., Morel, D. W. & Chisolm Iii, G. M. (1989) Superoxide anion participation in human monocyte-mediated oxidation of low-density lipoprotein and conversion of low-density lipoprotein to a cytotoxin. *Journal of Immunology,* 142**,** 1963-1969.

Chernyak, B. V., Dedov, V. N. & Chernyak, V. Y. (1995) Ca^{2+}-triggered membrane permeability transition in deenergized mitochondria from rat liver. *FEBS Letters,* 365**,** 75-78.

Chung, B. H., Wilkinson, T., Geer, J. C. & Segrest, J. P. (1980) Preparative and quantitative isolation of plasma lipoproteins: Rapid, single discontinuous density gradient ultracentrifugation in a vertical rotor. *Journal of Lipid Research,* 21**,** 284-291.

Cifuentes, M. E., Rey, F. E., Carretero, O. A. & Pagano, P. J. (2000) Upregulation of p67(phox) and gp91(phox) in aortas from angiotensin-indufused mice. *American Journal of Physiology - Heart and Circulatory Physiology,* 279**,** 2234-2240.

Colles, S. M., Maxson, J. M., Carlson, S. G. & Chisolm, G. M. (2001) Oxidized ldl-induced injury and apoptosis in atherosclerosis - potential roles for oxysterols. *Trends in Cardiovascular Medicine,* 11**,** 131-138.

Cotgreave, I. A. & Moldeus, P. (1986) Methodologies for the application of monobromobimane to the simultaneous analysis of soluble and protein thiol components of biological systems. *J. Biochem. Biophys. Meth.,* 13**,** 231-249.

Cox, J. A., Jeng, A. Y. & Sharkey, N. A. (1985) Activation of the human neutrophil nicotinamide adenine dinucleotide phosphate (nadph)-oxidase by protein kinase c. *Journal of Clinical Investigation,* 76**,** 1932-1938.

Cross, A. R. & Curnutte, J. T. (1995) The cytosolic activating factors p47(phox) and p67(phox) have distinct roles in the regulation of electron flow in nadph oxidase. *Journal of Biological Chemistry,* 270**,** 6543-6548.

Cross, A. R. & Jones, O. T. G. (1986) The effect of the inhibitor diphenylene iodonium on the superoxide-generating system of neutrophils. Specific labelling of a component polypeptide of the oxidase. *Biochemical Journal,* 237**,** 111-116.

De Mendez, I., Adams, A. G., Sokolic, R. A., Malech, H. L. & Leto, T. L. (1996) Multiple sh3 domain interactions regulate nadph oxidase assembly in whole cells. *EMBO Journal,* 15**,** 1211-1220.

Deng, T., Zhang, L., Ge, Y., Lu, M. & Zheng, X. (2009) Redistribution of intracellular calcium and its effect on apoptosis in macrophages: Induction by oxidized ldl. *Biomedicine and Pharmacotherapy,* 63**,** 267-274.

Deng, T. L., Yu, L., Ge, Y. K., Zhang, L. & Zheng, X. X. (2005) Intracellular-free calcium dynamics and f-actin alteration in the formation of macrophage foam cells. *Biochemical and Biophysical Research Communications,* 338**,** 748-756.

Deniaud, A., Sharaf El Dein, O., Maillier, E., Poncet, D., Kroemer, G., Lemaire, C. & Brenner, C. (2008) Endoplasmic reticulum stress induces calcium-dependent permeability transition, mitochondrial outer membrane permeabilization and apoptosis. *Oncogene,* 27**,** 285-299.

Denke, X. D., Wang, D., Dumont, J. E. & Miot, F. (2002) Characterization of thox proteins as components of the thyroid h2o2-generating system. *Experimental Cell Research,* 273**,** 187-196.

Dong, Y., Wu, Y., Wu, M., Wang, S., Zhang, J., Xie, Z., Xu, J., Song, P., Wilson, K., Zhao, Z., Lyons, T. & Zou, M. H. (2009) Activation of protease calpain by oxidized and glycated ldl increases the degradation of endothelial nitric oxide synthase. *Journal of Cellular and Molecular Medicine,* 13**,** 2899-2910.

Doussiere, J. & Vignais, P. V. (1992) Diphenylene iodonium as an inhibitor of the nadph oxidase complex of bovine neutrophils. Factors controlling the inhibitory potency of diphenylene iodonium in a cell-free system of oxidase activation. *European Journal of Biochemistry,* 208**,** 61-71.

Duggan, S., Rait, C., Gebicki, J. M. & Gieseg, S. P. (2001) Inhibition of protein oxidation by the macrophage-synthesised antioxidant 7,8-dihydroneopterin. *Redox Rep,* 6**,** 188-90.

Duggan, S., Rait, C., Platt, A. & Gieseg, S. P. (2002) Protein and thiol oxidation in cells exposed to peroxyl radicals is inhibited by the macrophage synthesised pterin 7,8-dihydroneopterin. *Biochimica et Biophysica Acta (BBA) - Molecular Cell Research,* 1591**,** 139-145.

Duke, R. C., Ojcius, D. M. & Young, J. D. (1996) Cell suicide in health and disease. *Scientific American,* Dec**,** 48-55.

Dworakowski, R., Anilkumar, N., Zhang, M. & Shah, A. M. (2006) Redox signalling involving nadph oxidase-derived reactive oxygen species. *Biochemical Society Transactions,* 34**,** 960-964.

Finan, P., Shimizu, Y., Gout, I., Hsuan, J., Truong, O., Butcher, C., Bennett, P., Waterfield, M. D. & Kellie, S. (1994) An sh3 domain and proline-rich sequence mediate an interaction between two components of the phagocyte nadph oxidase complex. *Journal of Biological Chemistry,* 269**,** 13752-13755.

Foreman, J., Demidchik, V., Bothwell, J. H. F., Mylona, P., Miedema, H., Angel Torres, M., Linstead, P., Costa, S., Brownlee, C., Jones, J. D. G., Davies, J. M. & Dolan, L. (2003) Reactive oxygen species produced by nadph oxidase regulate plant cell growth. *Nature,* 422**,** 442-446.

Forman, H. J., Zhang, H. & Rinna, A. (2009) Glutathione: Overview of its protective roles, measurement, and biosynthesis. *Molecular Aspects of Medicine,* 30**,** 1-12.

Gackowski, D., Kruszewski, M., Jawien, A., Ciecierski, M. & Olinski, R. (2001) Further evidence that oxidative stress may be a risk factor responsible for the development of atherosclerosis. *Free Radical Biology and Medicine,* 31**,** 542-547.

Galis, Z. S., Sukhova, G. K., Kranzhofer, R., Clark, S. & Libby, P. (1995) Macrophage foam cells from experimental atheroma constitutively produce matrix-degrading proteinases. *Proceedings of the National Academy of Sciences of the United States of America,* 92**,** 402-406.

Gardner, P. R. & Fridovich, I. (1992) Inactivation-reactivation of aconitase in escherichia coli. A sensitive measure of superoxide radical. *Journal of Biological Chemistry,* 267**,** 8757-8763.

Gardner, P. R., Nguyen, D. D. H. & White, C. W. (1994) Aconitase is a sensitive and critical target of oxygen poisoning in cultured mammalian cells and in rat lungs. *Proceedings of the National Academy of Sciences of the United States of America,* 91**,** 12248-12252.

Gardner, P. R., Raineri, I., Epstein, L. B. & White, C. W. (1995) Superoxide radical and iron modulate aconitase activity in mammalian cells. *Journal of Biological Chemistry,* 270**,** 13399-13405.

Geiszt, M., Kopp, J. B., Varnai, P. & Leto, T. L. (2000) Identification of renox, an nad(p)h oxidase in kidney. *Proceedings of the National Academy of Sciences of the United States of America,* 97**,** 8010-8014.

Geiszt, M., Witta, J., Baffi, J., Lekstrom, K. & Leto, T. L. (2003) Dual oxidases represent novel hydrogen peroxide sources supporting mucosal surface host defense. *The FASEB journal : official publication of the Federation of American Societies for Experimental Biology,* 17**,** 1502-1504.

Gerber, C. E., Bruchelt, G., Ledinski, G., Greilberger, J., Niethammer, D. & Jurgens, G. (2002) Low-density lipoprotein modification by normal, myeloperoxidase-deficient and nadph oxidase-deficient granulocytes and the impact of redox active transition metal ions. *Redox Report,* 7**,** 111-119.

Gieseg, S. P., Amit, Z., Yang, Y.-T., Shchepetkina, A. & Katouah, H. (2010a) Oxidant production, oxldl uptake, and cd36 levels in human monocyte–derived macrophages are downregulated by the macrophage-generated antioxidant 7,8-dihydroneopterin. *ANTIOXIDANTS & REDOX SIGNALING,* 13.

Gieseg, S. P., Amit, Z., Yang, Y. T., Shchepetkina, A. & Katouah, H. (2010b) Oxidant production, oxldl uptake, and cd36 levels in human monocyte-derived macrophages are downregulated by the macrophage-generated antioxidant 7,8-dihydroneopterin. *Antioxidants and Redox Signaling,* 13**,** 1525-1534.

Gieseg, S. P., Crone, E. & Amit, Z. (2009a) Oxidised low density lipoprotein cytotoxicity and vascular disease. *Endogenous toxins: Diet, genetics, disease and treatment.*

Gieseg, S. P., Crone, E. M., Flavall, E. & Amit, Z. (2008) Potential to inhibit growth of atherosclerotic plaque development through modulation of macrophage neopterin/7,8-dihydroneopterin synthesis. *Brit J Pharmacol,* 153**,** 627-35.

Gieseg, S. P. & Esterbauer, H. (1994) Low density lipoprotein is saturable by pro-oxidant copper. *FEBS Letters,* 343**,** 188-194.

Gieseg, S. P., G., M. & Glubb, D. (2000) Inhibition of haemolysis by the macrophage synthesized antioxidant, 7,8-dihydroneopterin. *Redox Report,* 5**,** 97-100.

Gieseg, S. P., Leake, D. S., Flavall, E. M., Amit, Z., Reid, L. & Yang, Y. (2009b) Macrophage antioxidant protection within atherosclerotic plaques. *Frontiers in Bioscience,* 14**,** 1230-1246.

Gieseg, S. P., Leake, D. S., Flavall, E. M., Amit, Z., Reid, L. & Yang, Y. T. (2009c) Macrophage antioxidant protection within atherosclerotic plaques. *Front Biosci.,* 14**,** 1230-46.

Gieseg, S. P., Pearson, J. & Firth, C. A. (2003) Protein hydroperoxides are a major product of low density lipoprotein oxidation during copper, peroxyl radical and macrophage-mediated oxidation. *Free Radic Res.,* 37**,** 983-91.

Gieseg, S. P., Reibnegger, G., Wachter, H. & Esterbauer, H. (1995) 7,8 dihydroneopterin inhibits low density lipoprotein oxidation in vitro. Evidence that this macrophage secreted pteridine is an anti-oxidant. *Free Radic Res. ,* 23**,** 123-36.

Gieseg, S. P., Simpson, J. A., Charlton, T. S., Duncan, M. W. & Dean, R. T. (1993) Protein bound 3,4-dihydroxyphenylalanine is a major reductant formed during hydroxyl radical damage to proteins. *Biochemistry,* 32**,** 4780-4786.

Gieseg, S. P., Whybrow, J., Glubb, D. & Rait, C. (2001) Protection of u937 cells from free radical damage by the macrophage synthesized antioxidant 7,8-dihydroneopterin. *Free Radic Res.,* 35**,** 311-8.

Glass, C. K. & Witztum, J. L. (2001) Atherosclerosis: The road ahead. *Cell,* 104**,** 503-516.

Gores, G. J., Miyoshi, H., Botla, R., Aguilar, H. I. & Bronk, S. F. (1998) Induction of the mitochondrial permeability transition as a mechanism of liver injury during cholestasis: A potential role for mitochondrial proteases. *Biochimica et Biophysica Acta - Bioenergetics,* 1366**,** 167-175.

Griendling, K. K., Sorescu, D. & Ushio-Fukai, M. (2000) Nad(p)h oxidase: Role in cardiovascular biology and disease. *Circulation Research,* 86**,** 494-501.

Grijalba, M. T., Vercesi, A. E. & Schreier, S. (1999) Ca2+-induced increased lipid packing and domain formation in submitochondrial particles. A possible early step in the mechanism of ca2+- stimulated generation of reactive oxygen species by the respiratory chain. *Biochemistry,* 38**,** 13279-13287.

Halliwell, B. & Gutteridge, J. M. C. (1999) *Free radicals in biology and medicine, 3rd edition,,* Oxford, Oxford University Press.

Halliwell, B. & Gutteridge, J. M. C. (2007a) Free radicals in biology and medicine.

Halliwell, B. & Gutteridge, J. M. C. (2007b) *Free radicals in biology and medicine, fourth edition,*

, Oxford Univeristy Press, Oxford

Hamilton, C. A., Brosnan, M. J., Al-Benna, S., Berg, G. & Dominiczak, A. F. (2002) Nad(p)h oxidase inhibition improves endothelial function in rat and human blood vessels. *Hypertension,* 40**,** 755-762.

Hampton, M. B., Morgan, P. E. & Davies, M. J. (2002) Inactivation of cellular caspases by peptide-derived tryptophan and tyrosine peroxides. *FEBS Letters,* 527**,** 289-292.

Han, H. J., Tokino, T. & Nakamura, Y. (1998) Csr, a scavenger receptor-like protein with a protective role against cellular damage caused by uv irradiation and oxidative stress. *Human Molecular Genetics,* 7**,** 1039-1046.

Harada-Shiba, M., Kinoshita, M., Kamido, H. & Shimokado, K. (1998) Oxidized low density lipoprotein induces apoptosis in cultured human umbilical vein endothelial cells by common and unique mechanisms. *Journal of Biological Chemistry,* 273**,** 9681-9687.

Haramaki, N. & Packer, L. (1994) Oxidative stress indices in exercise. IN SEN, C. K., PACKER, L. & HANNINEN, O. (Eds.) *Exercise and oxygen toxicity.* Amsterdam, Elsevier.

Harrison, D., Griendling, K. K., Landmesser, U., Hornig, B. & Drexler, H. (2003) Role of oxidative stress in atherosclerosis. *American Journal of Cardiology,* 91**,** 7A-11A.

Haunstetter, A. & Izumo, S. (1998) Apoptosis - basic mechanisms and implications for cardiovascular disease. *Circulation Research,* 82**,** 1111-1129.

Hausladen, A. & Fridovich, I. (1994) Superoxide and peroxynitrite inactivate aconitases, but nitric oxide does not. *Journal of Biological Chemistry,* 269**,** 29405-29408.

Heales, S. J. R., Blair, J. A., Meinschard, C. & Ziegler, I. (1988) Inhibition of monocyte luminol-dependent chemiluminescence by tetrahydrobiopterin and free radical oxidation of tetrahydrobiopterin, dihydrobiopterin and dihydroneopterin. *Cell Biochemistry and Function,* 6**,** 191-195.

Holland, J. A. (1999) Prevention of atherosclerosis using nadph oxidase inhibitors. *US Patent*.

Holland, J. A., Meyer, J. W., Chang, M. M., O'donnell, R. W., Johnson, D. K. & Ziegler, L. M. (1998) Thrombin stimulated reactive oxygen species production in cultured human endothelial cells. *Endothelium: Journal of Endothelial Cell Research,* 6**,** 113-121.

Holland, P. C., Clark, M. G., Bloxham, D. P. & Lardy, H. A. (1973) Mechanism of action of the hypoglycemic agent diphenyleneiodonium. *Journal of Biological Chemistry,* 248**,** 6050-6058.

Hsich, E., Segal, B. H., Pagano, P. J., Rey, F. E., Paigen, B., Deleonardis, J., Hoyt, R. F., Holland, S. M. & Finkel, T. (2000) Vascular effects following homozygous disruption of p47(phox): An essential component of nadph oxidase. *Circulation,* 101**,** 1234-1236.

Huang, J. & Kleinberg, M. E. (1999) Activation of the phagocyte nadph oxidase protein p47(phox): Phosphorylation controls sh3 domain-dependent binding to p22(phox). *Journal of Biological Chemistry,* 274**,** 19731-19737.

Inoue, T., Suzuki, Y., Yoshimaru, T. & Ra, C. (2008) Reactive oxygen species produced up- or downstream of calcium influx regulate proinflammatory mediator release from mast cells: Role of nadph oxidase and mitochondria. *Biochimica et Biophysica Acta - Molecular Cell Research,* 1783**,** 789-802.

Ito, Y., Pagano, P. J., Tornheim, K., Brecher, P. & Cohen, R. A. (1996) Oxidative stress increases glyceraldehyde-3-phosphate dehydrogenase mrna levels in isolated rabbit aorta. *American Journal of Physiology Heart And Circulatory Physiology,* 39**,** H81-H87.

Jang, I. K., Lassila, R. & Fuster, V. (1993) Atherogenesis and inflammation. *Euro. Heart. J.,* 14**,** 2-6.

Jessup, W., Krithairides, L. & Stocker, R. (2004) Lipid oxidation in atherogenesis: An overview. *Biochemical Society Transactions,* 32**,** 134-138.

Jones, O. T. G. (1994) The regulation of superoxide production by the nadph oxidase of neutrophils and other mammalian cells. *BioEssays,* 16**,** 919-923.

Jones, S. A., O'donnell, V. B., Wood, J. D., Broughton, J. P., Hughes, E. J. & Jones, O. T. G. (1996) Expression of phagocyte nadph oxidase components in human endothelial cells. *American Journal of Physiology - Heart and Circulatory Physiology,* 40**,** H1626-H1634.

Juliet, P. A. R., Hayashi, T., Iguchi, A. & Ignarro, L. J. (2003) Concomitant production of nitric oxide and superoxide in human macrophages. *Biochemical and Biophysical Research Communications,* 310**,** 367-370.

Kagan, V. E., Gleiss, B., Tyurina, Y. Y., Tyurin, V. A., Elenstrom-Magnusson, C., Liu, S. X., Serinkan, F. B., Arroyo, A., Chandra, J., Orrenius, S. & Fadeel, B. (2002) A role for oxidative stress in apoptosis: Oxidation and externalization of phosphatidylserine is required for macrophage clearance of cells undergoing fas-mediated apoptosis. *J Immunol.,* 169**,** 487-499.

Kappler, M., Gerry, A. J., Brown, E., Reid, L., Leake, D. S. & Gieseg, S. P. (2007) Aqueous peroxyl radical exposure to thp-1 cells causes glutathione loss followed by protein oxidation and cell death without increased caspase-3 activity. *Biochemica et Biophysica Acta,* 1773**,** 945-953.

Kirk, E. A., Dinauer, M. C., Rosen, H., Chait, A., Heinecke, J. W. & Leboeuf, R. C. (2000) Impaired superoxide production due to a deficiency in phagocyte nadph oxidase fails to inhibit atherosclerosis in mice. *Arteriosclerosis, Thrombosis, and Vascular Biology,* 20**,** 1529-1535.

Kobayashi, T., Robinson, J. M. & Seguchi, H. (1998) Identification of intracellular sites of superoxide production in stimulated neutrophils. *Journal of Cell Science,* 111**,** 81-91.

Koch, C. A., Anderson, D., Moran, M. F., Ellis, C. & Pawson, T. (1991) Sh2 and sh3 domains: Elements that control interactions of cytoplasmic signaling proteins. *Science,* 252**,** 668-674.

Konstantinova, S. G. & Russanov, E. M. (1996) Aconitase activity in rat liver. *Comparative Biochemistry and Physiology - B Biochemistry and Molecular Biology,* 113**,** 125-130.

Kowaltowski, A. J., Vercesi, A. E. & Castilho, R. F. (1997) Mitochondrial membrane protein thiol reactivity with n-ethylmaleimide or mersalyl is modified by ca2+: Correlation with mitochondrial permeability transition. *Biochimica et Biophysica Acta - Bioenergetics,* 1318**,** 395-402.

Kugiyama, K., Ohgushi, M., Sugiyama, S., Murohara, T., Fukunaga, K., Miyamoto, E. & Yasue, H. (1992) Lysophosphatidylcholine inhibits surface receptor-mediated intracellular signals in endothelial cells by a pathway involving protein kinase c activation. *Circulation Research,* 71**,** 1422-1428.

Lecourieux, D., Mazars, C., Pauly, N., Ranjeva, R. & Pugin, A. (2002) Analysis and effects of cytosolic free calcium increases in response to elicitors in nicotiana plumbaginifolia cells. *Plant Cell,* 14**,** 2627-2641.

Leeuwenburgh, C., Rasmussen, J. E., Hsu, F., Mueller, D. M., Pennathur, S. & Heinecke, J. W. (1997) Mass spectrometric quantification of markers for protein oxidation by tyrosyl radical, copper, and hydroxyl radical in low density lipoprotein isolated from human atherosclerotic plaques. *The Journal of Biological Chemistry,* 272**,** 3520-3526.

Lelli, J. L. J., Becks, L. L., Dabrowska, M. I. & Hinshaw, D. B. (1998) Atp converts necrosis to apoptosis in oxidant injured endothelial cells. *Free radicals Biology and medicine,* 25**,** 694-702.

Leto, T. L., Adams, A. G. & De Mendez, I. (1994) Assembly of the phagocyte nadph oxidase: Binding of src homology 3 domains to proline-rich targets. *Proceedings of the National Academy of Sciences of the United States of America,* 91**,** 10650-10654.

Li, J. M., Mullen, A. M., Yun, S., Wientjes, F., Brouns, G. Y., Thrasher, A. J. & Shah, A. M. (2002) Essential role of the nadph oxidase subunit p47phox in endothelial cell superoxide production in response to phorbol ester and tumor necrosis factor-伪. *Circulation Research,* 90**,** 143-150.

Li, N., Ragheb, K., Lawler, G., Sturgis, J., Rajwa, B., Melendez, J. A. & Robinson, J. P. (2003) Dpi induces mitochondrial superoxide-mediated apoptosis. *Free Radical Biology and Medicine,* 34**,** 465-477.

Li, Y. & Trush, M. A. (1998) Diphenyleneiodonium, an nad(p)h oxidase inhibitor, also potently inhibits mitochondrial reactive oxygen species production. *Biochemical and Biophysical Research Communications,* 253**,** 295-299.

Libby, P. (2002) Inflammation in atherosclerosis. *Nature,* 420**,** 868-874.

Libby, P., Ridker, P. M. & Maseri, A. (2002) Inflammation and atherosclerosis. *Circulation,* 105**,** 1135-1143.

Liu, G. & Pessah, I. N. (1994) Molecular interaction between ryanodine receptor and glycoprotein triadin involves redox cycling of functionally important hyperreactive sulfhydryls. *Journal of Biological Chemistry,* 269**,** 33028-33034.

Lougheed, M. & Steinbrecher, U. P. (1996) Mechanism of uptake of copper-oxidized low density lipoprotein in macrophages is dependent on its extent of oxidation. *J Biol Chem,* 271**,** 11798-11805.

Lusis, A. J. (2000) Atherosclerosis. *Nature,* 407**,** 233-241.

Maack, C. & O'rourke, B. (2007) Excitation-contraction coupling and mitochondrial energetics. *Basic Research in Cardiology,* 102**,** 369-392.

Madamanchi, N. R., Hakim, Z. S. & Runge, M. S. (2005) Oxidative stress in atherogenesis and arterial thrombosis: The disconnect between cellular studies and clinical outcomes. *Journal of Thrombosis and Haemostasis,* 3**,** 254-267.

Madamanchi, N. R. & Runge, M. S. (2007) Mitochondrial dysfunction in atherosclerosis. *Circulation Research,* 100**,** 460-473.

Maxeiner, H., Husemann, J., Thomas, C. A., Loike, J. D., El Khoury, J. & Silverstein, S. C. (1998) Complementary roles for scavenger receptor a and cd36 of human monocyte-derived macrophages in adhesion to surfaces coated with oxidized low-density lipoproteins and in secretion of h_2o_2. *Journal of Experimental Medicine,* 188**,** 2257-2265.

Meier, B., Jesaitis, A. J., Emmendorffer, A., Roesler, J. & Quinn, M. T. (1993) The cytochrome b-558 molecules involved in the fibroblast and polymorphonuclear leucocyte superoxide-generating nadph oxidase systems are structurally and genetically distinct. *Biochemical Journal,* 289**,** 481-486.

Meilhac, O., Escargueil-Blanc, I., Thiers, J. C., Salvayre, R. & Negre-Salvayre, A. (1999) Bcl-2 alters the balance between apoptosis and necrosis, but does not prevent cell death induced by oxidized low density lipoproteins. *FASEB Journal,* 13**,** 485-494.

Meister, A. (1988) Glutathione metabolism and its selective modification. *Journal of Biological Chemistry,* 263**,** 17205-17208.

Miyoshi, H., Umeshita, K., Sakon, M., Imajoh-Ohmi, S., Fujitani, K., Gotoh, M., Oiki, E., Kambayashi, J. I. & Monden, M. (1996) Calpain activation in plasma membrane bleb formation during tert-butyl hydroperoxide-induced rat hepatocyte injury. *Gastroenterology,* 110**,** 1897-1904.

Monier, S., Samadi, M., Prunet, C., Denance, M., Laubriet, A., Anne, A. A., Berthier, A., Steinmetz, E., Jurgens, G., Negre-Salvayre, A., Bessede, G., Lemaire-Ewing, S., Neel, D., Gambert, P. & Lizard, G. (2003) Impairment of the cytotoxic and oxidative activities of 7 beta-hydroxycholesterol and 7-ketocholesterol by esterification with oleate. *Biochemical and Biophysical Research Communications,* 303**,** 814-824.

Morgan, P. E., Dean, R. T. & Davies, M. J. (2002a) Inactivation of cellular enzymes by carbonyls and protein-bound glycation/glycoxidation products. *Archives of Biochemistry and Biophysics,* 403**,** 259-269.

Morgan, P. E., Dean, R. T. & Davies, M. J. (2002b) Inhibition of glyceraldehyde-3-phosphate dehydrogenase by peptide and protein peroxides generated by singlet oxygen attack. *European Journal of Biochemistry,* 269**,** 1916-1925.

Morton, R. L., Ikle, D. & White, C. W. (1998) Loss of lung mitochondrial aconitase activity due to hyperoxia in bronchopulmonary dysplasia in primates. *American Journal of Physiology - Lung Cellular and Molecular Physiology,* 274**,** L127-L133.

Mosmann, T. (1983) Rapid colorimetric assay for cellular growth and survival: Application to proliferation and cytotoxicity assays. *Journal Immunological Methods,* 65**,** 55-63.

Movitz, C., Sjolin, C. & Dahlgren, C. (1997) A rise in ionized calcium activates the neutrophil nadph-oxidase but is not sufficient to directly translocate cytosolic p47(phox) or p67(phox) to b cytochrome containing membranes. *Inflammation,* 21**,** 531-540.

Murakami, K. & Yoshino, M. (1997) Inactivation of aconitase in yeast exposed to oxidative stress. *Biochemistry and Molecular Biology International,* 41**,** 481-486.

Murray, C. J. L. & Lopez, A. D. (1997) Global mortality, disability, and the contribution of risk factors: Global burden of disease study. *Lancet,* 349**,** 1436-1442.

Napoli, C., D'armiento, F. P., Mancini, F. P., Postiglione, A., Witztum, J. L., Palumbo, G. & Palinski, W. (1997) Fatty streak formation occurs in human fetal aortas and is greatly enhanced maternal, hypercholesterolemia. Intimal accumulation of low density lipoprotein and its oxidation precede monocyte recruitment into early atheroeclerotic lesions. *Journal of Clinical Investigation,* 100**,** 2680-2690.

Negre-Salvayre, A., Fitoussi, G., Reaud, V., Pieraggi, M. T., Thiers, J. C. & Salvayre, R. (1992) A delayed and sustained rise of cytosolic calcium is elicited by oxidized ldl in cultured bovine aortic endothelial cells. *FEBS Letters,* 299**,** 60-65.

Nguyen-Khoa, T., Massy, Z. A., Witko-Sarsat, V., Canteloup, S., Kebede, M., Lacour, B., Drueke, T. & Descamps-Latscha, B. (1999) Oxidized low-density lipoprotein induces macrophage respiratory burst via its protein moiety: A novel pathway in atherogenesis? *Biochemical and Biophysical Research Communications,* 263**,** 804-809.

Nicotera, P. & Orrenius, S. (1998) The role of calcium in apoptosis. *Cell Calcium,* 23**,** 173-180.

Nisimoto, Y., Motalebi, S., Han, C. H. & Lambeth, J. D. (1999) The p67(phox) activation domain regulates electron flow from nadph to flavin in flavocytochrome b558. *Journal of Biological Chemistry,* 274**,** 22999-23005.

Nushjira, P. (2009) Atherosclerosis and nadph oxidase. *Silpakorn U Science & Tech J,* 3**,** 13-24.

O'donnell, V. B., Tew, D. G., Jones, O. T. G. & England, P. J. (1993) Studies on the inhibitory mechanism of iodonium compounds with special reference to neutrophil nadph oxidase. *Biochemical Journal,* 290**,** 41-49.

Oettl, K., Dikalov, S., Freisleben, H. J., Mlekusch, W. & Reibnegger, G. (1997) Spin trapping study of antioxidant properties of neopterin and 7,8-dihydroneopterin. *Biochem Biophys Res Commun.,* 234**,** 774-8.

Oettl, K., Greilberger, J., Dikalov, S. & Reibnegger, G. (2004) Interference of 7,8-dihydroneopterin with peroxynitrite-mediated reactions. *Biochemical and Biophysical Research Communications,* 321**,** 379-385.

Ohgushi, M., Kugiyama, K., Fukunaga, K., Murohara, T., Sugiyama, S., Miyamoto, E. & Yasue, H. (1993) Protein kinase c inhibitors prevent impairment of endothelium-dependent relaxation by oxidatively modified ldl. *Arteriosclerosis and Thrombosis,* 13**,** 1525-1532.

Paffenholz, R., Bergstrom, R. A., Pasutto, F., Wabnitz, P., Munroe, R. J., Jagla, W., Heinzmann, U., Marquardt, A., Bareiss, A., Laufs, J., Russ, A., Stumm, G., Schimenti, J. C. & Bergstrom, D. E. (2004) Vestibular defects in head-tilt mice result from mutations in nox3, encoding an nadph oxidase. *Genes and Development,* 18**,** 486-491.

Palinski, W., Ord, V. A., Plump, A. S., Breslow, J. L., Steinberg, D. & Witztum, J. L. (1994) Apoe-deficient mice are a model of lipoprotein oxidation in atherogenesis: Demonstration of oxidation-specific epitopes in lesions and high titers of autoantibodies to malondialdehyde-lysine in serum. *Arteriosclerosis and Thrombosis,* 14**,** 605-616.

Park, S. E., Song, J. D., Kim, K. M., Park, Y. M., Kim, N. D., Yoo, Y. H. & Park, Y. C. (2007) Diphenyleneiodonium induces ros-independent p53 expression and apoptosis in human rpe cells. *FEBS Letters,* 581**,** 180-186.

Parkos, C. A., Dinauer, M. C., Walker, L. E., Allen, R. A., Jesaitis, A. J. & Orkin, S. H. (1988) Primary structure and unique expression of the 22-kilodalton light chain of human neutrophil cytochrome b. *Proceedings of the National Academy of Sciences of the United States of America,* 85**,** 3319-3323.

Patterson, C., Ruef, J., Madamanchi, N. R., Barry-Lane, P., Hu, Z., Horaist, C., Ballinger, C. A., Brasier, A. R., Bode, C. & Runge, M. S. (1999) Stimulation of a vascular smooth muscle cell nad(p)h oxidase by thrombin: Evidence that p47(phox) may participate in forming this oxidase in vitro and in vivo. *Journal of Biological Chemistry,* 274**,** 19814-19822.

Petronilli, V., Costantini, P., Scorrano, L., Colonna, R., Passamonti, S. & Bernardi, P. (1994) The voltage sensor of the mitochondrial permeability transition pore is tuned by the oxidation-reduction state of vicinal thiols. Increase of the gating potential by oxidants and its reversal by reducing agents. *Journal of Biological Chemistry,* 269**,** 16638-16642.

Plank, M. J., Wall, D. J. N. & David, T. (2007) The role of endothelial calcium and nitric oxide in the localisation of atherosclerosis. In press. *Math. Biosci.*

Porn-Ares, M. I., Ares, M. P. S. & Orrenius, S. (1998) Calcium signalling and the regulation of apoptosis. *Toxicology in Vitro,* 12**,** 539-543.

Powell, C. S. & Jackson, R. M. (2003) Mitochondrial complex i, aconitase, and succinate dehydrogenase during hypoxia-reoxygenation: Modulation of enzyme activities by

mnsod. *American Journal of Physiology - Lung Cellular and Molecular Physiology,* 285**,** L189-L198.

Prabhakar, N. R. (2000) Oxygen sensing by the carotid body chemoreceptors. *Journal of Applied Physiology,* 88**,** 2287-2295.

Qin, F., Patel, R., Yan, C. & Liu, W. (2006) Nadph oxidase is involved in angiotensin ii-induced apoptosis in h9c2 cardiac muscle cells: Effects of apocynin. *Free Radical Biology and Medicine,* 40**,** 236-246.

Reid, V. C., Mitchinson, M. J. & Skeper, J. N. (1993) Cytotoxicity of oxidised low density lipoprotein towards mouse peritoneal macrophages: An ultrastructural study. *Journal of Pathology,* 171**,** 321-328.

Riganti, C., Costamagna, C., Bosia, A. & Ghigo, D. (2006) The nadph oxidase inhibitor apocynin (acetovanillone) induces oxidative stress. *Toxicology and Applied Pharmacology,* 212**,** 179-187.

Riganti, C., Costamagna, C., Doublier, S., Miraglia, E., Polimeni, M., Bosia, A. & Ghigo, D. (2008) The nadph oxidase inhibitor apocynin induces nitric oxide synthesis via oxidative stress. *Toxicology and Applied Pharmacology,* 228**,** 277-285.

Riganti, C., Gazzano, E., Polimeni, M., Costamagna, C., Bosia, A. & Ghigo, D. (2004) Diphenyleneiodonium inhibits the cell redox metabolism and induces oxidative stress. *Journal of Biological Chemistry,* 279**,** 47726-47731.

Rinckel, L. (1999) Rac1 disrupts p67phox/p40phox binding: A novel role for rac in nadph oxidase activation. *Biochemical and Biophysical Research Communications,* 263**,** 118-5.

Rodaway, A. R. F., Teahan, C. G., Casimir, C. M., Segal, A. W. & Bentley, D. L. (1990) Characterization of the 47-kilodalton autosomal chronic granulomatous disease protein: Tissue-specific expression and transcriptional control by retinoic acid. *Molecular and Cellular Biology,* 10**,** 5388-5396.

Rosenfeld, M. (1996) Cellular mechanisms in the development of atherosclerosis. *Diabetes Research and Clinical Practice,* 30**,** S139-S141.

Ross, R. (1993) Atherosclerosis: A defense mechanism gone awry. *American Journal of Pathology,* 143**,** 987-1002.

Rotrosen, D. & Leto, T. L. (1990) Phosphorylation of neutrophil 47-kda cytosolic oxidase factor. Translocation to membrane is associated with distinct phosphorylation events. *Journal of Biological Chemistry,* 265**,** 19910-19915.

Rotrosen, D., Yeung, C. L., Leto, T. L., Malech, H. L. & Kwong, C. H. (1992) Cytochrome b558: The flavin-binding component of the phagocyte nadph oxidase. *Science,* 256**,** 1459-1462.

Rutherford, L. D. (2010) Toxicity of 7-ketocholesterol as a mechanism of oxidised low density lipoprotein-induced cellular death. *Master Thesis,* University of Canterbury, New Zealand.

Ryter, S. W., Xi, S., Hartsfield, C. L. & Choi, A. M. K. (2002) Mitogen activated protein kinase (mapk) pathway regulates heme oxygenase-1 gene expression by hypoxia in vascular cells. *Antioxidants and Redox Signaling,* 4**,** 587-592.

S.Janes, M., M.Hill, D., Cardon, C. M., Robinson, K. M., Walls, J. R., Leung, W.-Y., Beckman, J. S. & J.Ignatius, M. (2004) Fluorogenic detection of mitochondrial superoxide in live cells.

Scott, J. (2004) Pathophysiology and biochemistry of cardiovascular disease. *Current Opinion in Genetics and Development,* 14**,** 271-279.

Shen, R. (1994) Inhibition of luminol enhanced chemiluminescence by reduced pterins. *Archives of Biochemistry and Biophysics,* 310**,** 60-63.

Simons, J. M., T Hart, B. A., Ip Vai Ching, T. R. A. M., Van Dijk, H. & Labadie, R. P. (1990) Metabolic activation of natural phenols into selective oxidative burst agonists by activated human neurophils. *Free Radical Biology and Medicine,* 8**,** 251-258.

Singh, U. & Jialal, I. (2006) Oxidative stress and atherosclerosis. *Pathophysiology,* 13**,** 129-142.

Skepper, J. N., Karydis, I., Garnett, M. R., Hegyi, L., Hardwick, S. J., Warley, A., Mitchinson, M. J. & Cary, N. R. B. (1999) Changes in elemental concentrations are associated with early stages of apoptosis in human monocyte macropahes exposed to oxidised low density lipoprotein: An x-ray microanalytical study. *Journal of Pathology,* 188**,** 100-106.

Souza, J. M. & Radi, R. (1998) Glyceraldehyde-3-phosphate dehydrogenase inactivation by peroxynitrite. *Archives of Biochemistry and Biophysics,* 360**,** 187-194.

Stadtman, E. R. & Berlett, B. S. (1998) Reactive oxygen-mediated protein oxidation in aging and disease. *Drug Metabolism Reviews,* 30**,** 225-243.

Stary, H. C., Chandler, A. B., Dinsmore, R. E., Fuster, V., Glagov, S., Insull, W. J., Rosenfeld, M.E., Schwartz, C. J., Wagner, W. D. & Wissler, R. W. (1995) A definition of advanced types of atherosclerotic lesions and a histological classification of atherosclerosis. A report from the committee on vascular lesions of the council on arteriosclerosis, american heart association. *Arteriosclerosis Thrombosis Vascular Biology,* 15**,** 1512-1531.

Steinberg, D., Parthasarathy, S., Carew, T. E., Khoo, J. C. & Witztum, J. L. (1989) Beyond cholesterol: Modifications of low-density lipoprotein that increase its atherogenicity. *The New England Journal of Medicine,* 320**,** 915-924.

Stocker, R. & Keaney, J. F. (2004) Role of oxidative modifications in atherosclerosis. *Physiological Reviews,* 84**,** 1381-1478.

Stolk, J., Hiltermann, T. J., Dijkman, J. H. & Verhoeven, A. J. (1994) Characteristics of the inhibition of nadph oxidase activation in neutrophils by apocynin, a methoxy-substituted catechol. *American journal of respiratory cell and molecular biology,* 11**,** 95-102.

Stuehr, D. J., Fasehun, O. A., Kwon, N. S., Gross, S. S., Gonzalez, J. A., Levi, R. & Nathan, C. F. (1991) Inhibition of macrophage and endothelial cell nitric oxide synthase by diphenyleneiodonium and its analogs. *FASEB Journal,* 5**,** 98-103.

Sukhanov, S., Higashi, Y., Shai, S. Y., Itabe, H., Ono, K., Parthasarathy, S. & Delafontaine, P. (2006) Novel effect of oxidized low-density lipoprotein - cellular atp depletion via downregulation of glyceraldehyde-3-phosphate dehydrogenase. *Circulation Research,* 99**,** 191-200.

Sumimoto, H., Hata, K., Mizuki, K., Ito, T., Kage, Y., Sakaki, Y., Fukumaki, Y., Nakamura, M. & Takeshige, K. (1996) Assembly and activation of the phagocyte nadph oxidase: Specific interaction of the n-terminal src homology 3 domain of p47(phox) with p22(phox) is required for activation of the nadph oxidase. *Journal of Biological Chemistry,* 271**,** 22152-22158.

Sumimoto, H., Kage, Y., Nunoi, H., Sasaki, H., Nose, T., Fukumaki, Y., Ohno, M., Minakami, S. & Takeshige, K. (1994) Role of src homology 3 domains in assembly and activation of the phagocyte nadph oxidase. *Proceedings of the National Academy of Sciences of the United States of America,* 91**,** 5345-5349.

Sun, J., Xu, L., Eu, J. P., Stamler, J. S. & Meissner, G. (2001) Classes of thiols that influence the activity of the skeletal muscle calcium release channel. *Journal of Biological Chemistry,* 276**,** 15625-15630.

Sundstrom, C. & Nilsson, K. (1976) Establishment and characterization of a human histiocytic lymphoma cell line (u 937). *International Journal of Cancer,* 17**,** 565-577.

Szanto, I., Rubbia-Brandt, L., Kiss, P., Steger, K., Banfi, B., Kovari, E., Herrmann, F., Hadengue, A. & Krause, K. H. (2005) Expression of noxi, a superoxide-generating nadph oxidase, in colon cancer and inflammatory bowel disease. *Journal of Pathology,* 207**,** 164-176.

T Hart, B. A. & Simons, J. M. (1992) Metabolic activation of phenols by stimulated neutrophils: A concept for a selective type of anti-inflammatory drug. *Biotechnology Therapeutics,* 3**,** 119-135.

Tabas, I. (2005) Consequences and therapeutic implications of macrophage apoptosis in atherosclerosis - the importance of lesion stage and phagocytic efficiency. *Arteriosclerosis Thrombosis and Vascular Biology,* 25**,** 2255-2264.

Vejrazka, M., Micek, R. & Stipek, S. (2005) Apocynin inhibits nadph oxidase in phagocytes but stimulates ros production in non-phagocytic cells. *Biochimica et Biophysica Acta - General Subjects,* 1722**,** 143-147.

Vicca, S., Hennequin, C., Nguyen-Khoa, T., Massy, Z. A., Descamps-Latscha, B., Drueke, T. B. & Lacour, B. (2000) Caspase-dependent apoptosis in thp-1 cells exposed to oxidized low-density lipoproteins. *Biochemical and Biophysical Research Communications,* 273**,** 948-954.

Vicca, S., Massy, Z. A., Hennequin, C., Rihane, D., Dr 眉 eke, T. B. & Lacour, B. (2003) Apoptotic pathways involved in u937 cells exposed to ldl oxidized by hypochlorous acid. *Free Radical Biology and Medicine,* 35**,** 603-615.

Vindis, C., Elbaz, M., Escargueil-Blanc, I., Auge, N., Heniquez, A., Thiers, J. C., Negre-Salvayre, A. & Salvayre, R. (2005) Two distinct calcium-dependent mitochondrial pathways are involved in oxidized ldl-induced apoptosis. *Arteriosclerosis Thrombosis and Vascular Biology,* 25**,** 639-645.

Wang, W., Pang, L. & Palade, P. (2010) Angiotensin ii upregulates cav1.2 protein expression in cultured arteries via endothelial h2o2 production. *Journal of Vascular Research,* 48**,** 67-78.

Wang, X. S., Greilberger, J. & Jurgens, G. (2000) Calcium and lipoprotein lipase synergistically enhance the binding and uptake of native and oxidized ldl in mouse peritoneal macrophages. *Atherosclerosis,* 150**,** 357-363.

Wang, X. S., Greilberger, J., Ratschek, M. & Jurgens, G. (2001) Oxidative modifications of ldl increase it's binding to extracellular matrix from human aortic intima: Influence of lesion development, lipoprotein lipase and calcium. *Journal of Pathology,* 195**,** 244-250.

Wang, Y. X., Poon, C. I., Poon, K. S. & Pang, C. C. Y. (1993) Inhibitory actions of diphenyleneiodonium on endothelium-dependent vasodilatations in vitro and in vivo. *British Journal of Pharmacology,* 110**,** 1232-1238.

Warnholtz, A., Nickenig, G., Schulz, E., Macharzina, R., Br 盲 sen, J. H., Skatchkov, M., Heitzer, T., Stasch, J. P., Griendling, K. K., Harrison, D. G., B 枚 hm, M., Meinertz, T. & M 眉 nzel, T. (1999) Increased nadh-oxidase-mediated superoxide production. In the early stages of atherosclerosis evidence for involvement of the renin-angiotensin system. *Circulation,* 99**,** 2027-2033.

Weber, H., H 眉 hns, S., L 眉 then, F., Jonas, L. & Schuff-Werner, P. (2005) Calpain activation contributes to oxidative stress-induced pancreatic acinar cell injury. *Biochemical Pharmacology,* 70**,** 1241-1252.

Whiteman, M., Armstrong, J. S., Cheung, N. S., Siau, J. L., Rose, P., Schantz, J. T., Jones, D. P. & Halliwell, B. (2004) Peroxynitrite mediates calcium-dependent mitochondrial dysfunction and cell death via activation of calpains. *FASEB Journal,* 18**,** 1395-1397.

Wientjes, F. B., Segal, A. W. & Hartwig, J. H. (1997) Immunoelectron microscopy shows a clustered distribution of nadph oxidase components in the human neutrophil plasma membrane. *Journal of Leukocyte Biology,* 61**,** 303-312.

Wintergerst, E. S., Jelk, J., Rahner, C. & Asmis, R. (2000) Apoptosis induced by oxidized low density lipoprotein in human monocyte-derived macrophages involves cd36 and activation of caspase-3. *European Journal of Biochemistry,* 267**,** 6050-6058.

Ximenes, V. F., Kanegae, M. P. P., Rissato, S. R. & Galhiane, M. S. (2007) The oxidation of apocynin catalyzed by myeloperoxidase: Proposal for nadph oxidase inhibition. *Archives of Biochemistry and Biophysics,* 457**,** 134-141.

Yan, L. J., Levine, R. L. & Sohal, R. S. (1997) Oxidative damage during aging targets mitochondrial aconitase. *Proceedings of the National Academy of Sciences of the United States of America,* 94**,** 11168-11172.

Yang, T. (2009) Mechanism and inhibition of hypochlorous acid-mediated cell death in human monocytes-derived macrophages. *PhD Thesis*.

Yang, Y. T., Whiteman, M. & Gieseg, S. P. (2012) Hocl causes necrotic cell death in human monocyte derived macrophages through calcium dependent calpain activation. *Biochimica et Biophysica Acta - Molecular and Cell Biology* 420-429.

Yap, Y. W., Whiteman, M., Bay, B. H., Li, Y., Sheu, F. S., Qi, R. Z., Tan, C. H. & Cheung, N. S. (2006) Hypochlorous acid induces apoptosis of cultured cortical neurons through activation of calpains and rupture of lysosomes. *JOURNAL OF NEUROCHEMISTRY,* 98**,** 1597-1609.

Yarian, C. S., Rebrin, I. & Sohal, R. S. (2005) Aconitase and atp synthase are targets of malondialdehyde modification and undergo an age-related decrease in activity in mouse heart mitochondria. *Biochemical and Biophysical Research Communications,* 330**,** 151-156.

Yarian, C. S. & Sohal, R. S. (2005) In the aging housefly aconitase is the only citric acid cycle enzyme to decline significantly. *Journal of Bioenergetics and Biomembranes,* 37**,** 91-96.

Yarian, C. S., Toroser, D. & Sohal, R. S. (2006) Aconitase is the main functional target of aging in the citric acid cycle of kidney mitochondria from mice. *Mechanisms of Ageing and Development,* 127**,** 79-84.

Ylaherttuala, S., Palinski, W., Rosenfeld, M. E., Parthasarathy, S., Carew, T. E., Butler, S., Witztum, J. L. & Steinberg, D. (1989) Evidence for the presence of oxidatively modified low-density lipoprotein in atherosclerotic lesions of rabbit and man. *Journal of Clinical Investigation,* 84**,** 1086-1095.

Young, M. P., Febbraio, M. & Silverstein, R. L. (2009) Cd36 modulates migration of mouse and human macrophages in response to oxidized ldl and may contribute to macrophage trapping in the arterial intima. *Journal of Clinical Investigation,* 119**,** 136-145.

Yuan, X. M., Li, W., Brunk, U. T., Dalen, H., Chang, Y. H. & Sevanian, A. (2000) Lysosomal destabilization during macrophage damage induced by cholesterol oxidation products. *Free Radical Biology and Medicine,* 28**,** 208-218.

Zmijewski, J. W., Moellering, D. R., Le Goffe, C., Landar, A., Ramachandran, A. & Darley-Usmar, V. M. (2005) Oxidized ldl induces mitochondrially associated

reactive oxygen/nitrogen species formation in endothelial cells. *American Journal of Physiology-Heart and Circulatory Physiology,* 289**,** H852-H861.

Zweier, J. L., Hu, Q., Ziegelstein, R. C., Zheng, G., Irani, K. & Deshpande, S. (2000) Nadph oxidase activation increases the sensitivity of intracellular ca2+ stores to inositol 1,4,5-trisphosphate in human endothelial cells. *The Journal of biological chemistry,* 275**,** 15749-9.